COMPARISON OF THE EFFECT OF REPRESENTATIVE METAL AND TRANSITION METAL SALTS ON THE FORMATION OF HEXAGONAL BORON NITRIDE

ERHAN BUDAK

JULY 2009

COMPARISON OF THE EFFECT OF REPRESENTATIVE METAL AND TRANSITION METAL SALTS ON THE FORMATION OF HEXAGONAL BORON NITRIDE

by

ERHAN BUDAK

THESIS SUBMITTED TO
THE GRADUATE SCHOOL OF NATURAL AND APPLIED SCIENCES
OF
THE ABANT IZZET BAYSAL UNIVERSITY
IN PARTIAL FULFILLMENT OF THE REQUIREMENTS FOR THE DEGREE OF
DOCTOR OF PHILOSOPHY
IN
THE DEPARTMENT OF CHEMISTRY

JULY 2009

Approval of the Graduate School of Natural and Applied Sciences.

Prof.Dr. Nihat ÇELEBİ
Director

I certify that this thesis satisfies all the requirements as a thesis for the degree of Doctor of Philosophy.

Prof.Dr.Çetin BOZKURT
Head of Department

This is to certify that we have read this thesis and that in our opinion it is fully adequate, in scope and quality as a thesis for the degree of Doctor of Philosophy.

Prof.Dr.Çetin BOZKURT
Supervisor

Examining Committee Members

1. Prof.Dr. İbrahim BELENLİ .....
2. Prof.Dr. Çetin BOZKURT .....
3. Prof.Dr. Canan ÜNALEROĞLU .....
4. Prof.Dr. İzzet MORKAN .....
5. Assoc.Prof.Dr. Engin ÖZDAŞ .....

ABSTRACT

COMPARISON OF THE EFFECT OF REPRESENTATIVE METAL AND TRANSITION METAL SALTS ON THE FORMATION OF HEXAGONAL BORON NITRIDE

Budak, Erhan
Ph.D., Department of Chemistry
Supervisor: Prof. Dr. Çetin Bozkurt

July 2009, 123 pages

Boron nitride is an extraordinary structure in the area of materials science. Due to the special bonding behaviors of boron and nitrogen BN can exist in many different structures. Graphite like hexagonal boron nitride with amazing properties was subjected to many studies in the last twenty years.

In this study, hexagonal boron nitride was synthesized with the modified O'Connor method in presence of different metal salts. Structural properties of the synthesized materials were determined by X-Ray Diffraction, (XRD), Fourier Transform Infrared Spectroscopy, (FTIR), and Scanning Electron Microscopy, (SEM).

FTIR results confirmed the formation of hexagonal boron nitride and main peaks of hexagonal boron nitride were observed in XRD analysis. Lattice parameters

were calculated for the samples and the results were found very close to original hexagonal boron nitride In addition, it was found that the synthesized products in nano-scale.

Key words: Hexagonal Boron Nitride, O'Connor Method, Synthesis, Characterization, XRD, Nanocrystal.

ÖZET

TEMSİLCİ METAL VE GEÇİŞ METAL TUZLARININ
BOR NİTRÜR OLUŞUMUNA
ETKİLERİNİN KARŞILAŞTIRILMASI

Budak, Erhan
Doktora, Kimya Bölümü
Tez Danışmanı: Prof.Dr. Çetin Bozkurt

Temmuz 2009, 123 sayfa

Bor nitrür, malzeme bilimleri alanında sıradışı konudur. Borun ve azotun özel bağlama davranışları nedeniyle, bor nitrür birçok farklı yapılarda bulunabilir. Grafit benzeri yapısı ve mükemmel özellikleriyle hekzagonal bor nitür son yirmi yılda bir çok araştırmaya çalışmaya konu olmuştur.

Bu çalısmada, hekzagonal bor nitrür modifiye O'Connor metodu ile farklı metal tuzlarının varlığında sentezlenmistir. Sentezlenen maddelerin yapısal özellikleri X-Isını Kırınım Ölçeri (XRD), Fourier Dönüsüm Kızılötesi Spektroskopisi (FTIR) ve Taramalı Elektron Mikroskobu (SEM) kullanılarak belirlenmistir.

FTIR sonuçları hekzagonal bor nitrür oluşumunu doğrulamakta ve XRD analizlerinde hekzagonal bor nitrürün ana pikleri görülmüştür. Örnekler için örgü

parametreleri hesaplanmış ve orjinal hexagonal bor nitrüre çok yakın bulunmuştur. Ayrıca sentezlenen maddelerin nano ölçekte olduğu gözlenmiştir.

Anahtar kelimeler: Hekzagonal Bor Nitrür, O'Connor Metot, Sentez, Karekterizasyon, XRD, Nanokristal.

To My Family

ACKNOWLEDGMENT

I would like to express my sincere gratitude to my supervisor Prof.Dr. Çetin Bozkurt for his continuous support of my Ph.D study and research. His guidance helped me in all the time of research and writing of this thesis. I could not have imagined having a better advisor this Ph.D study.

Besides my advisor, I would like to thank the rest of my thesis committee: Prof.Dr. İbrahim Belenli, Prof.Dr. İzzet Morkan and Prof.Dr. Canan Ünaleroğlu and Assoc.Prof.Dr. Engin Özdaş for their encouragement, insightful comments.

My sincere thanks also goes to Assoc.Prof. Dr. Engin Özdaş, Assoc.Prof. Dr. Ahmet Varilci, Bora Kalkan, Mustafa Akdoğan, and Dinçer Yeğen for providing and informing SEM and XRD analysis.

I want to express my gratitude to my office mates Sevim Demirözü Şenol and Bahadır Altıntaş for their motivation and patience. I am also grateful to Efkan Çatıker, İsmail Uğur Tiryaki, Canan Sapmaz, and Ahmet Erden for their friendship and motivation during this study.

Last but not the least; I would like to thank to my family for their endless support, love, patience for me that made the accomplishment of this work.

ABBREVIATIONS

2θ	Bragg angle degree
BN	Boron Nitride
AFM	Atomic Force Microscope
cBN	Cubic Boron Nitride
EDX	Energy Dispersive X-Ray Spectroscopy
FTIR	Fourier Transform Infrared Spectroscopy
hBN	Hexagonal Boron Nitride HRTEM
ICDD	The International Centre for Diffraction Data
rBN	Rhombohedral Boron Nitride
SEM	Scanning Electron Microscopy
tBN	Turbostratic Boron Nitride
TEM	Transmission Electron Microscope
wBN	Wurtzitic Boron Nitride
XRD	X-ray Diffractometer

CONTESTS

LIST OF TABLES

Table **Page**

LIST OF FIGURES

Figure **Page**

1. INTRODUCTION

Boron compounds, especially borax, have been used for more than thousand years by Babylon, ancient Egypt, and ancient Greek for cleaning, melting valuable jewels, mummifying, and curing illness. Today Turkey has the largest boron ore deposits in the World. However, the production of **"specialty boron chemicals**" which is very important for industrial applications is very low. Also, boron and its compounds were declared by USA and NATO as strategically important material in 1961 [1].

Boron nitride (BN) - in all its various structures - is a synthetic product and not found in nature. The first synthesis for hexagonal boron nitride (hBN) was described in 1842 by Balmain [2], but hBN became a commercial material after 100 years. Due to its excellent properties hBN is useful for industrial applications:

i. As the lubricity mechanism does not involve water molecules trapped between the layers, so hBN lubricants can be used even in vacuum, e.g. for space applications.
ii. Due to its excellent dielectric and insulating properties, hBN is used in electronics eg. as a substrate for semiconductors, microwave-transparent windows, structural material for seals, electrodes and catalyst carriers in fuel cells and batteries.

iii. hBN is fairly chemically inert and is not wetted by many melted materials (e.g. aluminum, copper, zinc, iron and steels, germanium, silicon, boron, cryolite, glass and halide salts).

iv. Addition of hBN to silicon nitride ceramics improves the thermal shock resistance of the resulting material [3].

2. BORON NITRIDE

2.1. Structure of Boron Nitride Phases

Boron nitride is an extraordinary structure in the area of materials science. Due to the special bonding behaviors of boron and nitrogen, BN exists in many different phases. The well-defined crystallographic structures are hexagonal BN (hBN), rhombohedral BN (rBN), wurtzitic BN (wBN), and cubic BN (cBN). Additionally, other crystalline and amorphous structures exist. In Table 2.1 the types of boron nitride can be seen in detailed.

Table 2.1. Types of Boron Nitride.

Boron Nitride	
sp^2 – BN	**sp^3 – BN**
hBN	cBN
rBN	wBN
tBN (amorphous)	aBN (amorphous)

2.1.1. Hexagonal Boron Nitride

Hexagonal boron nitride, hBN, has trigonal sp^2 bonding and their structures are similar to, but not the same as, the graphite structure (Figure 2.1.1.1). hBN is composed of series of stacked parallel layer planes. The stacking of these layer planes occurs with the hexagon immediately above each other. The boron and nitrogen atoms alternate from one layer to the other; in other words, each nitrogen atom has a boron atom directly above and below and vice versa. The stacking is thus different from graphite which has the same planar arrangement but offset planes so that only half the carbon atoms have neighbors directly above and directly below.

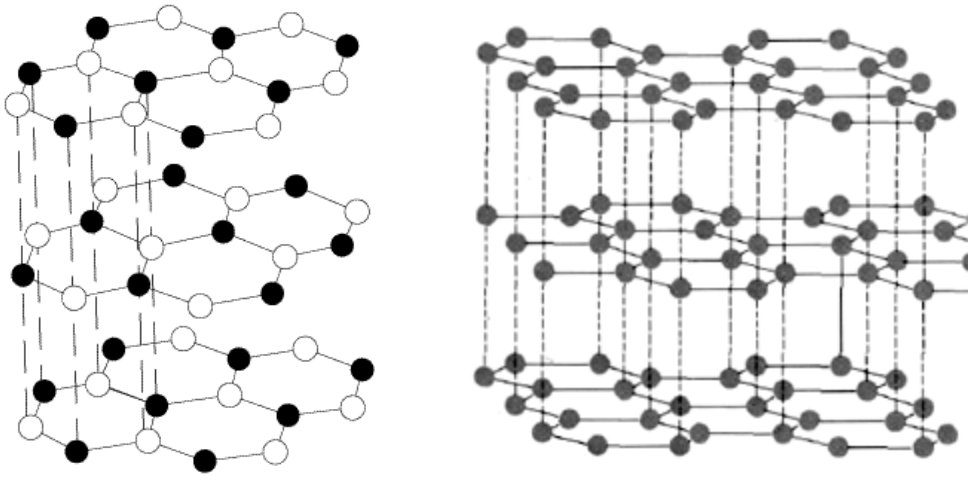

Fig. 2.1.1.1. Crystal lattice of hexagonal boron nitride (left) and graphite (right). Because boron nitride and graphite show similar layer structures, boron nitride is often called "white graphite".

Within the layer plane, each nitrogen atom is bonded to three boron atoms (and vice versa) with a short bond length (0.1446 nm), forming a series of continuous hexagons in what can be considered as an essentially infinite two-dimensional array. The spacing between layer planes is relatively large (0.3615 nm) or more than twice the spacing between atoms within the layer plane. This means that hBN, like graphite, should be able to accommodate intercalation elements or compounds. As a result of the large anisotropy in its crystal, hexagonal boron nitride has very anisotropic properties.

The distribution of the three bonds of each boron and nitrogen atom within the layer plane derives from the sp^2 hybridization of the respective atoms. This bonding is thus similar to the sp^2 bonding within the planes of graphite. It is a strong covalent bond with a short bond length as mentioned above and high bond dissociation energy (4.0 f 0.5 eV, 385 k.I/mol).

In contrast, the bond between the planes of hBN is very weak and even weaker than that of graphite. It is readily broken and layers can be cleaved with a knife like an onion skin. However this bond is electronically different from that in graphite. In graphite, it stems from the hybridized fourth valence electron which is paired with another delocalized electron of the adjacent plane by a weak van der Waals bond. The high electrical conductivity of graphite is attributed to these delocalized electrons. In hBN, no free electrons are available since the corresponding p_Z orbitals in the boron atom are vacant and those of the nitrogen atom are occupied by two electrons. Overlap to form π- bonds is not possible. In addition, the relatively large difference in

electronegativity between nitrogen (3.0) and boron (2.0) imparts greater localization of π- electrons than in graphite. As a result, boron nitride is an electrical insulator [4].

Turbostratic BN (tBN) [5] is low-temperature product of BN. It is prepared at about 1000ºC and often has a disordered structure. In accordance with disordered carbons which show only two X-Ray diffraction peaks (002) and (101), such a structure called *turbostratic* (Figure 2.1.1.2). The turbostratic structure can readily be converted to an ordered layer-lattice hexagonal form by high temperature treatment.

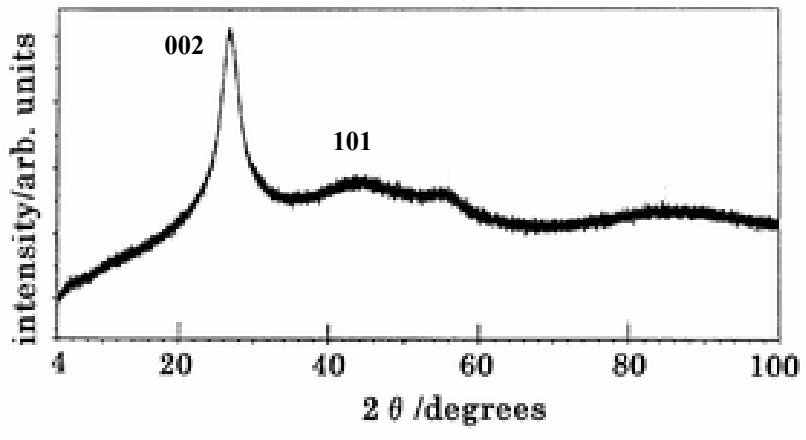

Fig. 2.1.1.2. XRD pattern of tBN.

2.1.2. Cubic Boron Nitride

The structure (Figure 2.1.2.1) of cubic boron nitride is of the zincblende (or sphalerite) type which is similar to that of diamond and β-SiC and is characterized by extreme hardness and excellent chemical resistance. This structure is relatively simple in the sense that it is essentially isotropic, in contrast with the pronounced anisotropy of hBN. It can be visualized as a stacking of puckered infinite (111) layers or as two face-centered interpenetrating cubic sublattices, one consisting entirely of boron atoms and the other entirely of nitrogen atoms.

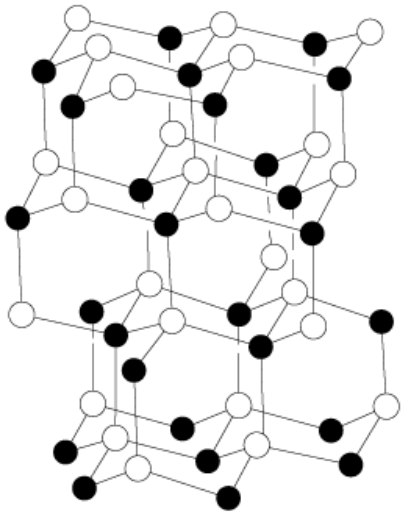

●: B, ○: N

Fig.2.1..2.1 Structure of cBN.

Each boron atom is bonded to four nitrogen atoms in a fourfold coordinated tetrahedral (sp^3) arrangement with a short bond length (0.158 nm). The bonding is essentially covalent although some degree of ionic bonding has been reported. The difference between the atomic spacing of cBN and the sum of the covalent radii of nitrogen and boron and that atomic spacing and the sum of their ionic radii, shows that the bonding is mainly covalent but that a sizeable degree of ionicity is retained. The calculated covalent bond energy is 13.33 eV and the ionic bond energy is 3.12 eV.

The cBN structure, with its tetrahedral bonding, is isotropic and, except on the (111) plane, is more compact than that of hBN (with its sp^2 anisotropic structure and wide interlayer spacing). Consequently cBN has higher theoretical density than hBN (3.43 g/cm3 vs. 2.34 g/cm3). It should be pointed out that the diamond-like structure of cubic boron nitride is similar to those of the other two refractory covalent nitrides, i.e., aluminum nitride and silicon nitride, as well as silicon carbide [6].

2.2. Characterization of Boron Nitride Products

Due to the complexity of BN-structures and atomic bonding situations, the characterization of BN-phases by spectroscopic methods (e.g., IR and Raman) is difficult. It is not possible to identify BN phases using only one analytical method. For example, the X-Ray diffraction peaks of cBN correspond to those of Cu, Ni, and many other cubic phases. Elemental composition must be known or measured to be sure that no other phases are present.

2.2.1. Infrared Spectroscopy (IR)

Infrared spectroscopy (IR) is often used to characterize BN products. Because of the strong covalent bonding of cBN is expected to have high-frequency lattice vibration but the bonding in the flat sp^2 6-ring of hBN is stronger than in the cBN (Figure 2.2.1), as indicated by the higher frequency B-N vibrations exhibited by hBN υ_{LO} = 1610 cm^{-1} –IR inactive- and υ_{LO} = 1370 cm^{-1}-IR active- on the other hand, frequency B-N vibrations exhibited by cBN are υ_{LO} = 1304 cm^{-1} –IR inactive- and υ_{LO} = 1054 cm^{-1}-IR active [7].

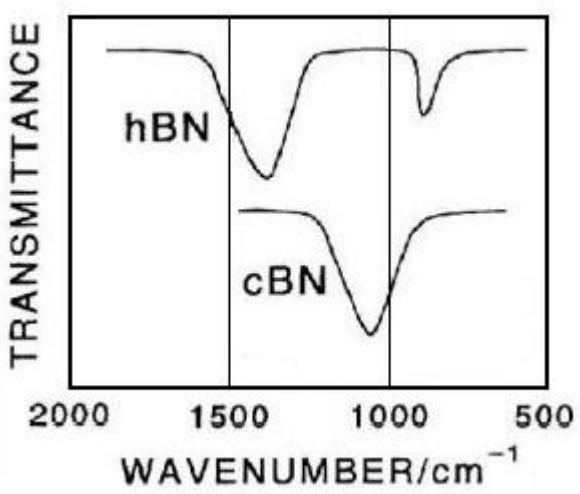

Fig.2.2. 1. IR spectra of hBN and cBN.

2.2.2. X-Ray Diffraction (XRD)

X-Ray diffraction (XRD) is another possibility to distinguish between cBN and hBN. In that case again the elemental composition of the sample is important, because the diffractograms of many cubic substances can mimic the one of cBN (e.g. Cu, Ni, etc.). The peak positions and their intensities are mainly influenced by grain size, stress in the layers and impurities.

The X-Ray diffraction data of sp^2- and sp^3- bonded of BN (Figure 2.2.2) gives information about the layer types and the distances.

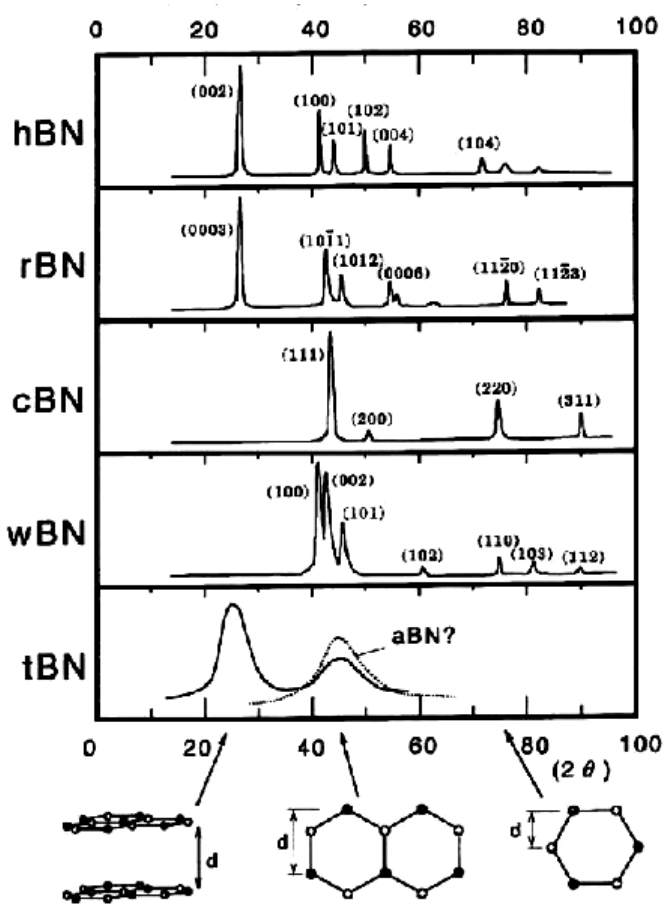

Fig. 2.2.2. The X-Ray diffraction data of hBN, rBN, tBN, cBN, and wBN.

The spectral peaks around 2θ = 25° correspond to the distance (~333 pm) between the layers of the sp^2 networks. Some peaks around 2θ = 40-50° are due to the atoms in the sp^2 or sp^3-6-layer rings. tBN shows two broad diffraction peaks around 2θ = 25° and 40-50°. However, the species having sp^3 layers gives peak 2θ = 40-50° with ~210 pm layer distance [8].

2.3 Synthesis of Hexagonal Boron Nitride

Preparation of a binary compound of boron with nitrogen was first reported as early in 1842 by Balmain by using the action of molten boric acid on potassium cyanide but the compound was unstable. Since then, there have been many routes found to synthesize hBN (Figure 2.3.).

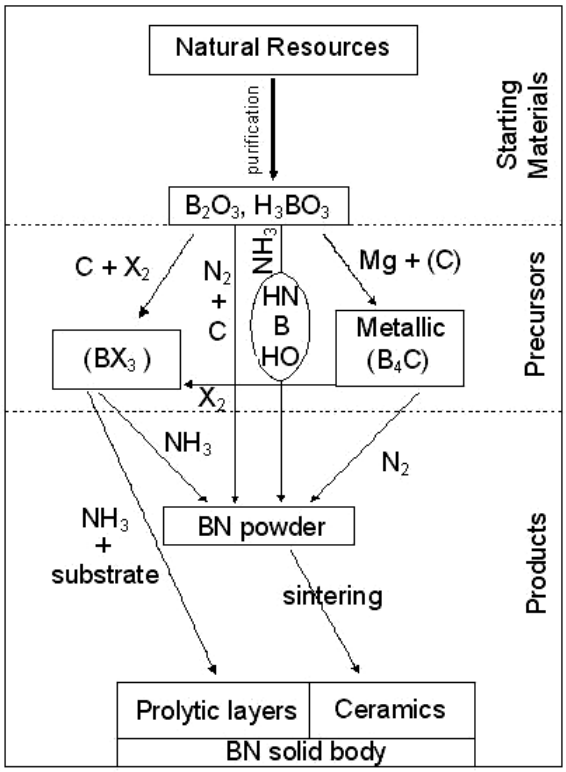

Fig. 2.3. The routes of synthesis of BN [9].

Although there are a lot of other general methods for producing hBN, principally two reactions are used on the industrial scale.

2.3.1. Boric Acid with Carrier Substances

Boric acid with ammonia reacts in the presence of carrier substances ($Ca_3(PO_4)_2$, $CaCO_3$, CaO, BN, Zn-borate). The carrier substances prevent the formation of a homogeneous melt of boric acid, which is not suitable because of its minimal surface: At reaction temperatures exceeding 700 °C a thin film of molten boric acid covers each carrier substance particle. Because of the large surface a full reaction of the boric compound with ammonia is possible. After the reaction the carrier is leached with HC1 and the remaining hBN is washed with water. A second reaction at temperatures exceeding 1500 °C with ammonia follows, resulting in hBN powders with 97% purity. BN crystallites are thin hexagonal platelets with a thickness of about 0.1-0.5 μm and a diameter up to 5 μm [10].

2.3.2. Boric Acid with Organic Nitrogen Compounds

The second important way to produce hBN is the reaction of boric acid or alkali-borates with organic nitrogen compounds (melamin, urea, dicyanamide, guanidine) in nitrogen atmosphere. These reactions are carried out at temperatures between 1000 °C and 2100 °C in N_2 atmosphere. Before final thermal treatment, the product can be washed with methanol or diluted acids in order to remove all non-reacted products. For removing oxygen impurities a thermal treatment at 1500 °C in inert N_2 or Ar atmosphere is used. BN with tBN is obtained which is characterized by partial or complete absence of three-dimensional order in the stacking of its atomic planes [11].

2.3.3. Various BN Synthesis Methods

- In carbothermal reactions BN is synthesized by reduction of boric acid or borates in nitrogen atmosphere at 1000-1500 °C. One example is the reduction of boric acid or borates with carbon. The precursors* are mixed intensively and after drying, the mixture is heated up to 1200-1500 °C in nitrogen atmosphere, remaining at maximum temperature for 60-600 min. To enhance the yield of BN, catalysts ($CaCO_3$, MnO_2) are sometimes added to the mixture. However, too high carbon content of the mixture leads to the formation of boron carbide.

- Reaction of amides, cyanides, cyanamides, and thiocyanates with boron compounds. $NaNH_2$ forms boron nitride with boric acid or sodium borates at 300-500 °C in ammonia atmosphere. At the end of the reaction the temperature is increased to 1000 °C for the decomposition of the remaining nitrogenous compounds. After washing with water, the BN powder is stabilized by annealing at 1800 °C in inert atmosphere. Cyanides (NaCN, KCN) react with boric acid at 800-1500 °C by forming BN. As a byproduct, CO gas and C are produced. The reaction of cyanamides (CaNCN) with boric acid is carried out at 1400-1750 °C in a 93% N_2 - 7% H_2 atmosphere. After reaction the product is washed with diluted HCl. Carbon, which is produced as a by-product during the reaction, is burned in air at 1000 °C.

- Preparation of B-N containing precursors with subsequent decomposition is also a suitable method to produce BN. The adduct BF_3-NH_3 is formed by reaction of BF_3

* A substance having an unknown structure from which another substance or component is created

with gaseous, liquid, or aqueous ammonia. From aqueous solutions the BF_3-NH_3 adducts can be precipitated by adding NaOH. After drying the precipitate it is heated up to 800 °C in inert atmosphere (N_2> H_2, or NH_3), and afterwards the BN is formed by pyrolytic reaction. After washing with hot water the h-BN is obtained.

- Fine and ultra-fine BN is used for lubricants and toners and can be produced by combustion of boron powder at 5500 °C in a nitrogen-plasma.

- Other ways for preparing BN are the reactions of calcium-boride (CaB_6) with additions of boric acid in nitrogen atmosphere at temperatures exceeding 1500 °C, or the synthesis from iron boride (FeB) with ammonia at 550 °C and subsequent annealing in ammonia at 1000 °C.

- Growing of h-BN crystals is possible in molten sodium at temperatures between 700 and 800 °C. Starting materials are boron and NaN_3 powders which are sealed in a stainless steel tube and heated up [12].

The O'Connor method [13] is the easiest and obvious method to obtain powder hBN. According to O'Connor the mixture of boron oxide (B_2O_3) and urea ($(NH_2)_2CO$) was heated under ammonia atmosphere at ca.1600 °C. Not requiring some expensive laboratory devices and poison gases (for example boron trichloride) and doing modifications at preparation of precursor step are the advantages of the O'Connor method.

According to Hubacek [14] the O'Connor method was performed in three steps. In the first step, an ammonia molecule has to approach the surface of a boric acid grain. Due to the redistribution of electron densities in the system, new bonds are created. HO-B-N-H monomer is formed and water is released as the consequence of the redistribution (Figure 2.3.2.1). In the second step, the monomer is stabilized by the trimerization (Figure 2.3.2.2).

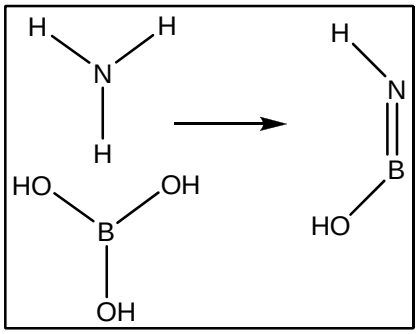

Fig. 2.3.2.1. Redistribution of HO-B-N-H

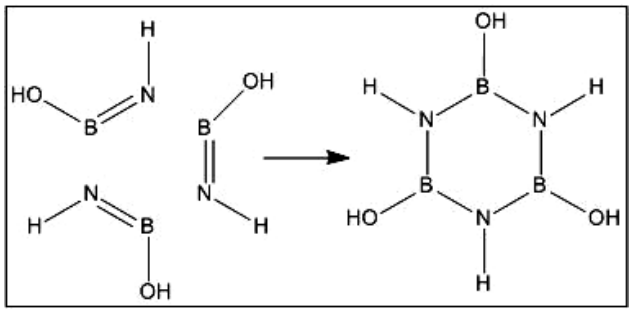

Fig.2.3.2.2. Trimerization of the monomer

In the last step we can get a macromolecule as shown in the Figure 2.3.2.3. The growth can continue till the macromolecule was reached (Figure 2.3.2.4).

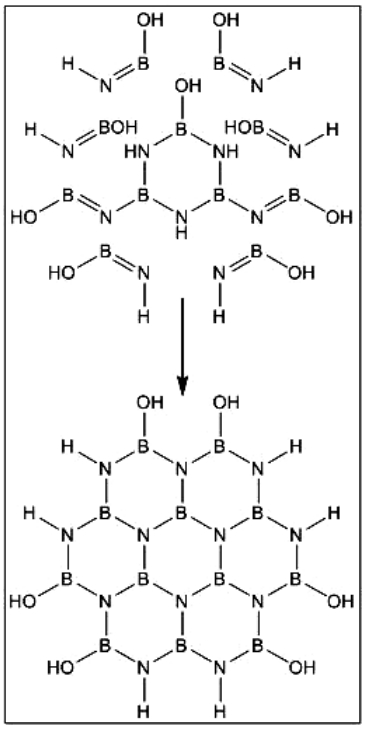

Fig. 2.3.2.3. Macromolecules of BN.

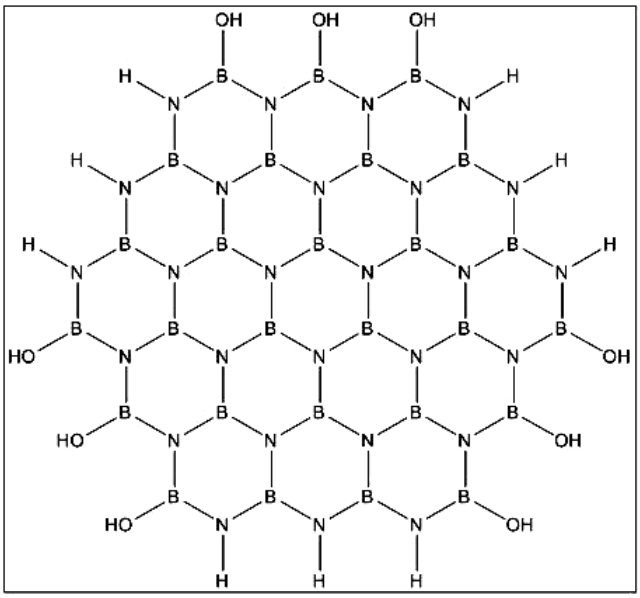

Fig. 2.3.2.4. Crystalline BN.

As shown in Figure 2.3.2.4, oxygen and hydrogen must not be understood as impurities [14], but they represent constitutional elements terminating the two-dimensional hBN macromolecules. Since the contents of these elements are inversely proportional to the circumference-to-area ratio, it can be assumed that the larger are BN crystals, the higher is the purity of BN. This relationship is actually the principle of the purification process, where BN is first crystallized by the thermal treatment in nitrogen gas, and oxygen impurities converted to boron oxide are washed out.

2.4. Synthesis of hBN Intercalation Compounds

Intercalation compound are formed by insertion of a guest chemical species -an intercalate- between layers in a host material. Because of its simple structure, high-quality pyrolytic graphite is the most often the preferred choice of host lattice for purposes of enhancing its electrical conductivity and chemical reactivity. Another simple lattice is pyrolytic BN, the crystal structure of which is closely related to that of graphite and being built of hexagonal layers of the same kind, but arrange so that atoms of one layer lie vertically above those in the layers below [15].

The synthesis of a graphite intercalation compound was first reported by Schaffäutl in 1841. However, the first systematic studies of these compounds began in the early 1930s with the introduction of X-Ray diffraction techniques for stage index determinations (Hoffman and Frenzel 1931, Schleede and Wellman 1932) and study of their physical properties began in the late 1940's [16].

After these developments, attempt of hBN intercalation compounds synthesis began due to structural similarities between hBN and graphite and Croft announced the first hBN intercalation compound [17]. hBN intercalation compound was prepared by heating a mixture of boric acid, urea and metal halides such as $FeCl_3$, $CuCl_2$, $AlCl_3$, etc. at high temperature in this study and it was found that an electronic interaction between boron nitride and intercalated substances appeared possible by means of

either electron transfer involving normally latent fourth sp^3 boron bonds, or coordination of intercalated cations by unshared pairs of nitrogen valence electrons.

Freeman and Larkindale found [18] approved Croft's pink colored hBN-intercalation compound ($FeCl_3$-hBN) finding. They were found evidence which confirmed that boron nitride forms intercalation compounds with a number of metal halides ($FeCl_3$, CuCl, Hg_2l_2, and $AsCl_3$). According to the Mössbauer spectrum of the iron (III) chloride compound indicated that the intercalated iron nucleus lied in a strong electrical-field gradient, and the d-electron population was reduced compared to that of high-spin iron (III) in free iron (III) chloride. They suggested that bonding, in these compounds, was caused by electron transfer from the intercalated molecule to the BN layers, and the intercalated molecules were isolated from each other.

However, Ohhashi and Shinjo [19] made an extensive study of this system and they did not confirm $FeCl_3$ intercalation in to hBN. In this study, Mössbauer spectra and X-ray diffraction measurements were made in order to clear up the ambiguity on the existence of intercalation compound of BN with $FeCl_3$. It was confirmed that the intercalation did not occur when the mixture of BN and $FeC1_3$ was heated in a sealed tube, independently of temperatures (280-450 °C) and durations (1-5 days). Under a certain condition, pink specimen was obtained which were the same as those produced by Freeman and Larkindale. However, these were proved to be the hydrolysis product, FeOCl, by the Mössbauer and X-Ray measurements.

Sakamoto and co-workers [20] reported that cesium and bromine intercalated in to hBN in 1986. They were found that only a few percent weight increase was observed by doping BN with Cs and Br_2. The electron paramagnetic resonance (EPR) signal was significantly modified by Cs doping, which is attributed to the reaction between the Cs atoms and spin resonance centers (N vacancies) in BN; no change in the EPR spectra was observed with Br_2 doping.. Though no evidence of systematic intercalation reaction in BN was observed in contrast to graphite host materials, intercalation islands induced by the introduction of Cs atoms were suggested by the transmission electron microscopy (TEM) observations.

Doll and co-workers announced K-hBN intercalation compound in 1989 [21]. They performed photoluminescence, photoexcitation, and transmission electron rnicroscopy measurements on boron nitride films grown by chemical vapor deposition and later reacted with potassium. After reaction, the potassium atoms were found to intercalate the BN host. Optic transitions with ~2.7 eV onsets were found to occur within the ~5eV BN band gap and was interpreted as Γ- point transitions between the K (4s) band and the BN (2p) bands. The absence of an appreciable shift in the E_{2g2} phonon frequency of the pristine and reacted films suggests that the charge transfer between the K and BN bands is very small.

Oku and co-workers [22] synthesized BN and carbon nanocapsules with Ag, Ge and SiC nanoparticles by the new chemical solution process. High-resolution electron microscopy, energy dispersive spectroscopy and X-ray diffraction showed the formation of silver and silver oxide nanoparticles encapsulated in boron nitride

nanocages, which were synthesized from mixtures of boric acid, urea and silver nitrate by reduction at 300–700°C in hydrogen gas. This work indicated that the boron nitride and carbon nanocage structures with electronic conductors, superhard materials, semiconductor nano- particles and nanowires can be synthesized by these new methods.

Besides experimental studies, theoretical studies of hBN intercalation have been taken much more attentions. Dai and Zhang [23] made a calculation for intercalation compounds of alkali metal and hBN, and compared with graphite in forming alkali metal intercalation compounds using the density functional theory (DFT) method. It was found that the difference in electron affinity between hBN and graphite, and the difference in electronic structures of their alkali metal intercalation compounds, show that it was difficult for hBN to be intercalated with metals.

In other study, Dai and Zhang [24] made ab initio self consistent field –molecular orbital (SCF-MO) calculations for intercalation compound Cu–hBN by using molecular cluster model. From the calculated interlayer distances, orbital interactions, atomic net charges and frontier orbital energy levels, the electronic structure and stability of Cu–hBN were discussed. It was confirmed by vibration analysis that this intercalation compound was merely a metastable structure.

Also, possibility of Li-hBN intercalation compound was calculated theoretically by Altıntaş [25]. It was found that the calculated formation energy of hBN was positive

and negative phonon vibrations were observed. As a result, Li-hBN intercalation compound was unstable structure and it may be possible at high pressure.

2.5 Synthesis of hBN with Presence of Metals

Two methods [26] were used to obtain metal- hBN samples. The first one consists of the chemical treatment of the mixtures of boric oxides, urea and metal salts, while the second one includes mechanical mixing and heating of hBN with metal powder. Both methods are considered to yield the same product.

Hubacek and co-workers obtained Cu-hBN composites by heating mixture of boric acid, urea and $Cu(NO_3)_2$. [26, 27]. They claimed that copper atoms inserted between hBN layers and a donor– acceptor interaction exists between copper electronic orbitals and p-electrons of adjacent BN facets, d- π interaction, similar to ferrocenes; therefore, the positive role of the copper was observed on the growth of the grain size of hBN.

In our previous study M-hBN (M: Cr, Mn, Fe, Co, Ni, Cu, Zn, and Ag) compounds were synthesized and crystallinity, grain size, and interlaying spacing of hBN was examined [28]. It was found that transition metal nitrates increased the crystallinity of hBN and arranged the layers of hBN at low temperature (1050°C), especially when the second row transition metal member silver was used, it provided the best result.

Cd-hBN compound was prepared [29] to understand much more the effect of the second row transition metals. The crystallization of Cd-hBN were tested with using different amount of cadmium(II) nitrate and similar results were obtained with previous study [28].

In an another study different hBN compounds were prepared with using metal carbonyls ($Cr(CO)_6$, $Mo(CO)_6$, and $W(CO)_6$) at different temperatures [30]. The crystallization degree and grain growth of hexagonal boron nitride was improved by various transition metal carbonyls at a relatively lower temperature (850°C).

Terrones and friends [31] mixed mechanically hBN and tantalum, and they obtained graphite like nanostructure. The particles were synthesized by arcing hBN and Ta in a nitrogen atmosphere. High resolution electron microscopy (HRTEM), electron energy loss spectroscopy (EELS) and XRD studies was used to study these materials, which contain B:N ratios of 1:1. The observations reveal interesting new information on the dynamics of metal cluster catalyzed nanostructure formation. The structures provided strong circumstantial evidence for the presence of B_2N_2 squares at the tips, in addition to B_3N_3 hexagons in the main body of the tubes.

Benko and co-workers [32] applied mechanical mixture of hBN, and Al so increased the mechanical strength of the hBN. hBN and Al were mechanically mixed in ethyl alcohol and then sintered by high pressure hot pressing. The structure of sintered material before and after annealing was studied using transmission electron

microscope. From the microscopic observations it was concluded that the samples prepared both before and after annealing exhibit a compact structure. Hardness of the samples increases twice after annealing. Thermal treatment also results in an increase in mechanical strength of the sintered BN-Al system.

In other study Kondo and co-workers [33] investigated the structural and hydrogen absorption properties for Ti mechanically milled with hBN for various milling times and compared the results with those obtained with graphite. The hydrogen absorption kinetics for both Ti milled with hBN and Ti milled with graphite was improved with increasing milling time although a longer time was required with hBN than with graphite.

3. EXPERIMENTAL PART

3.1. Materials

Boron oxide (Fluka, 97%), urea (Fluka, 99%), potassium nitrate (Fluka, 98%) calcium nitrate (Fluka, 99%), scandium(III) nitrate (Aldrich, 99.9%), titanium(IV) nitrate (Aldrich, 99.9%), vanadium(IV) oxide (Aldrich, 99.9%), iron(III) bromide (Aldrich, 98%), iron(III) fluoride (Aldrich, 99%), iron(III) nitrate (Aldrich, 99.99%), iron(III) sulfate (Aldrich, 97%), methanol (Fluka, 99.9%), and hydrochloric acid (Merck, 37%) obtained commercially were used without any purification.

4.2. Synthesis of hBN Samples

The modified O'Connor method was used to synthesize and hBN compounds. The mixture of 2 g of boron oxide was mixed with 4 g of urea pulverized in ball-mill grinder. After that, 0.04 g of metal salt (KNO_3, $Ca(NO_3)_2$, $Sc(NO_3)_3$, $Ti(NO_3)_4$, VO_2, $FeBr_3$, FeF_3, $Fe(NO_3)_3$, and $Fe_2(SO_4)_3$) was added on to this mixture and ground in mortar. Then it was pre-heated at 200°C for 2 hours in furnace and precursor was obtained. Finally, the obtained precursor was re-pulverized in mortar and heated in tube furnace under ammonia atmosphere (120 mL/min) at different temperatures (for each precursor 1050, 1250 and 1450 °C) under open atmosphere for 2 hours.

The product was boiled in 10% HCl solution then leached in methanol and dried in an oven at 100°C. The obtained powder was pressed by 100 bar at room temperature.

3.3. Preparation of hBN Samples

3.3.1. Ball-Mill Grinder

A mixture of boron oxide, urea and metal salts were ground in a ball mill rotated on a roll mixer (Pascall Engineering, 1600-VS-A roll mixer) at medium speed for 4 hours to obtain homogenous mixture. The resultant powder was sieved and 149 μm mixture particles were collected.

Fig. 3.3.1.1. Pascall Engineering, 1600-VS-A roll mixer)

Fig. 3.3.1.2. Alumina Jar

3.3.2. Camera Furnace

The precursor preparation was performed with Proterm PLF 140/5 (average heating speed: 10°C/min) camera furnace at 200°C under open atmosphere for 2 hours.

Fig. 3.3.2. Proterm PLF 140/5

3.3.3. Tube Furnace

Final heating process was done with Proterm PTF 15/75/450 tube furnace (average heating speed: 16°C/min) at different temperatures (1050°C, 1250°C, and 1450°C) under ammonia atmosphere (ammonia flowrate adjusted as 120mL/min. by using flowmeter) under open atmosphere for 2 hours.

Fig. 3.3.3. Proterm PTF 15/75/450

3.4. Characterization of hBN Samples

3.4.1. FT-IR Spectroscopy

FTIR spectra of hBN samples in KBr pellets were recorded on a Jasco 430 Spectrometer in the range of 400 - 4000 cm^{-1}. To compare IR spectra of the samples all KBr pellets which composed of 0.0002 g of sample and 0.0198 g of KBr, were prepared in the same weight.

Fig. 3.4.1. Jasco 430 Spectrometer.

3.4.2. XRD Measurement

XRD characterization of hBN samples was done with Rigaku DMAX 2000/PC and Rigaku Multiflex diffractometer using CuK_{α} radiation. (40 kV / 30 mA, Goniometer: MultiFlex+ goniometer (with a shutter), Div Slit: ½ deg., Sct Slit: ½ deg., Rec Slit: 0.15 mm, Scan Speed: 3 deg / min., Attachment: Standard sample holder)

Fig. 3.4.2. Rigaku Multiflex.

3.4.3. SEM Analysis

SEM photographs were taken Zeiss Evo 50 and Jeol JSM 6390LV and the samples used for SEM were coated with carbon.

Fig.3.4.3. Jeol JSM 6390LV

3.5. Sample Calculations

3.5.1. Calculation of Lattice Parameters

Lattice parameters of the samples were calculated by using Equation 1 for hexagonal systems.

$$\frac{1}{d^2} = \frac{4}{3} \times \left[\frac{h^2 + hk + k^2}{a^2} \right] + \frac{l^2}{c^2} \qquad (1)$$

d: Interlayer spacing

h, k ,l : Related Miller indeces

a, c: Lattice parameter

Calculation of "a" parameter of hBN:

For 110 peak of hBN d is 1.2521 Å

$$\frac{1}{(1.2521)^2} = \frac{4}{3} \times \frac{1^2 + 1 \times 1 + 1^2}{a^2} + \frac{0^2}{c^2}$$

a = 2.504 Å

Calculation of "c" parameter of hBN:

For 002 peak of hBN d is 3.3280 Å

$$\frac{1}{(3.3280)^2} = \frac{4}{3} \times \frac{0^2 + 0 \times 0 + 0^2}{a^2} + \frac{2^2}{c^2}$$

a = 6.656 Å

3.5.2. Calculation of Grain Size

Scherrer equation (Equation 2) relates the peak breadth of a specific phase of a material to the mean crystallite size of that material.

$$L = \frac{K\lambda}{\beta \cos\theta} \qquad (2)$$

β is difference of the width of the peak at half maximum intensity of a specific phase (hkl) in radians of reference material and sample.

K is a constant that varies with the method of taking the breadth (0.9)

λ is the wavelength of incident X-Rays (CuK_α=1.504 Å).

2θ is the center angle of the peak of sample

L is the crystallite size

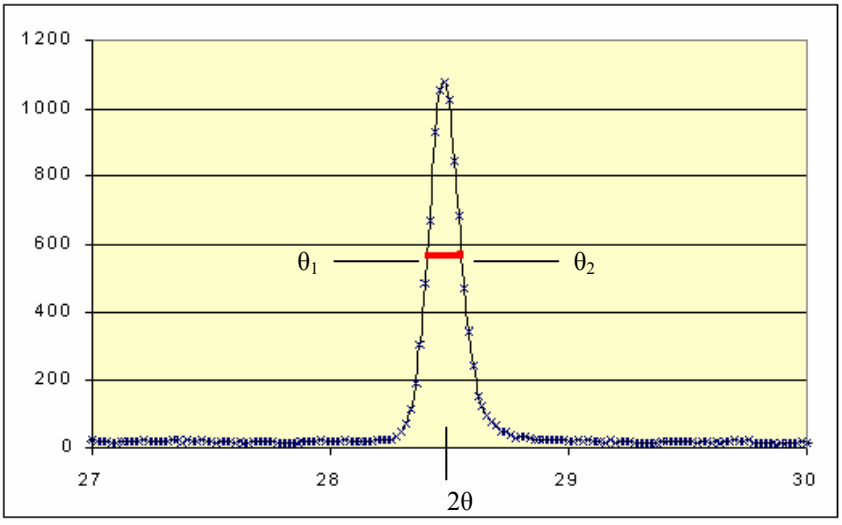

$\theta_{Ref.1}$ (26.64°) and $\theta_{Ref.2}$ (26.97°)are angels of the width of the peak at half maximum intensity in radians of reference material. $\theta_{Samp.1}$ (25.94°) and $\theta_{Samp.2}$(26.97°) are angels of the width of the peak at half maximum intensity in radians of sample and 2θ is 26.54° for sample.

$$\beta = \sqrt{((26.97\text{-}26.64)\times\frac{\pi}{180})^2 - ((26.88\text{-}25.94)\times\frac{\pi}{180}))^2}$$

$$\beta = 0.02$$

$$L = \frac{K\lambda}{\beta\cos\theta} = \frac{0.9\times1.504}{0.02\times(\cos13.27\times\frac{\pi}{180})}$$

$$L = 92.4\ \text{Å}$$

$$L = 9.24\text{nm}$$

4. RESULTS

4.1. Characterization of hBN Samples in the Presence of K and Ca

4.1.1 FTIR Spectroscopy of hBN Samples

The FTIR measurement was performed to examine the types of chemical bonds of the obtained hBN samples and there are several studies in the literature characterizing the formation and structure of hBN by IR spectroscopy [34, 35, 36]. FTIR spectra of hBN samples prepared at 1050, 1250 and 1450°C are given in Figure 4.1.1.1 and 4.1.1.2 (*see Appendix A for all FTIR spectra of hBN samples*). Two strong characteristic bands locate at ~1390 cm^{-1} and ~780 cm^{-1} which were attributed to in-plane vibrations and out-of-plane bending vibrations of hBN, respectively [34, 36, 37]. The broad absorption band near 3200 cm^{-1}, 3400 cm^{-1} and a shoulder peak near ~1050 cm^{-1} can be ascribed to the N-H, –BO–H and B-O stretching vibrations of the terminal –OH, -NH and –B-OH groups that always appears when the boric acid or boron oxide and urea systems were applied [38, 39, 40]. It can be easily understood that as the temperature increases, the intensity of the N-H, –BO–H and B-O stretching decreases or disappears.

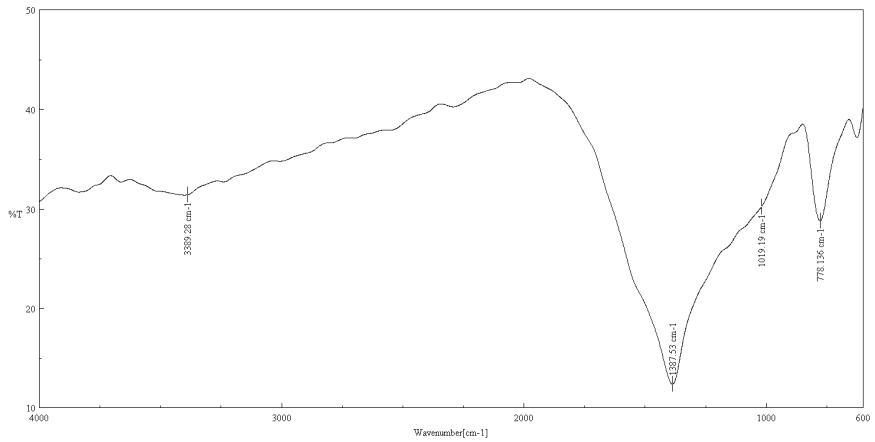

Fig. 4.1.1.1. Typical FTIR spectrum hBN in presence of KNO_3.

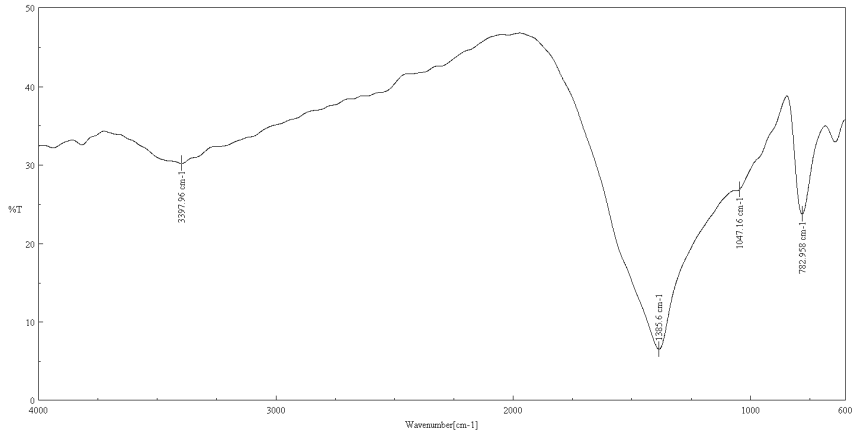

Fig. 4.1.1.2. Typical FTIR spectrum of hBN in presence of $Ca(NO_3)_2$.

4.1.2 XRD Pattern of hBN Samples

The composition and crystallinity of BN samples were examined by XRD and the results were compared with standard hBN (ICDD card no: 34 - 421). In all diffractograms, Fig. 4.1.2.1 and Figure 4.1.2.2 (*see Appendix B for all XRD patterns of hBN samples*), the main peaks of hBN (002, 10*, 004, 110, and 112) are observed.

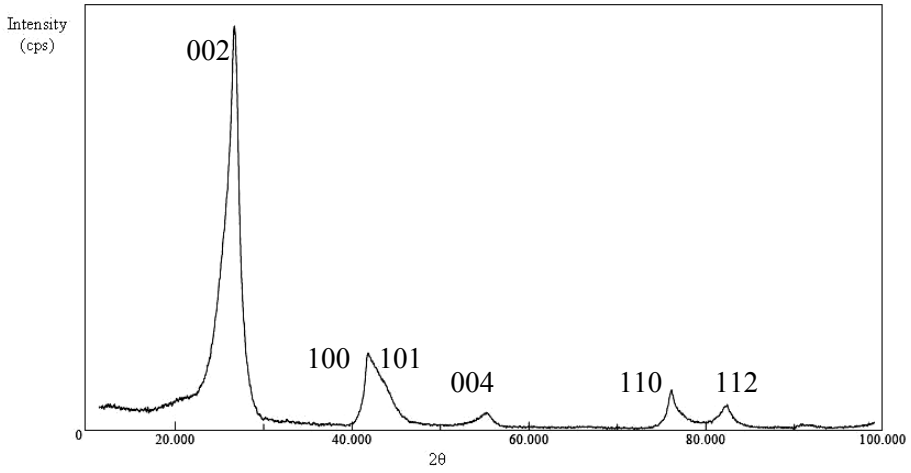

Fig. 4.1.2.1 Typical XRD patterns of hBN in presence of KNO_3.

* Not separated 100 and 101 peaks of hBN.

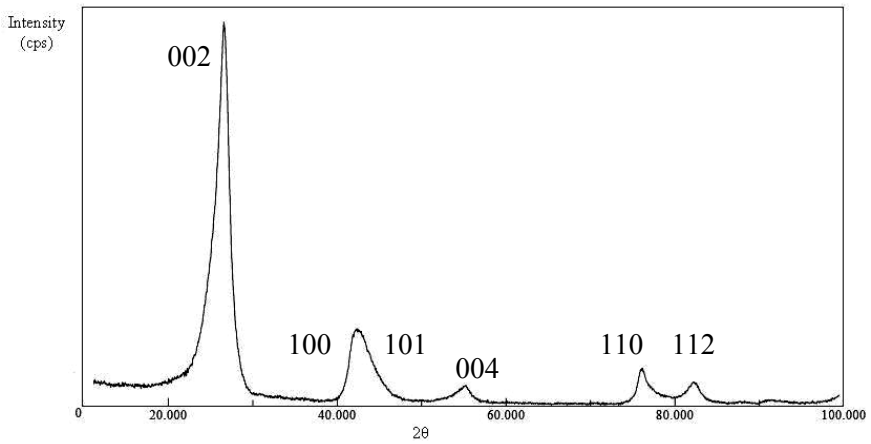

Fig. 4.1.2.2 Typical XRD patterns of hBN in presence of $Ca(NO_3)_2$.

The lattice constant of BN samples calculated from the XRD patterns (Table 4.1.2.1) are well consistent with the literature values (ICDD card no: 34 – 421, a= 2.5044 Å, c= 6.6562 Å, d= 3.3281 Å).

Table 4.1.2.1 Calculated lattice constant of hBN the Presence of K and Ca.

Synthesis Temperature	**Used Salts** / **Lattice parameters**	**KNO_3**	**$Ca(NO_3)_2$**
1050 ºC	a (Å)	2.498	2.500
	c (Å)	6.668	6.702
	d (Å)	3.334	3.351
1250 ºC	a (Å)	2.504	2.502
	c (Å)	6.702	6.686
	d (Å)	3.351	3.343
1450 ºC	a (Å)	2.504	2.502
	c (Å)	6.712	6.706
	d (Å)	3.356	3.353

The broadening nature of the XRD peaks indicates that the particle size of the samples is within nanometer scale [36, 41]. By using the Scherrer equation the grain sizes of hBN are calculated (Table 4.1.2.2.).

Table 4.1.2.2. Grain size of BN samples the Presence of K and Ca.

Used salt for preparing hBN	Grain size (nm) at 1050 ºC	Grain size (nm) at 1250 ºC	Grain size (nm) at 1450 ºC
KNO_3	4.72	10.58	11.08
$Ca(NO_3)_2$	4.38	7.84	10.93

4.1.3 SEM Analysis of hBN Samples

SEM images, Fig. 4.1.3.1 and 4.1.1.2, (*see Appendix C for all SEM images of hBN samples*) indicate that irregular grained powder with fractures and the particles are jagged shapes. The fractures for these samples are intergranular and cracks nucleate at BN boundaries because of the low bonding strength of BN grains.

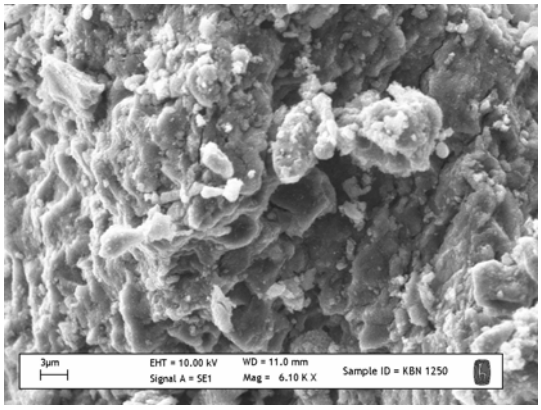

Fig. 4.1.3.1

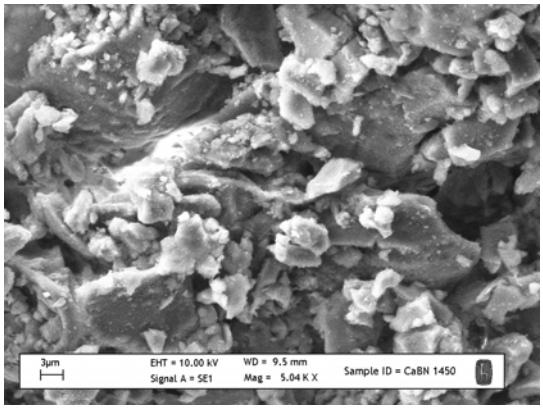

Fig. 4.1.3.2.

Fig. 4.1.3.1 Sample SEM image of hBN in presence of KNO_3.

Fig. 4.1.3.2. Sample SEM image of hBN in presence of $Ca(NO_3)_2$.

4.2. Characterization of hBN Samples in the Presence of Sc, Ti and V

4.2.1 FTIR Spectroscopy of hBN Samples

FTIR spectra of hBN samples prepared at 1050, 1250 and 1450°C is presented in Figure 4.2.1.1, 4.2.1.2 and 4.2.1.3 (*see Appendix A for all FTIR spectra of hBN samples*). BN formation is confirmed since the in-plane and out-of- plane vibrations of hBN are observed at ~1390 cm^{-1} and ~780 cm^{-1}. Two broad absorption band near 3200 cm^{-1} and 3400 cm^{-1} can be ascribed to the N-H, –BO–H stretching vibrations of the terminal B–OH, -NH. A shoulder peak near ~1050 cm^{-1} can be attributed to B-O stretching vibration.

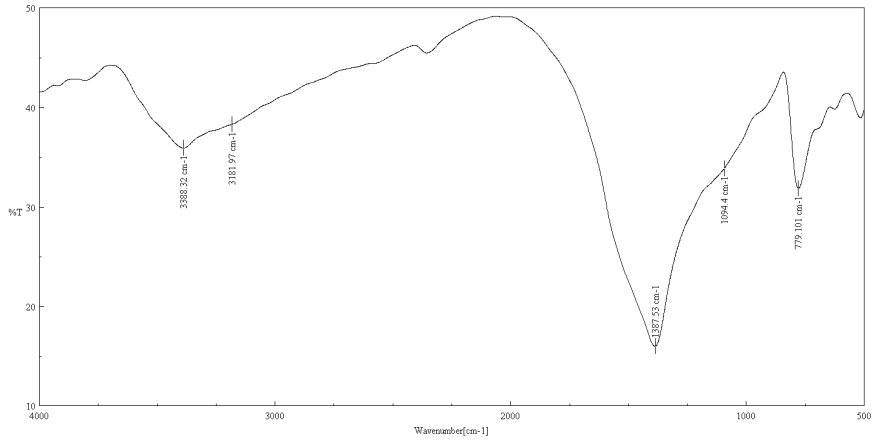

Fig. 4.2.1.1. Typical FTIR spectrum of hBN in presence of $Sc(NO_3)_3$.

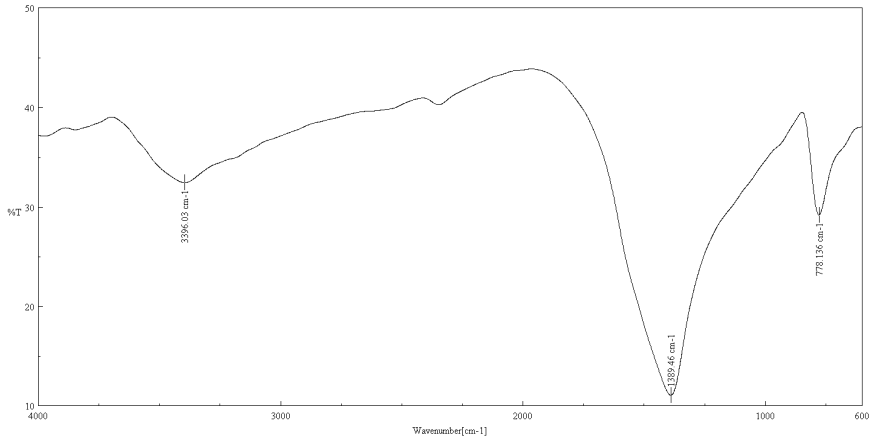

Fig. 4.2.1.2. Typical FTIR spectrum of hBN in presence of $Ti(NO_3)_4$.

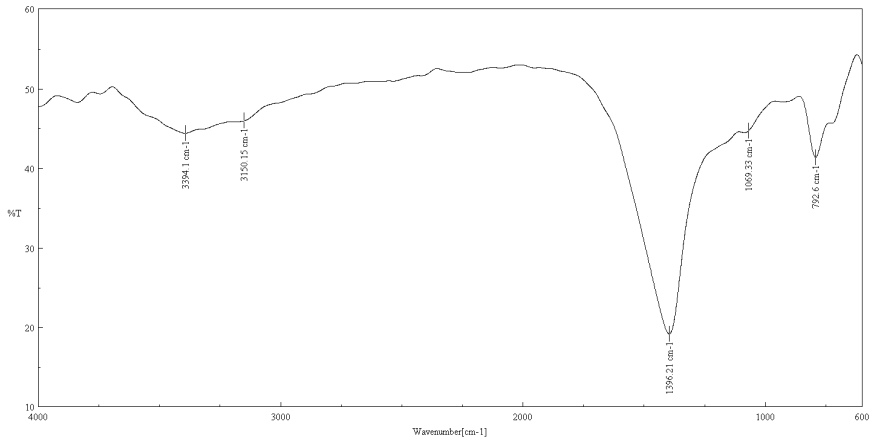

Fig. 4.2.1.3. Typical FTIR spectrum of hBN in presence of VO_2.

4.2.2 XRD Pattern of hBN Samples

Typical XRD patterns of hBN samples are shown in Figure 4.2.2.1, Figure 4.2.2.2, and Figure 4.2.2.3 (*see Appendix B for all XRD patterns of hBN samples*). All the peaks (002, 10, 004, 110, and 112) can be assigned to hBN. The lattice constant (Table 4.2.2.1.) are very close to reported values of hBN (ICDD card no: 34 – 421, a= 2.5044 Å, c= 6.6562 Å, d= 3.3281 Å).

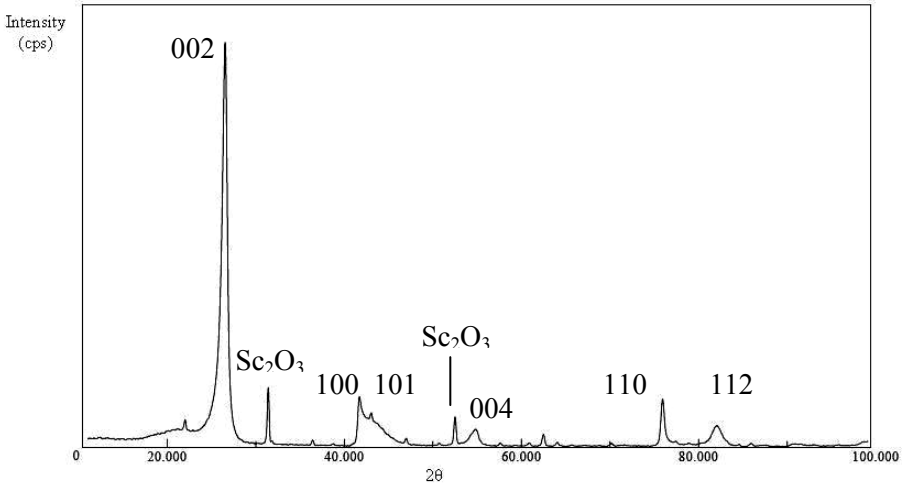

Fig. 4.2.2.1 Typical XRD patterns of hBN in presence of $Sc(NO_3)_3$.

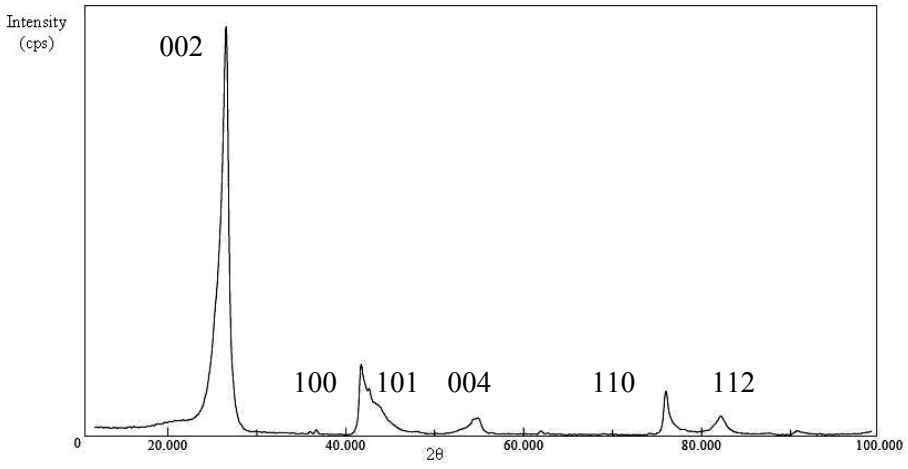

Fig. 4.2.2.2 Typical XRD patterns of hBN in presence of $Ti(NO_3)_4$.

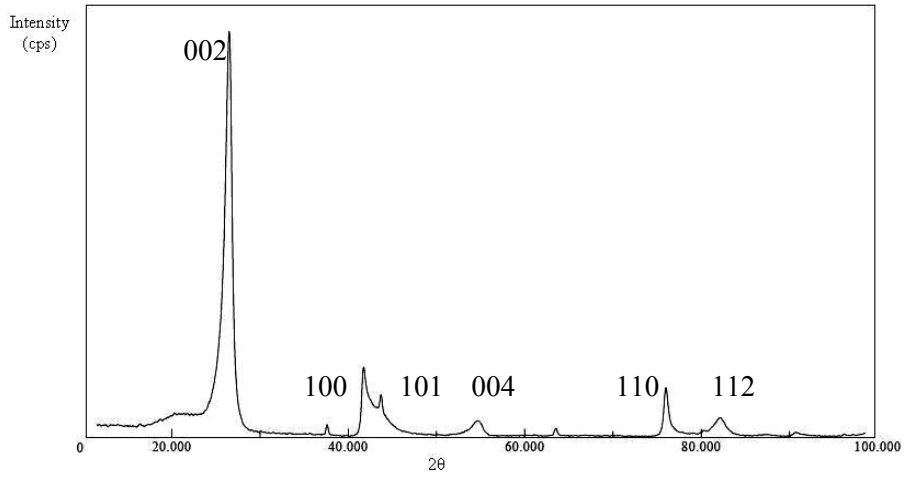

Fig. 4.2.2.3. Typical XRD patterns of hBN in presence of VO_2.

Table 4.2.2.1 Calculated lattice constant of hBN in the Presence of Sc, Ti and V.

Synthesis Temperature	**Used Salts** / **Lattice Parameters**	**$Sc(NO_3)_3$**	**$Ti(NO_3)_4$**	**VO_2**
1050 ºC	a (Å)	2.498	2.500	2.496
	c (Å)	6.696	6.682	6.696
	d (Å)	3.348	3.341	3.348
1250 ºC	a (Å)	2.502	2.502	2.502
	c (Å)	6.686	6.692	6.706
	d (Å)	3.343	3.346	3.353
1450 ºC	a (Å)	2.504	2.502	2.502
	c (Å)	6.712	6.706	6.712
	d (Å)	3.356	3.353	3.356

The broadening of XRD peaks suggest that grain size of hBN samples are in nanometer scale according to Scherrer equation.

Table 4.2.2.2. Grain size of BN samples in the Presence of Sc, Ti and V.

Used salt for preparing hBN	**Grain size (nm) at 1050 ºC**	**Grain size (nm) at 1250 ºC**	**Grain size (nm) at 1450 ºC**
$Sc(NO_3)_3$	3.70	6.98	13.29
$Ti(NO_3)_4$	5.65	8.55	8.74
VO_2	4.46	7.55	9.24

4.2.3 SEM Analysis of hBN Samples

SEM images (Figure 4.2.3.1, Figure 4.2.3.2, and Figure 4.2.3.3) of hBN (*see Appendix C for all SEM images of hBN samples*) indicate that the grains of hBN samples have irregular shape and order. In addition, in some images indicate that the surfaces of hBN are coated by amorphous materials.

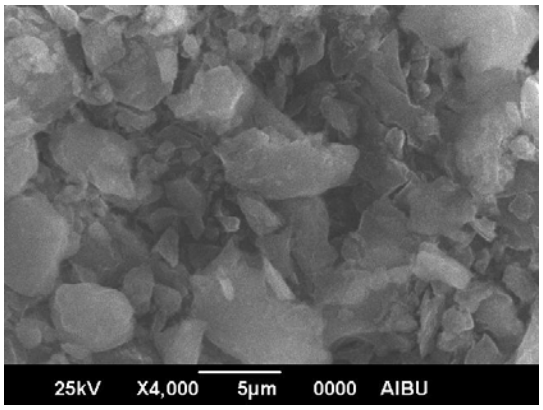

Fig. 4.2.3.1 Sample SEM image of hBN in presence of $Sc(NO_3)_3$.

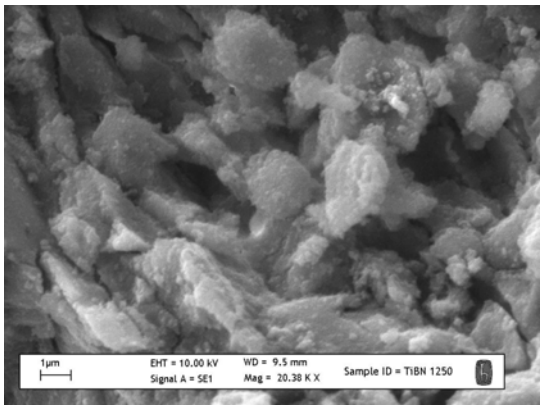

Fig. 4.2.3.2 Sample SEM image of hBN in presence of $Ti(NO_3)_4$.

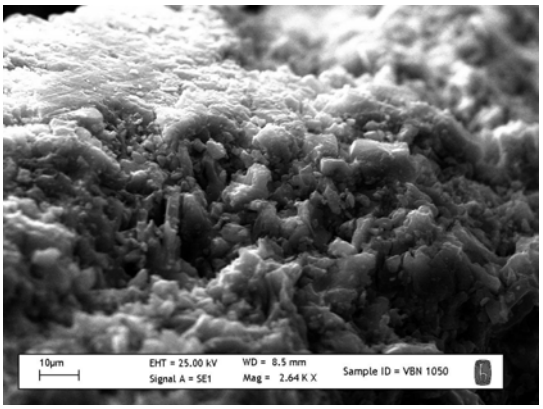

Fig. 4.2.3.3 Sample SEM image of hBN in presence of VO_2.

4.3. Characterization of hBN Samples in the Presence of Different Iron(III) Salts

4.3.1 FTIR Spectroscopy of hBN Samples

FTIR spectra of hBN samples prepared at 1050, 1250 and 1450°C are presented in Figure 4.3.1.1 (*see Appendix A for all FTIR spectra of hBN samples*). Two strong characteristic peaks located at ~1390 cm^{-1} and ~780 cm^{-1} are identified with in-plane and out-of- plane vibrations of hBN. The broad bands near 3400 cm^{-1} can be attributed to –BO–H bonds from terminal group of BN and the peak at 3200cm^{-1} can be assigned to N-H bonds located the end group of hBN. A shoulder peak near ~1050 cm^{-1} can be attributed to B-O stretching vibration.

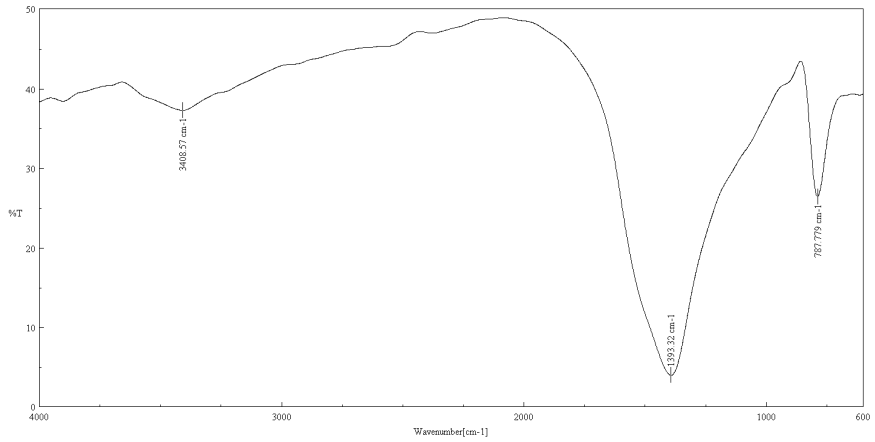

Fig. 4.3.1.1. Typical FTIR spectrum of hBN in presence of iron salts.

4.3.2 XRD Pattern of hBN Samples

Fig 4.3.2.1 indicates that typical XRD pattern of hBN samples (*see Appendix B for all XRD patterns of hBN samples*). All of the peaks can be indexed as hBN (002), (10), (004), (110), and (112) phases.

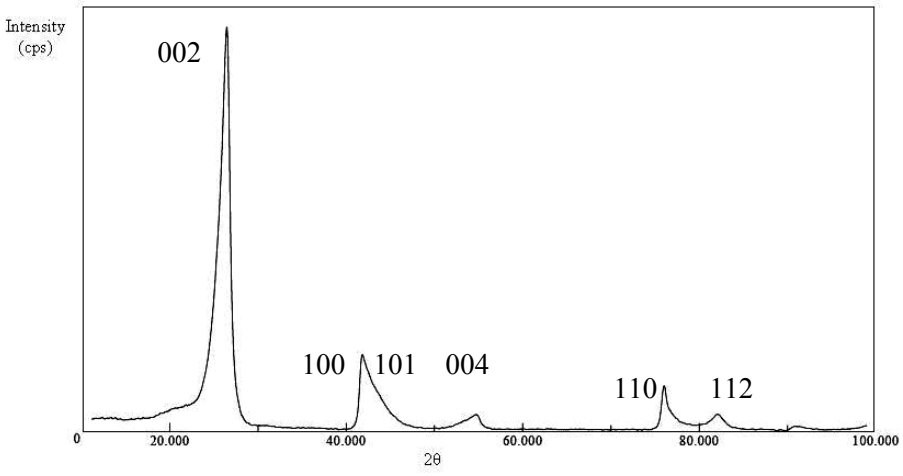

Fig. 4.3.2.1. Typical XRD patterns of hBN in presence of iron salts.

The lattice constants are calculated from XRD patterns and presented in Table 4.3.2.1.

Table 4.3.2.1. Calculated lattice constant of hBN in the Presence of Different Iron(III) Salts.

Synthesis Temperature	**Used Salts** / **Lattice Parameters**	**$FeBr_3$**	**FeF_3**	**$Fe(NO_3)_3$**	**$Fe_2(SO_4)_3$**
1050 ºC	a (Å)	2.498	2.502	2.498	2.500
	c (Å)	6.696	6.692	6.686	6.720
	d (Å)	3.348	3.346	3.343	3.360
1250 ºC	a (Å)	2.502	2.502	2.502	2.502
	c (Å)	6.706	6.686	6.692	6.696
	d (Å)	3.353	3.343	3.346	3.348
1450 ºC	a (Å)	2.502	2.502	2.500	2.502
	c (Å)	6.736	6.706	6.706	6.736
	d (Å)	3.368	3.353	3.353	3.368

The broadening in the XRD peaks show that the particle size of the samples is within nanometer scale. The grain size of hBN are calculated (Table 4.1.2.2.) by using the Scherrer equation.

Table 4.3.2.2. Grain size of BN samples in the Presence of Different Iron(III) Salts.

Used salt for preparing hBN	**Grain size (nm) at 1050 ºC**	**Grain size (nm) at 1250 ºC**	**Grain size (nm) at 1450 ºC**
$FeBr_3$	3.39	7.76	6.15
FeF_3	6.93	8.42	5.91
$Fe_2(SO_4)_3$	5.99	7.97	5.95
$Fe(NO_3)_3$	4.24	7.36	4.27

4.3.3 SEM Analysis of hBN Samples

SEM images of BN samples (*see Appendix C for all SEM images of hBN samples*) show a regularly grained powder (Figure 4.3.3.1) and some of them appear flaky and have an irregular shape (Figure 4.3.3.2). However, in some SEM images indicate that the surfaces of hBN were coated by amorphous materials (Figure 4.3.3.3). In some images, large pores are detected (Figure 4.3.3.4). This porous structure may be resulted from the escape of ammonia from BN lattice as proposed by Perdigon-Melon and Yoo [42, 43].

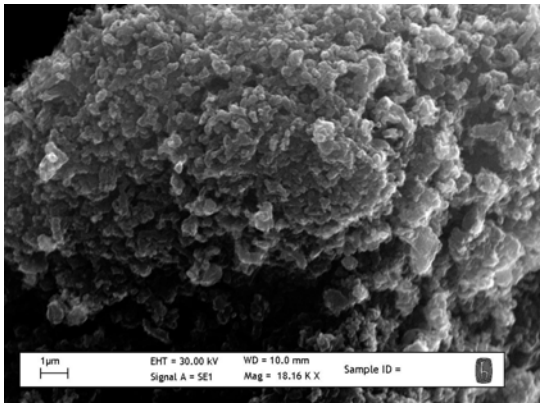

Fig. 4.3.3.1

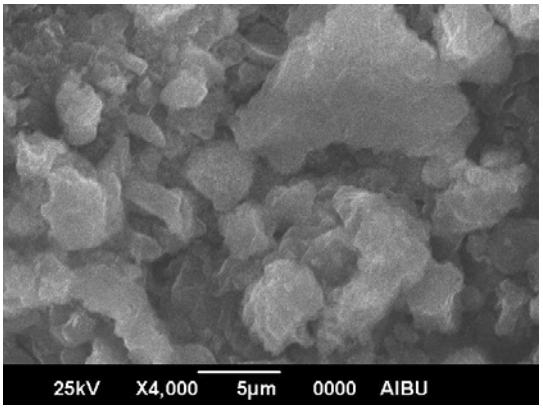

Fig. 4.3.3.2

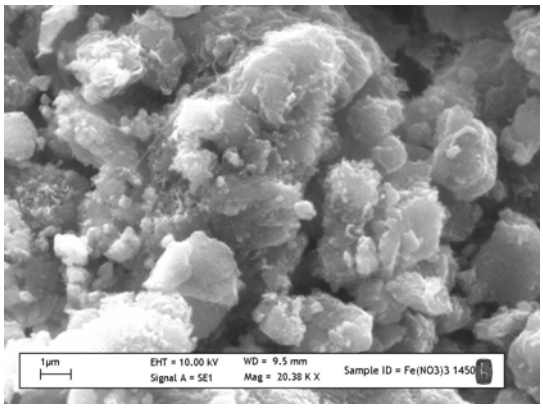

Fig. 4.3.3.3

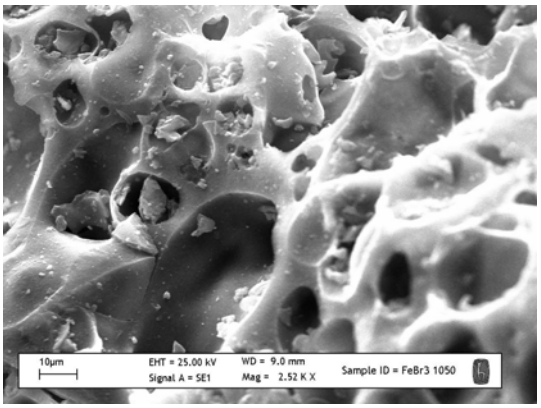

Fig. 4.3.3.4

Fig. 4.3.3.1 Sample SEM image of hBN in presence of $Fe_2(SO_4)_3$.

Fig. 4.3.3.2 Sample SEM image of hBN in presence of FeF_3.

Fig. 4.3.3.3 Sample SEM image of hBN in presence $Fe(NO_3)_3$.

Fig. 4.3.3.4 Sample SEM image of hBN in presence $Fe(NO_3)_3.FeF_3$.

5. DISCUSSION

All hBN samples were synthesized using the modified O'Connor method with the presence of various metal salts. The modified O'Connor method was chosen to synthesize of boron nitride for this study because it is the simplest method to form hBN and worked successfully in previous studies [28, 29, 30]. Not requiring some expensive laboratory devices and poison gases and doing modifications at preparation of precursor step are the advantages of this method.

All FTIR measurements confirm the formation of hBN and two strong characteristic peaks locate at ~1390 cm^{-1} and ~780 cm^{-1} which were attributed to in-plane vibrations and out-of-plane bending vibrations of hBN, respectively. In addition, other peaks near ~3400 cm^{-1}, ~3200 cm^{-1}, and ~1050 cm^{-1}, were ascribed to the –BO–H, N-H, and B-O stretching vibrations of the terminal –OH, -NH and –B-OH groups that always appears when the boric acid or boron oxide and urea systems is applied. –BO–H, and N-H groups must not be understood as impurities [14] but they represent constitutional elements terminating the two-dimensional hBN macromolecules. Since the contents of these elements are inversely proportional to the circumference-to-area ratio, it can be assumed that the larger are BN crystals, the higher is the purity of BN. This relationship is actually the principle of the purification process, where BN is first crystallized by the thermal treatment in

ammonia gas, and oxygen impurities converted to boron oxide are washed out. Also, it was understood that as the temperature increases, the intensity of these groups decreases or disappears (Fig.5.1). Also, the peak at near ~1050 cm^{-1} can be assigned as cBN [44] but there is no evidence for formation of cBN in XRD pattern.

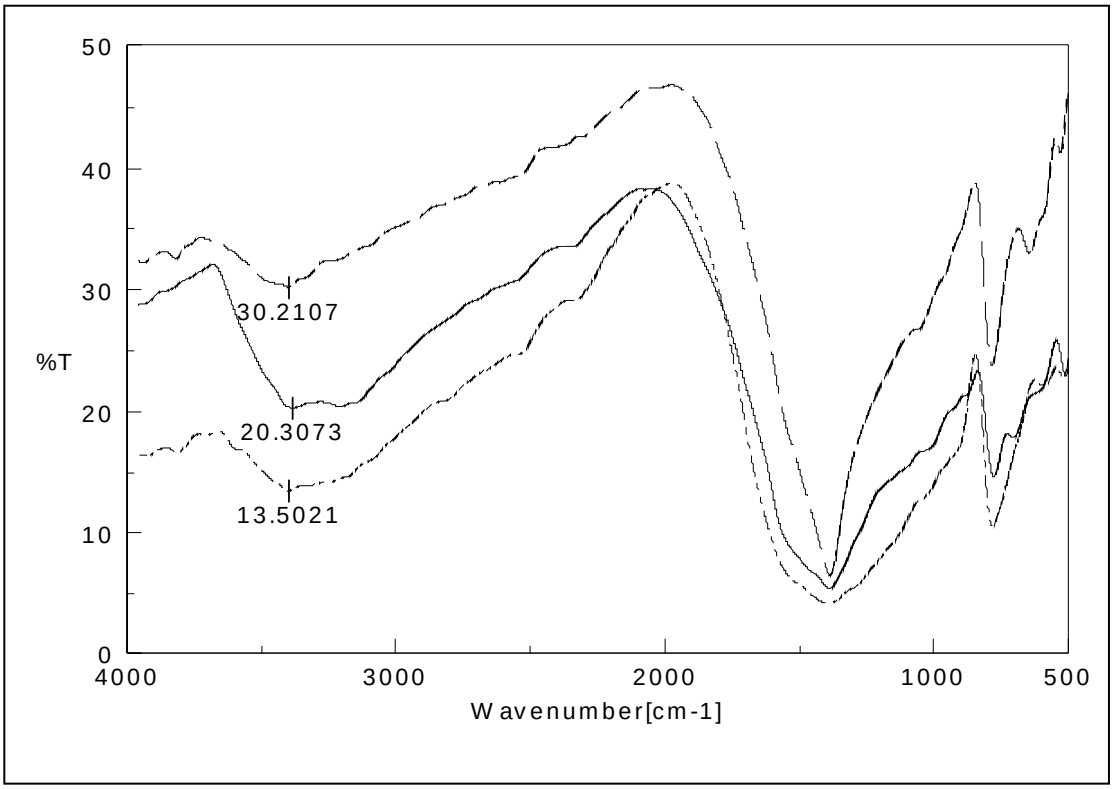

Fig. 5.1. Decreasing of intensity of N-H, –BO–H stretching with increasing temperature.

-.-.-. %T value at 1050°C: 13.5021

_____ %T value at 1250°C: 20.3073

- - - - - %T value at 1450°C: 30.2107

In our previous study [28] the presence of the metals was determined by X-Ray fluorescence. In this study the presence of the metals was observed by Energy Dispersive X-Ray Spectroscopy (EDX). Although EDX analysis (*see Appendix D for EDX results*) indicate that the presence of the metals, there is no intercalation between hBN and metals according to FTIR spectra. Because metal intercalation is weaken the out-of-plane B-N vibration (780 cm^{-1}). In all FTIR spectrum of hBN the out-of-plane B-N vibration can be easily observed, like Hubacek's work [14]. In this work B-C-N system was synthesized and three atoms occupy the same planar macromolecules. The number of modes must increase due to additional chemical bonds such as C-N, and B-C. Increasing the carbon content in the sample led to decreasing absorption due to the out-of-plane mode of hBN, which finally disappeared. Moreover, in previous study [29] the ratio of B_3N_3 units to cadmium atoms was calculated as 5000:1 on molar basis. This value points out that metal intercalation to hBN by modified O'Connor synthesis should be questionable.

In all diffractograms the well-known peaks of hBN (002, 10, 004, 110, and 112) were observed in XRD. According to previous studies [42, 45] the obtained products could be accepted as turbostratic because of inseparable (100) and (101) XRD peaks of hBN (Fig. 5.2). However, recent works [36, 41, 46] emphasized that absence of 10 peaks indicated the formation of nano crystalline substance. It is known that both usage of ammonia and transition metals permit lowering the formation temperature of hBN; the transition metals behave as catalyst [40, 45, 47] while ammonia acts as nitriding agent for metals and alloys at low temperature [14, 34, 48].

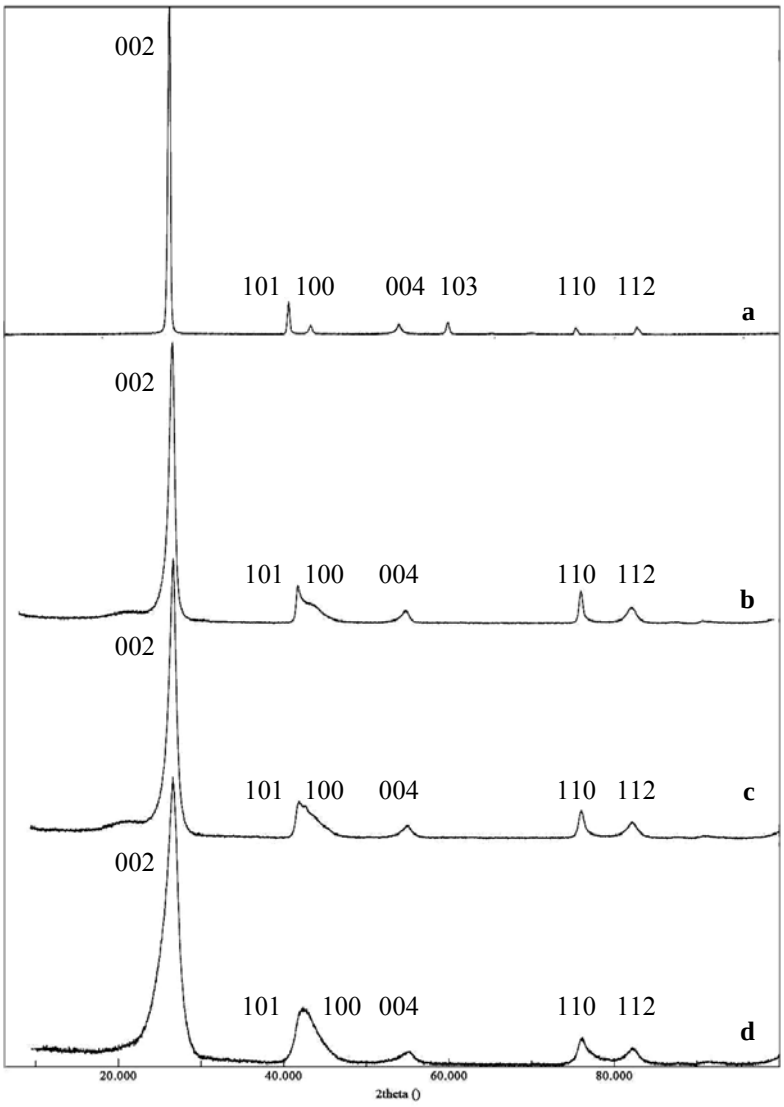

Fig. 5.2 Comparison of XRD pattern of hBN prepared at different temperatures with original hBN.

a. Original hBN

b. XRD pattern of hBN at 1450ºC in presence of $FeBr_3$

c. XRD pattern of hBN at 1250ºC in presence of $FeBr_3$

d. XRD pattern of hBN at 1050ºC in presence of $FeBr_3$

Moreover, the internal stress decreases in the presence of the transition metals because of the reduction of the content of cBN phase and increase of hBN phase [49] so BN is more easily formed than cBN at the low temperatures (Fig. 5.2), and hBN are the dominant phases in the samples [50]. Also, the broadening nature of the XRD peaks indicates that the particle size of the samples is within nanometer scale [41, 46]. According to Scherrer equation the grain size of hBN was calculated and it was found that there was an increase in the grain size with raising temperature (Fig. 5.3).

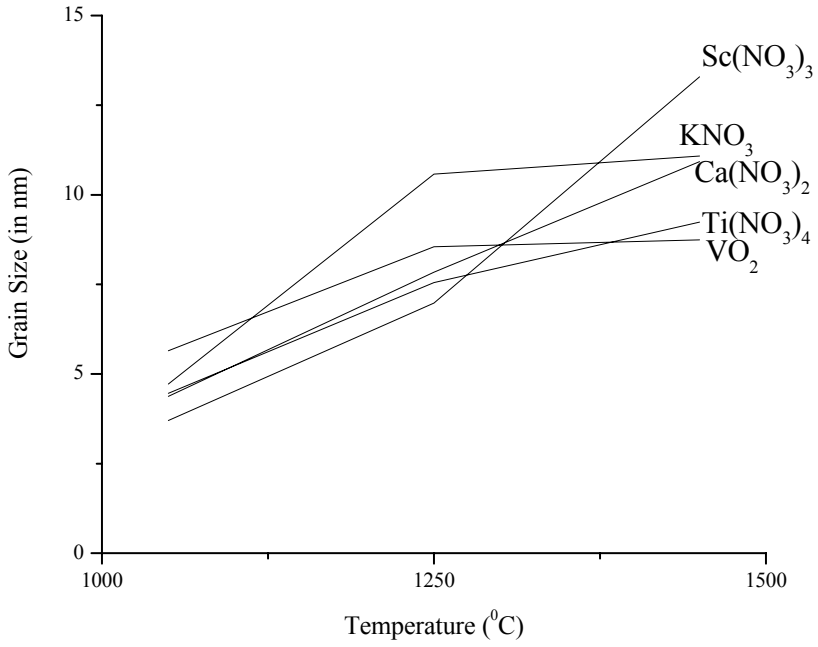

Fig. 5.3. Grain size of hBN vs temperature when representative and transition metals used.

However, when iron salts were used, there is no regularity in grain size of hBN. Even though, the grain size of hBN became smaller with increasing temperature (Fig 5.4).

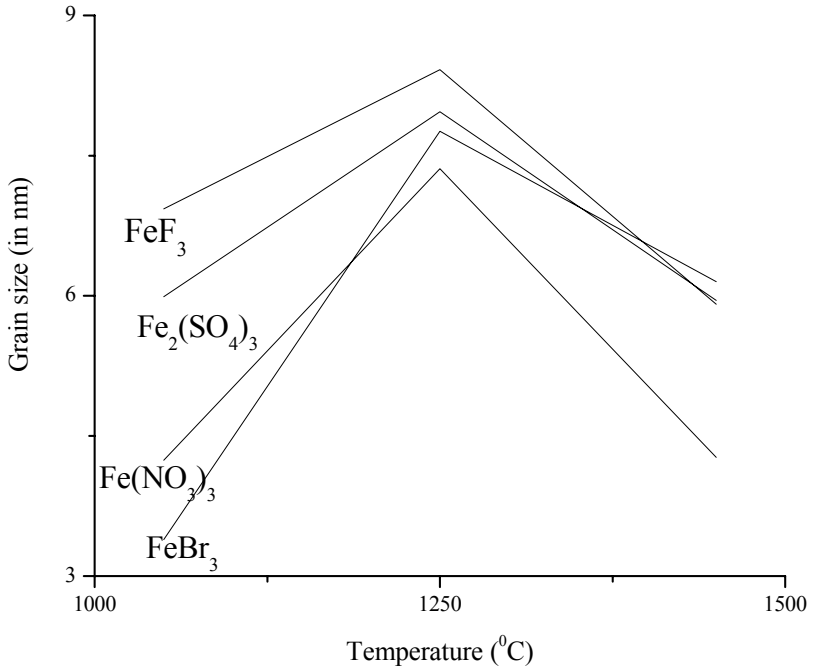

Fig. 5.4. Grain size of hBN vs temperature when iron salts were used.

Different iron salts were used to examine the anion effects on the crystallization of hBN and it was found that the used anions (SO_4^{2-}, Br^-, F^-) make no change on crystallization of hBN according to experimental results.

It was claimed in previous studies [17, 27, 28] that there is an electronic interactions between the metal atom and hBN, d-π interaction, which influence the grain growth in hBN. However, the experimental results indicate that the same results can always be obtained with usage of any metal even representative group metals such as K and Ca and grain size of the samples are significantly close each other (Figure 5.5). In this case, the d-π interaction is questionable.

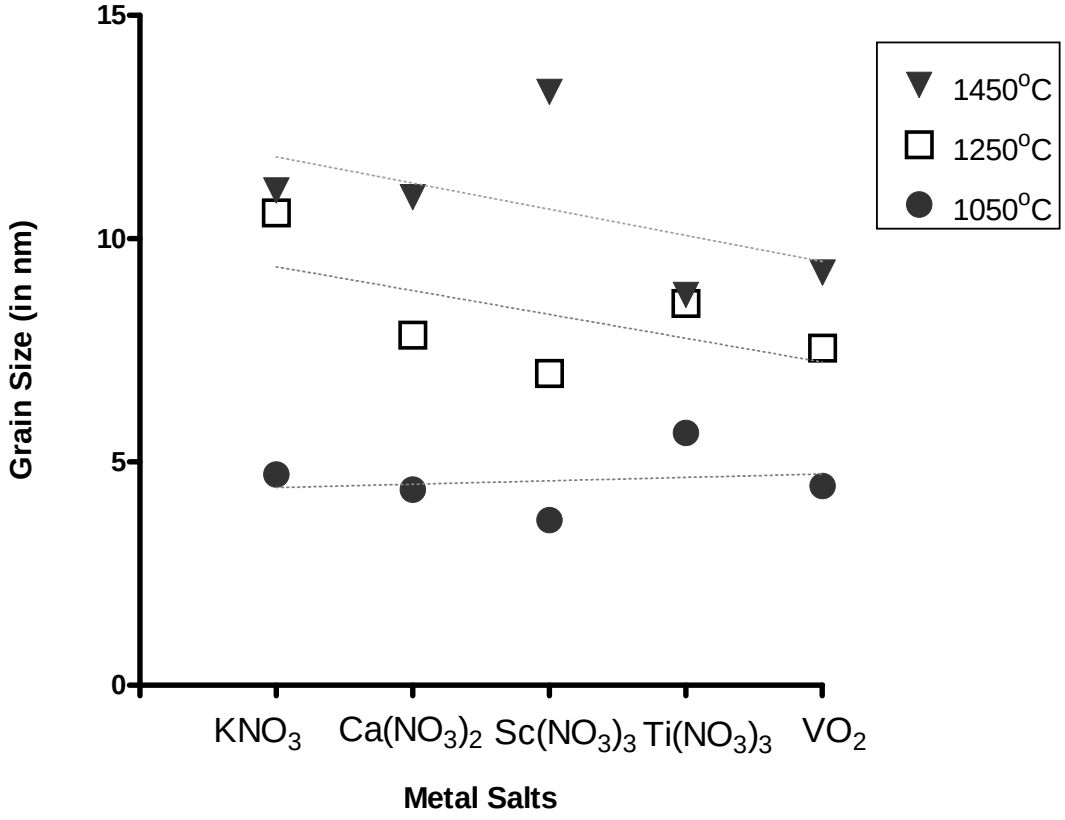

Fig. 5.5. Changing in grain size of the hBN at different temperatures in the presence of metal salts.

All SEM image interpretations were based on Shimomura [51]. In this work hBN was prepared at 2000°C and disc-shape homogeneous plates were observed. However, our SEM images indicate that the grains are irregular shape and order, and coated by amorphous material (Fig.5.5), some of them appear flaky (Fig. 5.6) with having irregular shape, and some of them are irregular grained powder with fractures (Fig.5.7) and the particles are jagged shapes (Fig 5.8). These unexpected results may be caused by insufficient instrumental conditions (not enough focusing and zooming) rather than structural problems because it was not able to observe single grain or layers due to very small grain size of hBN. Transmission Electron Microscope (TEM), High Resolution Transmission Electron Microscope (HRTEM) or Atomic Force Microscope (AFM) should be used instead of SEM.

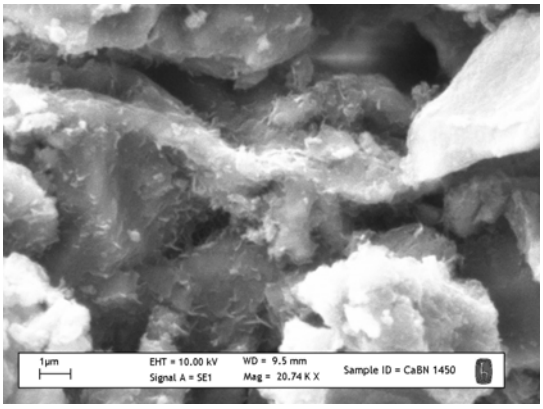

Fig 5.6.

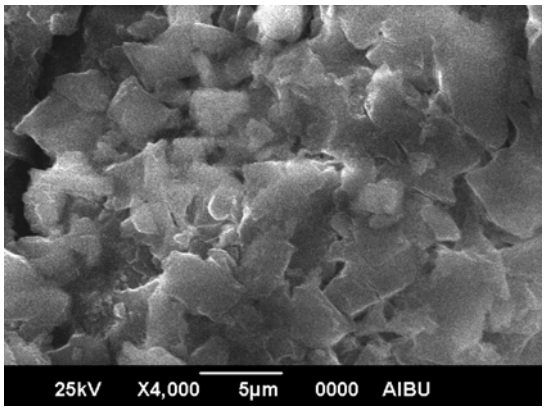

Fig.5.7.

Fig 5.6. SEM image of hBN sample coated by amorphous material.

Fig. 5.7. SEM image of flaky shape hBN.

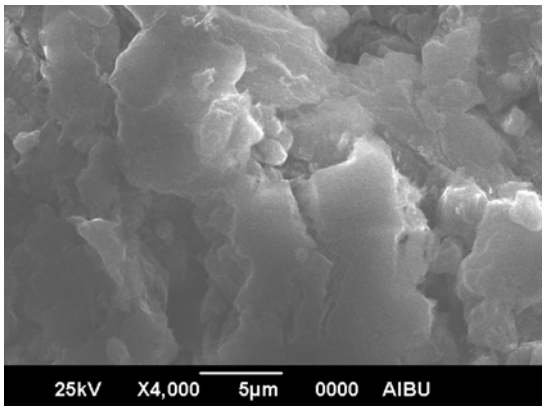

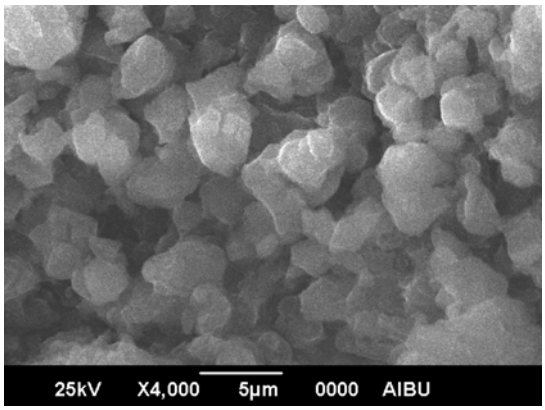

Fig 5.8. **Fig.5.9.**

Fig. 5.8. SEM image of hBN with fracture.

Fig. 5.9. SEM image of jagged shape hBN.

The presence of metals was proved by EDX but they can not be observed in SEM images. Because metals might be located in phase boundaries and / or cracks of hBN as ultradispersion clusters like the graphite intercalation compounds demonstrated in Shuvaev's study [52].

As a result, hBN samples were prepared at relatively at low temperature and formation of B-N confirmed by FTIR. Both usage of ammonia and metals decreased the synthesis temperature of hBN and helped the formation of nano-scale hBN which were proved by XRD pattern. The grain size of hBN was raised with increasing temperature and calculated lattice parameters were very close to reported value of original hBN. Although, the presence of metals was proved by EDX but they can not be observed in SEM images. Because metals might be placed in phase boundaries and / or cracks of hBN.

6. CONCLUSION

In summary, hBN samples were prepared with the modified O'Connor method at different temperatures under ammonia atmosphere and following conclusions can be stated:

1. FTIR investigations confirm the formation hBN.
2. XRD patterns of the samples are indexed as hBN and calculated lattice parameters are very close to reported values of hBN.
3. The broadening nature of the XRD peaks indicates that the particle size of the samples is within nanometer scale.
4. Usages of metals permit lowering the formation temperature of hBN and overcome the internal stress. Also, usages of metals help the formation of the nano structures at low temperature.
5. The accompanying anions to the metal do not affect the crystallization behavior of hBN.
6. An electronic interaction between the metal atom and hBN, d-π interaction, is questionable.
7. According to FTIR and the calculation of ratio of B_3N_3 units to metal atoms, there is no evidence for intercalation.
8. Crystallization degree of BN rises with increasing temperature which proved by XRD.

REFERENCES

1. Anonymous- 1. Chamber of Mining Engineers of Turkey Web Site. http://www.maden.org.tr/resimler/ekler/6358599b7afb250_ek.pdf?tipi=5&turu=R&sube=0..http://www.maden.org.tr/resimler/ekler/6358599b7afb250_ek.pdf?tipi=5&turu=R&sube=0.

2. Balmain, W. H. 1842. Bemerkungen über die Bildung von Verbindungen des Bors und Siliciums mit Stickstoff und gewissen Metallen. *J Prakt Chem*. 27: 422- 430.

3. Davis, R. F. 1991. III- IV Nitrides for Electronic and Optoelectronic Applications, *Proceedings of the IEEE*. 79 (5): 702- 712.

4. Pierson, H.O. Handbook of Refractory Carbides and Nitrides.1996. *Covalent Nitrides: Composition and Structure*. 213- 214. Noyes Publications, New Jersey, USA.

5. Hubacek, M. and Brozek, V. 1991. Kinetics of Deoxidizing of Hexagonal Boron Nitride Preparations. *J Solid State Chem*. 95: 253- 259.

6. Pierson, H.O. Handbook of Refractory Carbides and Nitrides.1996. *Covalent Nitrides: Composition and Structure*. 214- 216. Noyes Publications, New Jersey, USA.

7. Mishima, O., and Era, K. 2000. Science and Technology of Boron Nitride. *In*: Kumashiro, Y. (ed.): *Electric Refractory Materials*. 517- 518. Mercel Dekker, Inc. New York, USA.

8. Mishima, O., and Era, K. 2000. Science and Technology of Boron Nitride. *In:* Kumashiro, Y. (ed.): *Electric Refractory Materials*. 498. Mercel Dekker, Inc. New York.

9. Anonymous- 2. Milan Hubacek's Web Site. http://hubacek.jp/bn/bn.htm.

10. Haubner, R., Wilhelm, M., Weissenbacher, R., and Lux, B. 2002. Boron Nitrides- Properties, Synthesis and Applications. In: Jansen, M. (ed). *High Performance Non- Oxide Ceramics II*. 15. Springer Verlag. Berlin.

11. Haubner, R., Wilhelm, M., Weissenbacher, R., and Lux, B. 2002. Boron Nitrides-Properties, Synthesis and Applications. In: Jansen, M. (ed). *High Performance Non- Oxide Ceramics II*. 15. Springer Verlag. Berlin.

12. Haubner, R., Wilhelm, M., Weissenbacher, R., and Lux, B. 2002. Boron Nitrides-Properties, Synthesis and Applications. In: Jansen, M. (ed). *High Performance Non- Oxide Ceramics II*. 15- 16. Springer Verlag. Berlin.

13. O'Connor, T. E.1962. Synthesis of Boron Nitride. *J Am Chem Soc*. 84: 1753-1754.

14. Hubacek, M. and, Sato, T.1995. Preparation and Properties of a Compound in the B-C-N System. *J Solid State Chem*.114: 258-264.

15. Bardo, R. D. 1995. Reaction Mechanism in Shocked, Intercalated Graphite and Boron Nitride. *J Phys IV*. 5: C4 561- C4 570.

16. Dresselhaus, M. S., and Dresselhaus, G. 2002. Intercalation Compounds of Graphite. *Adv Phys*. 51 (1): 1- 186

17. Croft, R. C. 1955. A New Molecular Compound of Boron Nitride. *Aust J Chem*. 9: 206- 211.

18. Freeman, A. G., and Larkindale, J. P. 1969. Preparation, Mössbauer Spectra, and Structure of Intercalation Compounds of Boron Nitride with Metal Halides. *J. Chem. Soc*. A7: 1307- 1308.

19. Ohhashi, K., and Shinjo, T. 1977. On the Existence of Intercalation Compound of Boron Nitride with Ferric Chloride. *Bull Inst Chem Res Kyoto Univ*. 55 (5): 441-446.

20. Sakamoto. M., Speck, J. S., and Dresselhaus, M. S.1986. Cesium and Bromine Doping into Hexagonal Boron Nitride. *J Mater*. *Res*. 1: 685.

21. Doll, G. L., Nakamura, K., and Tanuma, S. I. 1989. Intercalation of Hexagonal Boron Nitride with Potassium. *J Appl Phys*. 66 (6): 2554- 2558.

22. Oku, T., Kusunose, T., Hirata, T., Hatakeyama, R., Sato, N., Niihara, K., and Suganuma, K. 2000. Formation and Structure of Ag, Ge and SiC Nanoparticles Encapsulated in Boron Nitride and Carbon Nanocapsules. Diam Relat Mater. 9: 911- 915.

23. Dai, B.Q., and Zhang, G.L. 2002. Ab initio MO studies on the stability of intercalation compound Cu–hBN. *Mater Chem Phys*. 78: 304–307.

24. Dai, B.Q., and Zhang, G.L. 2002. Ab initio MO studies on the stability of intercalation compound Cu–hBN. *Mater Chem Phys*. 77: 318–320.

25. Altıntaş, B. 2009. Ab Initio Investigations on Electronic and Lattice Dynamical Properties of Intercalation of Metals into Hexagonal Boron Nitride. PhD Thesis. Department of Chemistry, Abant Izzet Baysal University, Bolu. p. 120.

26. Hubacek, M., Ueki M. 1996. Orientation and Grain Growth in Copper-Activated Hot-Pressed Hexagonal Boron Nitride. *J Am Ceram Soc*.79 (1): 283-285.

27. Hubacek, M., Sato T., and Ueki M. 1997. Copper - Boron Nitride Interaction in Hot-Pressed Ceramics. *J. Mater. Res*. 12 (1): 113-118.

28. Budak E., Bozkurt, Ç. 2004. The Effect of Transition Metals on the Structure of hBN Intercalation Compounds. *J Solid State Chem*.177: 1768- 1770.

29. Koç, G. 2004. Synthesis of Cadmium Intercalated Hexagonal Boron Nitride. MSc Thesis. Department of Chemistry, Abant Izzet Baysal University, Bolu. p. 35.

30. Yücel, N. 2005. Effect of Metal Carbonyls on the Formation of Hexagonal Boron Nitride. MSc Thesis. Department of Chemistry, Abant Izzet Baysal University, Bolu. p. 28.

31. Terrones, M., Hsu, W.K., Terrones, H., Zhang, J.P., Ramos, S., Hare, J.P., Castillo, R., Prassides, K., Cheetham, A.K., Kroto, H.W., and Walton, D.R.M. 1996. Metal particle catalysed production of nanoscale BN structures. *Chem Phys Lett*. 259: 568-573.

32. Benko, E., Morgiel, J., and Czeppe, T. 1997. BN Sintered with Al: Microstructure and Hardness. Ceram. Inter.23: 89- 91.

33. Kondo, T., Shindo, K., and Sakurai, Yoji. 2005. Comparison of Hydrogen Absorption Properties of Ti Mechanically Milled with Hexagonal Boron Nitride and with Graphite. *J Alloy Compd*. 386: 202–206.

34. Hubacek, M., Sato, T., and Ishii, T. 1994. A Coexistence of Boron Nitride and Boric Oxide. *J Solid State Chem*. 109: 384– 390.

35. Hu, J. Q., Lu, Q. Y., Tang, K. B., Yu, S. H., Qian, Y. T., Zhou, G. E., Liu, X. M., and Wu, J. X. 1999. Synthesis and Characterization of Nanocrystalline Boron Nitride. *J Solid State Chem*. 148: 325- 328.

36. Chen, L., Gu, Y., Li, Z., Qian, Y., Yang, Z., and Ma, J. 2005. Low-Temperature Synthesis and Benzene-Thermal Growth of Nanocrystalline Boron Nitride. *J Cryst Growth*. 273: 646- 650.

37. Chen, L., Huang, M., Luo, T., Gu, Y., Shi, L., Yang, Z., and Qian, Y. 2004. A Low-Temperature Route to Nanocrystalline Boron Nitride Whiskers and Flakes. *Mater Lett*. 58 (27- 28): 3634-3636.

38. Hubacek, M. and Ueki, M. 1996. Chemical Reactions in Hexagonal Boron Nitride System.1996. *J Solid State Chem*. 123: 215- 222.

39. Dibandjo, P., Bois, L., Chassagneux, F., and Miele, P. 2007. Thermal Stability of Mesoporous Boron Nitride Templated with a Cationic Surfactant. *J Eur Ceram Soc.* 27 (1): 313- 317.

40. Zheng, M., Gu, Y., Xu, Z., and Liu, Y. 2007. Synthesis and Characterization of Boron Nitride Nanoropes. *Mater Lett*. 61 (8-9): 1943- 1945.

41. Shi, L., Gu, Y., Chen, L., Qian, Y., Yang, Z., and Ma, J. 2004. Synthesis and Morphology Control of Nanocrystalline Boron Nitride. *J Solid State Chem*. 177 (3): 721- 724.

42. Perdigon-Melon J. A., Auroux, A., Cornu, D., Miele, P., Toury, B., and Bonnetot, B. 2002. Porous Boron Nitride Supports Obtained From Molecular Precursors.: Influence of the Precursor Formulation and of the Thermal

Treatment on the Properties of BN Ceramic. *J Organomet Chem*. 657: 98-106.

43. Yoo, C. S., Akella, J., and Cynn, H.1997. Direct Elementary Reactions of Boron and Nitrogen at High Pressures and Temperatures. *Phys Rev B*. 56: 140- 146.

44. Hu, J. Q., Lu, Q. Y., Tang, K. B., Yu, S. H., Qian, Y. T., Zhou, G. E., Liu, X. M., and Wu, J. X. 1999. Synthesis and Characterization of Nanocrystalline Boron Nitride. *J Solid State Chem*. 148: 325- 328.

45. Choi, J. Y., Kang, S. J. L., Fukunaga, O., Park, J. K., and Eun, K. Y. 1993. Effect of B_2O_3 and hBN Crystallinity on cBN Synthesis. *J Am Ceram Soc*. 76 (10): 2525-2528.

46. Shi, L., Gu, Y., Chen, L., Yang, Z., Ma, J., and Qian, Y. 2004. Formation of Nanocrystalline BN with a Simple Chemical Route. *Mater Lett*. 58 (26): 3301- 3303.

47. Zhou, G. W., Zhang, Z., Bai, Z. G., and Yu, D. P. 1999. Catalyst Effects on Formation of Boron Nitride Nano-Tubules Synthesized by Laser Ablation. *Solid State Commun*. 109 (8): 555- 559.

48. Warner T. E. and Fray, D. J. 2000. Nitriding of Iron Boride to Hexagonal Boron Nitride. *J Mater Sci*. 38: 5341- 5345.

49. Kurooka, S., Ikeda, T., Kohama, K., Tanaka, T., and Tanaka, A. 2003. Formation and Characterization of BN Films with Ti Added. *Surf Coat Tech*. 166: 111- 116.

50. Hao, X., Yu, M., Cui, D., Xu, X., Wang, Q., and Jiang, M. 2002. The effect of temperature on the synthesis of BN nanocrystals. *J Cryst Growth*. 241: 124-128.

51. Shimomura, J., Funahashi, T., and Koitabashi, T. 1995. Electron Microscopy of Hexagonal Boron Nitride Powder. *J Mater Sci*. 30: 3193- 3199.

52. Shuvaev, A.T., Helmer, B.Y., Kraizman, V. L., Lyubesnova T. A., Mirmilstein, A. S., Kvacheva, L. D., Novikov Y. N., and Volpin, M. E. 1989. Graphite Intercalation Compounds with 3D Transition Metals: Graphite-Metal Intercalation. *Physica B*. 158 (1-3): 539-542.

APPENDIX A

FTIR SPECTRA OF hBN SAMPLES

A.1. FTIR spectra of hBN in presence of KNO_3.

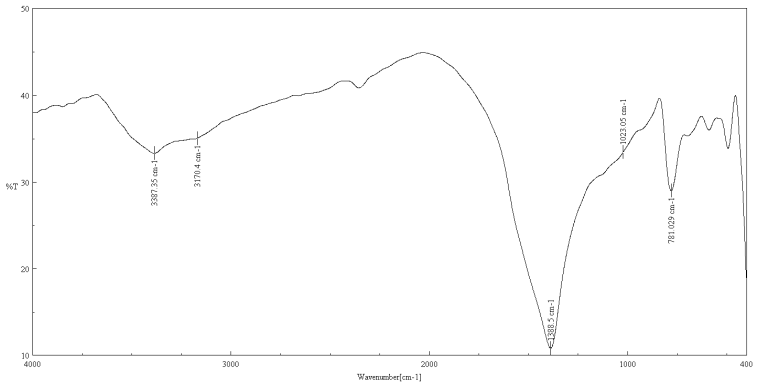

Fig. A.1.1. FTIR spectrum of hBN in presence of KNO_3 at 1050°C.

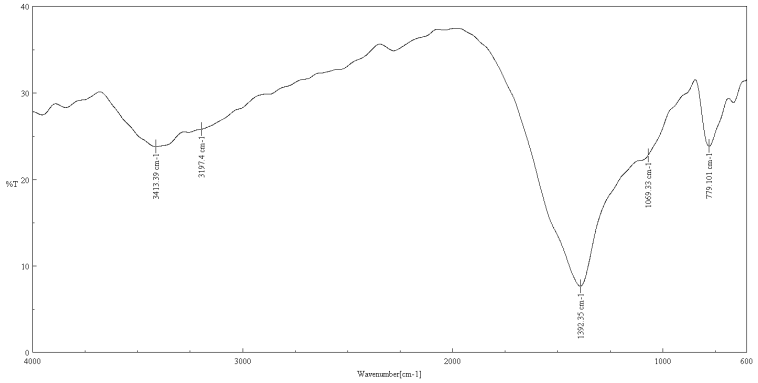

Fig. A.1.2. FTIR spectrum of hBN in presence of KNO_3 at 1250°C.

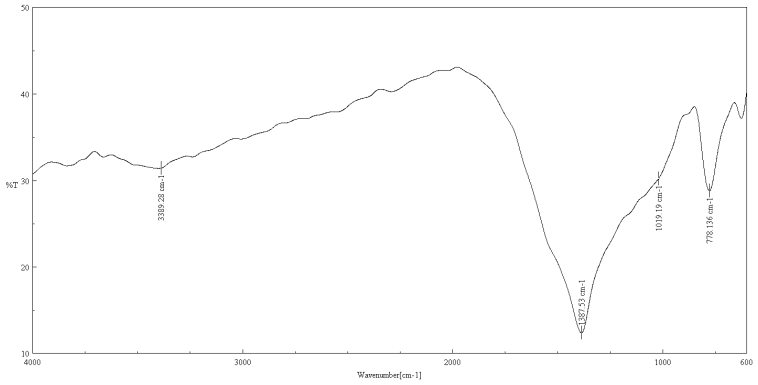

Fig. A.1.3. FTIR spectrum of hBN in presence of KNO_3 at 1450°C.

A.2. FTIR spectra of hBN in presence of $Ca(NO_3)_2$.

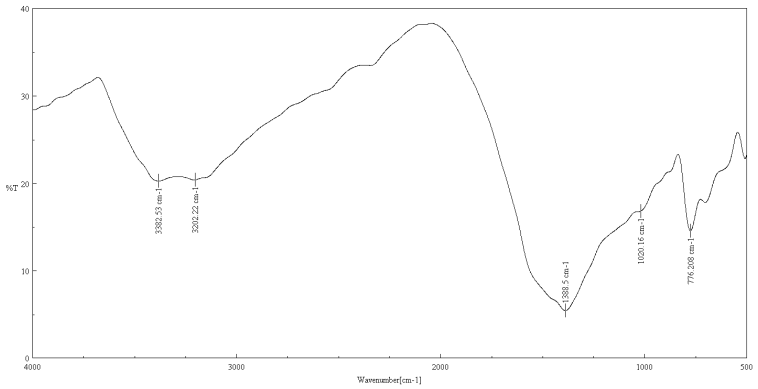

Fig. A.2.1. FTIR spectrum of hBN in presence of $Ca(NO_3)_2$ at 1050°C.

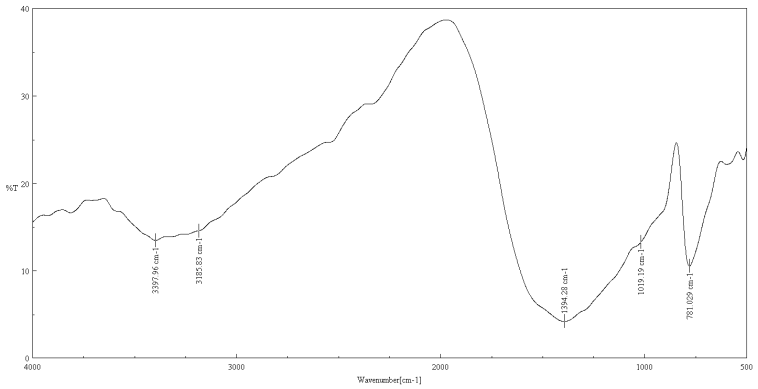

Fig. A.2.2. FTIR spectrum of hBN in presence of $Ca(NO_3)_2$ at 1250°C.

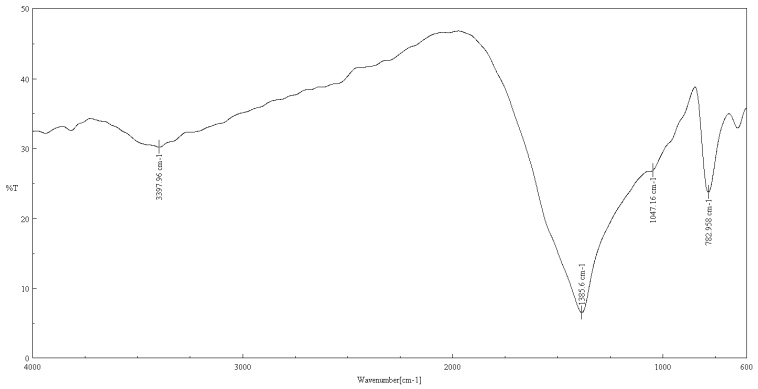

Fig. A.2.3. FTIR spectrum of hBN in presence of $Ca(NO_3)_2$ at 1450°C.

A.3. FTIR spectra of hBN in presence of $Sc(NO_3)_3$.

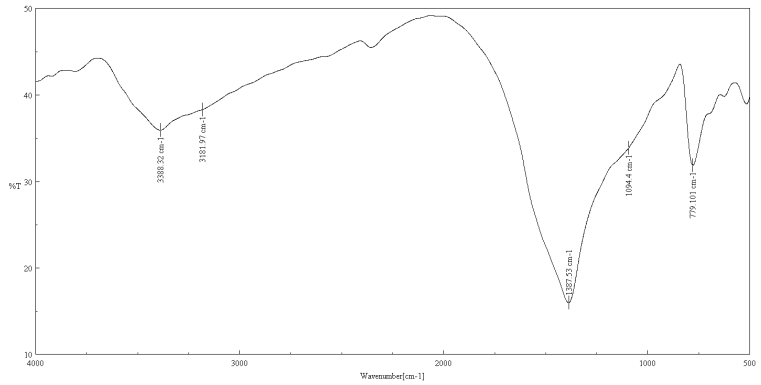

Fig. A.3.1. FTIR spectrum of hBN in presence of $Sc(NO_3)_3$ at 1050°C.

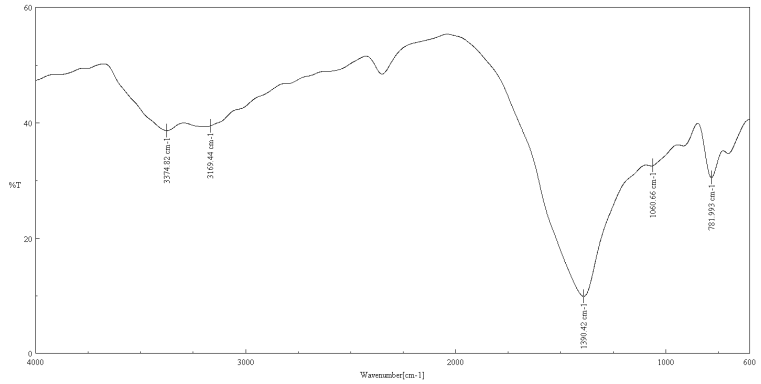

Fig. A.3.2. FTIR spectrum of hBN in presence of $Sc(NO_3)_3$ at 1250°C.

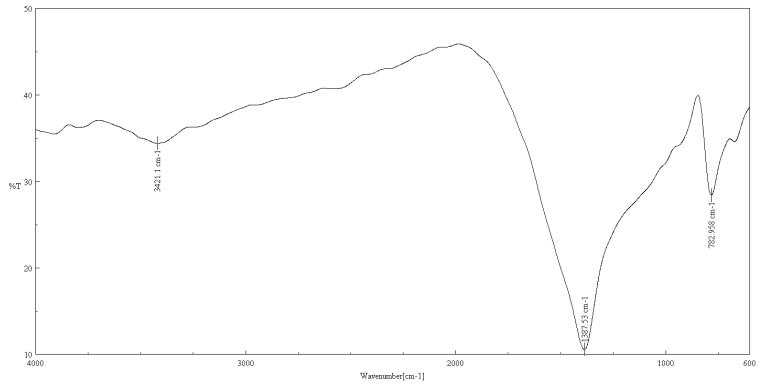

Fig. A.3.3. FTIR spectrum of hBN in presence of $Sc(NO_3)_3$ at 1450°C.

A.4. FTIR spectra of hBN in presence of $Ti(NO_3)_4$.

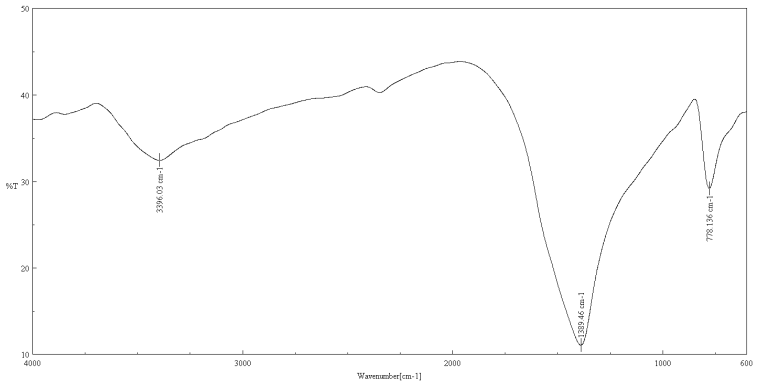

Fig. A.4.1. FTIR spectrum of hBN in presence of $Ti(NO_3)_4$ at 1050°C.

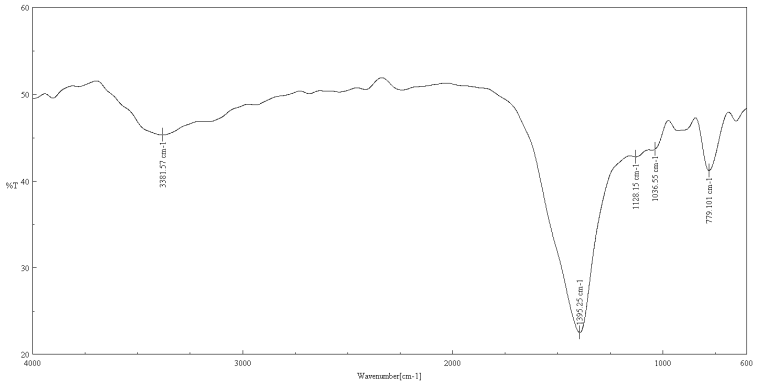

Fig. A.4.2. FTIR spectrum of hBN in presence of $Ti(NO_3)_4$ at 1250°C.

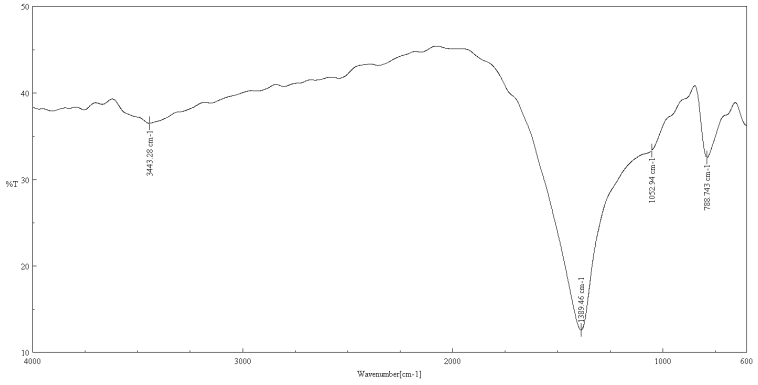

Fig. A.4..3. FTIR spectrum of hBN in presence of $Ti(NO_3)_4$ at 1450°C.

A.5. FTIR spectra of hBN in presence of VO_2.

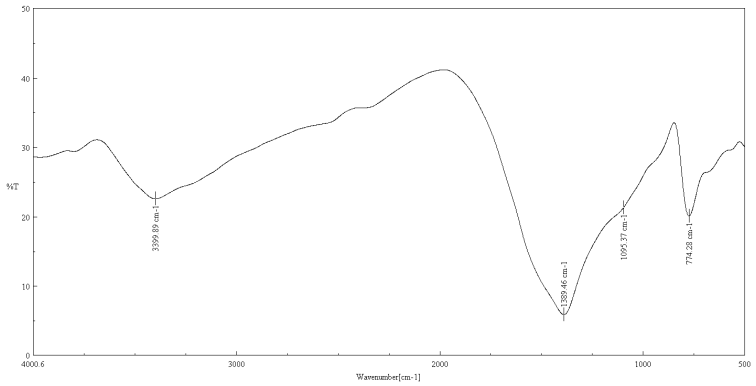

Fig. A.5.1. FTIR spectrum of hBN in presence of VO_2 at 1050°C.

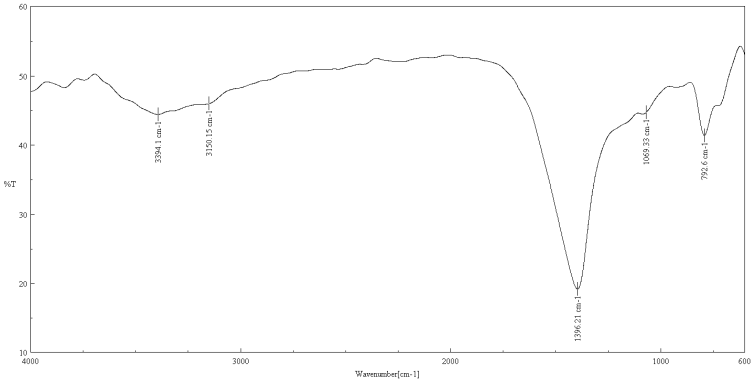

Fig. A.5.2. FTIR spectrum of hBN in presence of VO_2 at 1250°C.

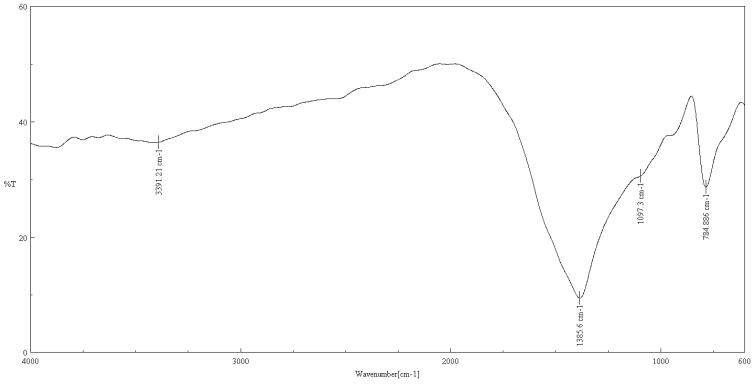

Fig. A.5.3. FTIR spectrum of hBN in presence of VO_2 at 1450°C.

A.6. FTIR spectra of hBN in presence of $Fe_2(SO_4)_3$.

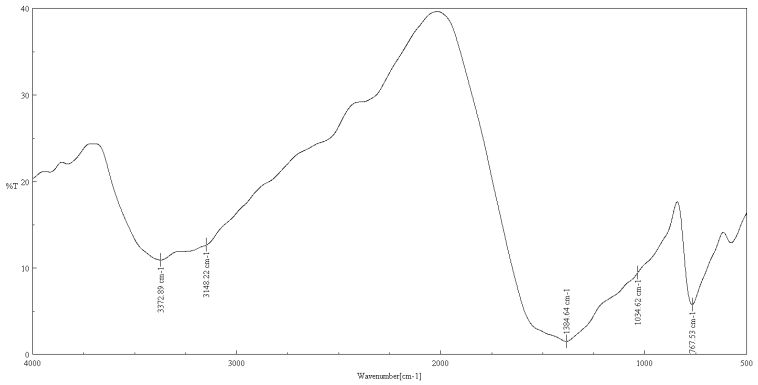

Fig. A.6.1. FTIR spectrum of hBN in presence of $Fe_2(SO_3)_4$ at 1050°C.

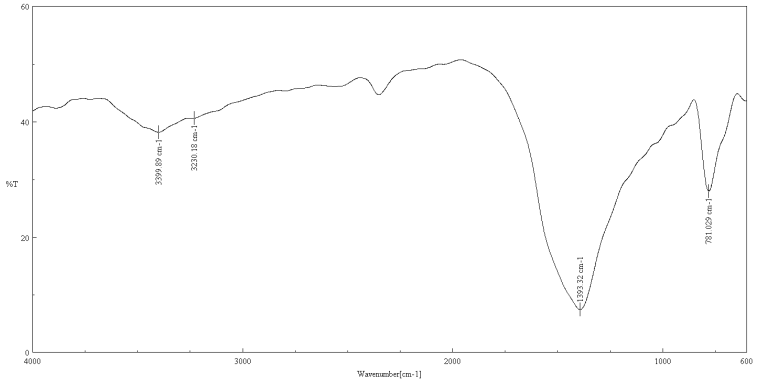

Fig. A.6.2. FTIR spectrum of hBN in presence of $Fe_2(SO_4)_3$ at 1250°C.

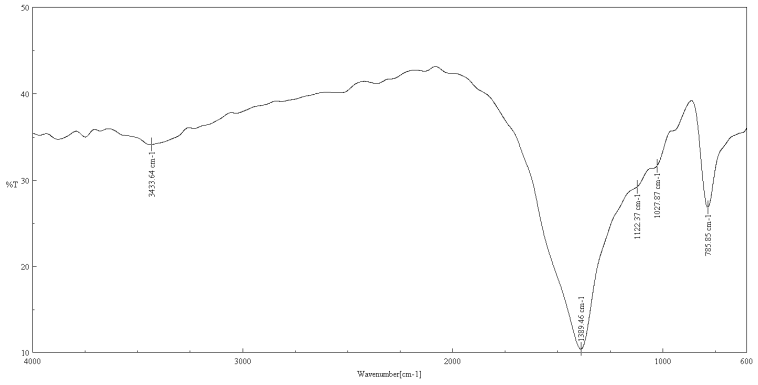

Fig. A.6.3. FTIR spectrum of hBN in presence of $Fe_2(SO_4)_3$ at 1450°C.

A.7. FTIR spectra of hBN in presence of $FeBr_3$.

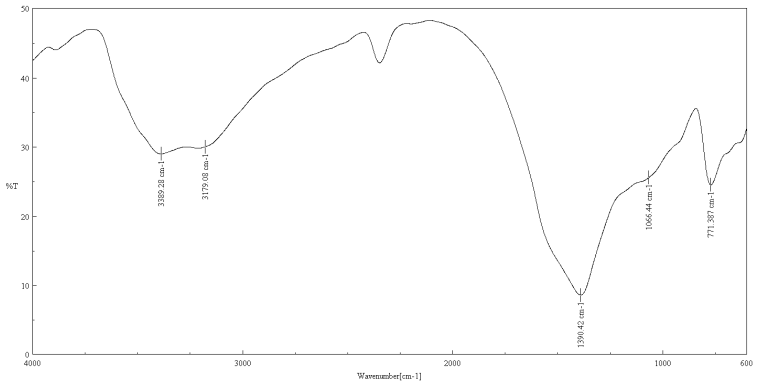

Fig. A.7.1. FTIR spectrum of hBN in presence of $FeBr_3$ at 1050°C.

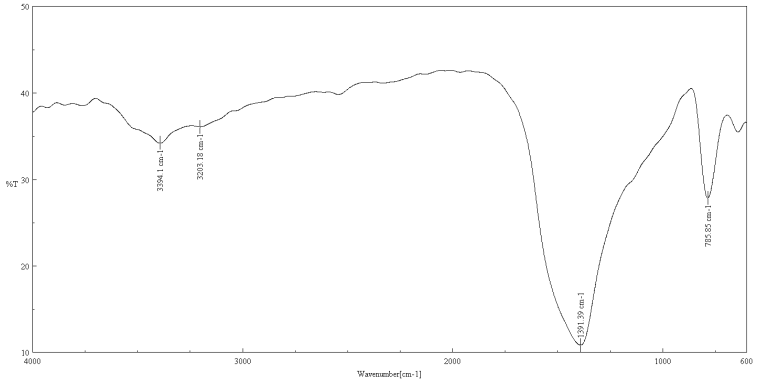

Fig. A.7.2 FTIR spectrum of hBN in presence of $FeBr_3$ at 1250°C.

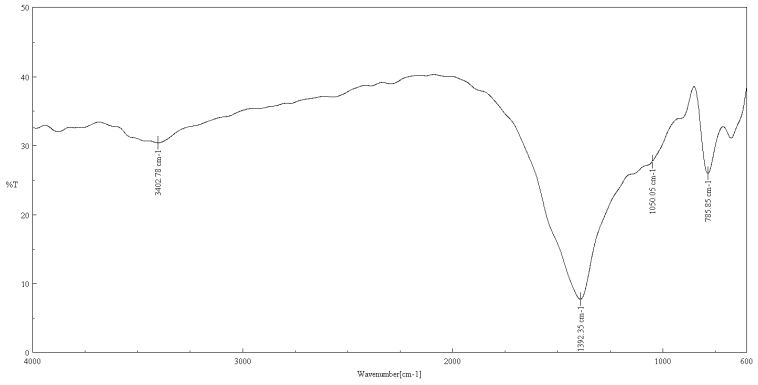

Fig. A.7.3. FTIR spectrum of hBN in presence of $FeBr_3$ at 1450°C.

A.8. FTIR spectra of hBN in presence of FeF_3.

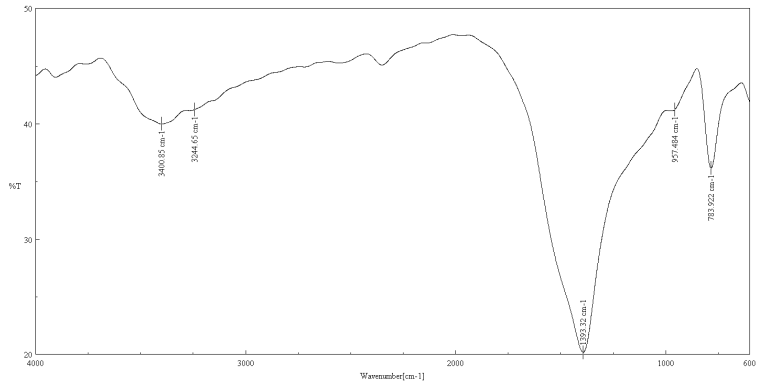

Fig. A.8.1. FTIR spectrum of hBN in presence of FeF_3 at 1050°C.

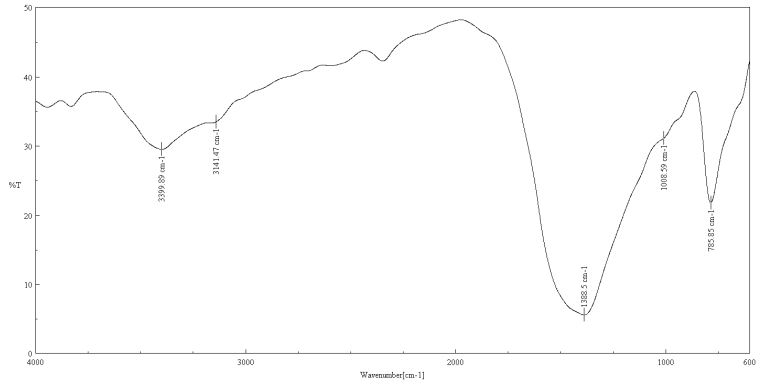

Fig. A.8.2. FTIR spectrum of hBN in presence of FeF_3 at 1250°C.

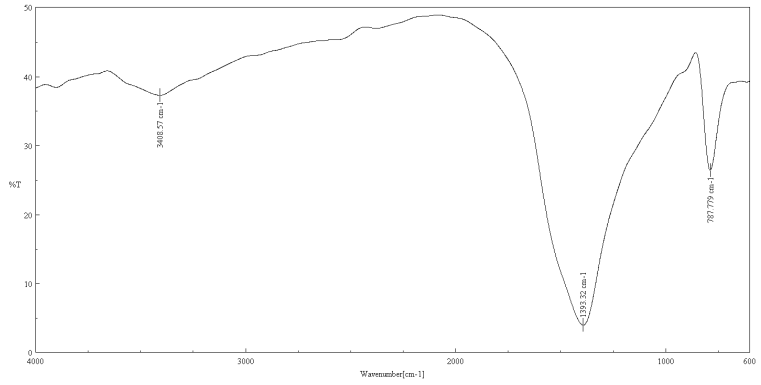

Fig. A.8.3. FTIR spectrum of hBN in presence of FeF_3 at 1450°C.

A.9. FTIR spectra of hBN in presence of $Fe(NO_3)_3$.

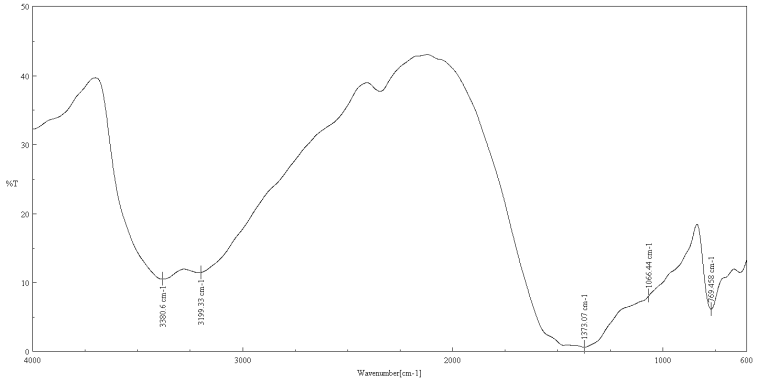

Fig. A.9.1. FTIR spectrum of hBN in presence of $Fe(NO_3)_3$ at 1050°C.

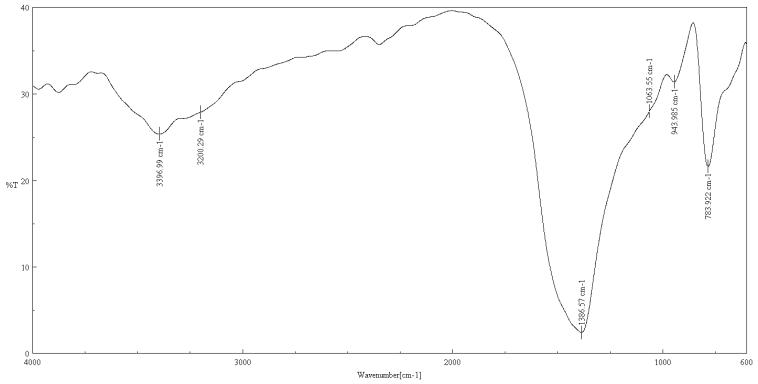

Fig. A.9.2. FTIR spectrum of hBN in presence of $Fe(NO_3)_3$ at 1250°C.

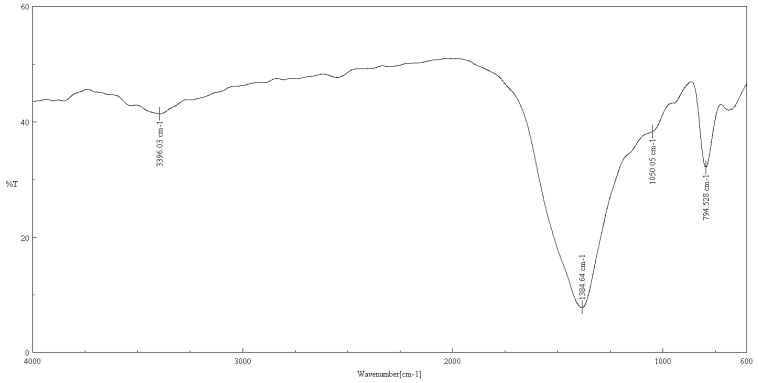

Fig. A.9.3. FTIR spectrum of hBN in presence of $Fe(NO_3)_3$ at 1450°C.

APPENDIX B

XRD PATTERN OF hBN SAMPLES

B.1. XRD pattern of hBN samples in presence of KNO_3.

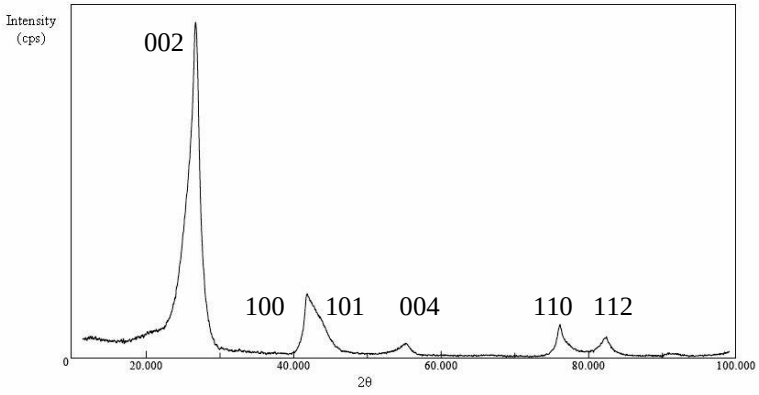

Fig. B.1.1. XRD pattern of hBN in presence of KNO_3 at 1050°C.

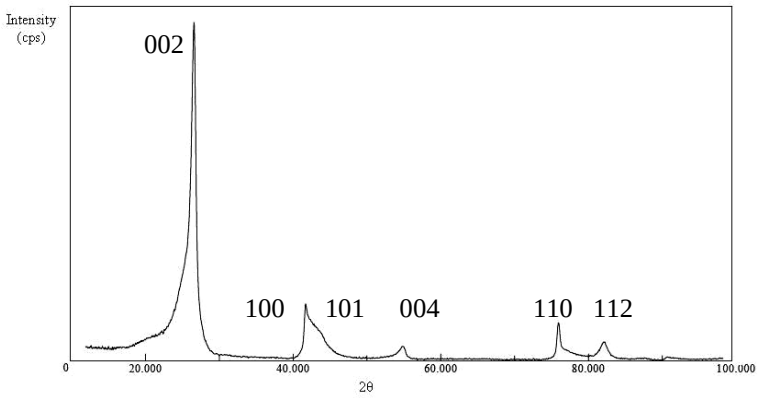

Fig. B.1.2. XRD pattern of hBN in presence of KNO_3 at 1250°C.

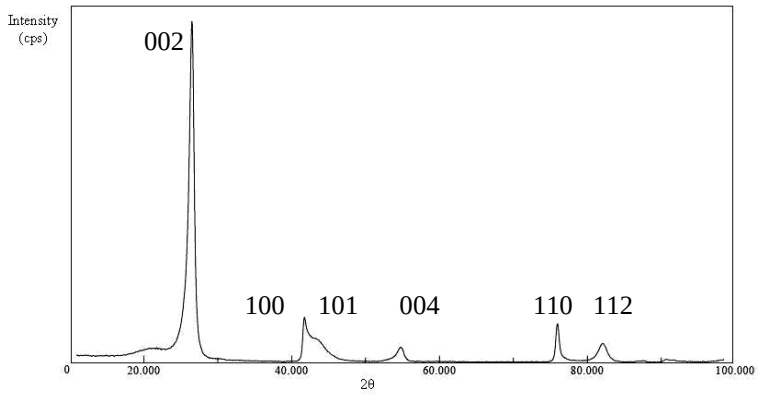

Fig. B.1.3. XRD pattern of hBN in presence of KNO_3 at 1450°C.

B.2. XRD pattern of hBN samples in presence of $Ca(NO_3)$.

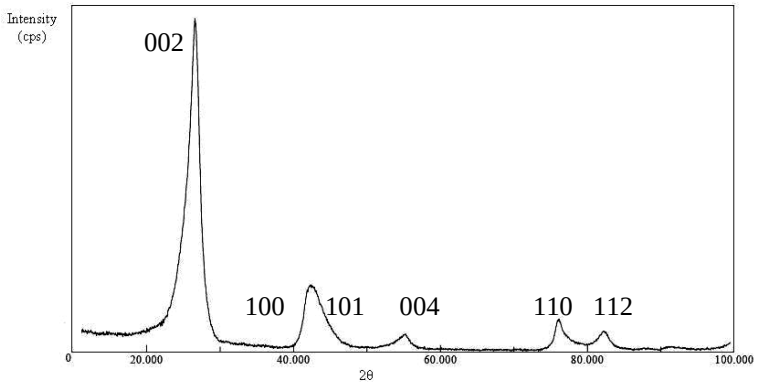

Fig. B.2.1. XRD pattern of hBN in presence of $Ca(NO_3)_2$ at 1050°C.

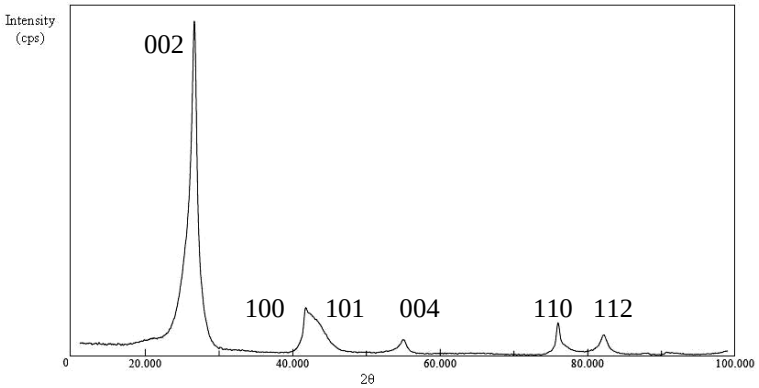

Fig. B.2.2. XRD pattern of hBN in presence of $Ca(NO_3)_2$ at 1250°C.

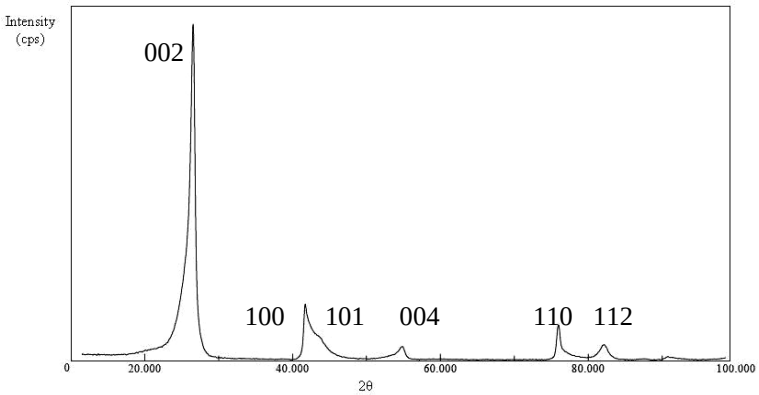

Fig. B.2.3. XRD pattern of hBN in presence of $Ca(NO_3)_2$ at 1450°C.

B.3. XRD pattern of hBN samples in presence of $Sc(NO_3)_3$.

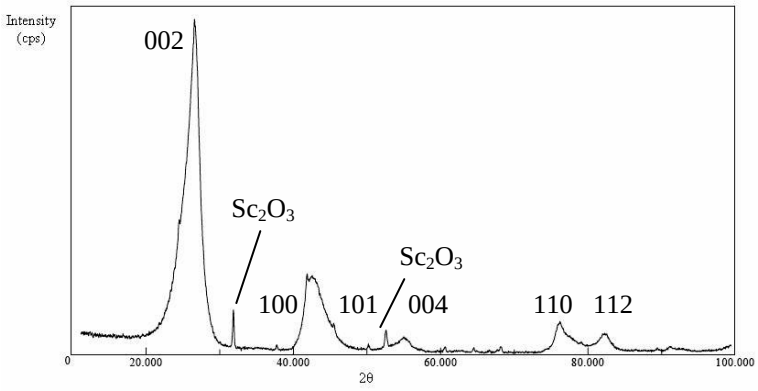

Fig. B.3.1. FTIR spectrum of hBN in presence of $Sc(NO_3)_3$ at 1050°C

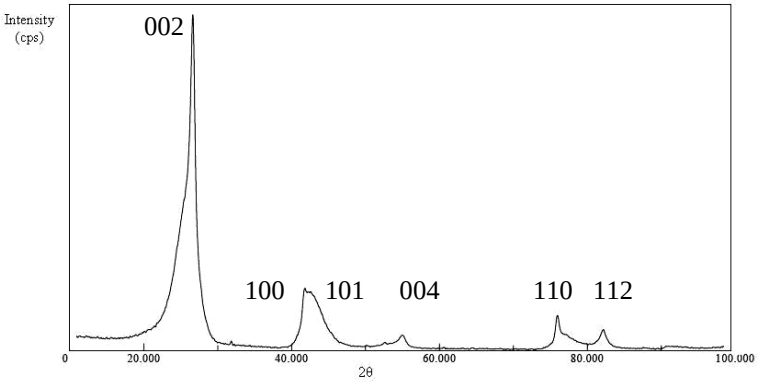

Fig. B.3.2. XRD pattern of hBN in presence of $Sc(NO_3)_3$ at 1250°C.

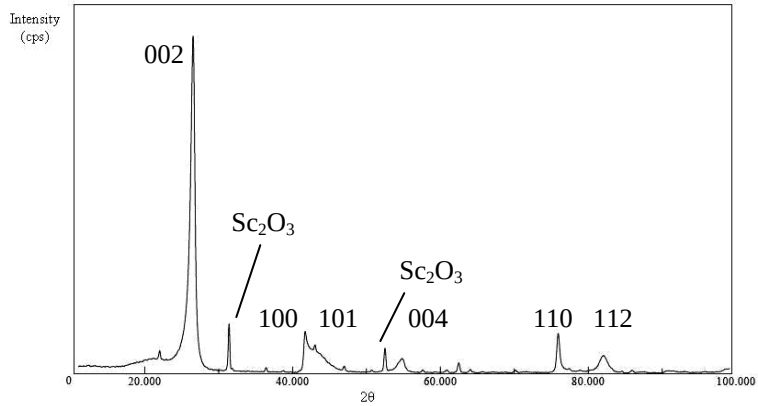

Fig. B.3.3. XRD pattern of hBN in presence of $Sc(NO_3)_3$ at 1450°C.

B.4. XRD pattern of hBN samples in presence of $Ti(NO_3)_4$.

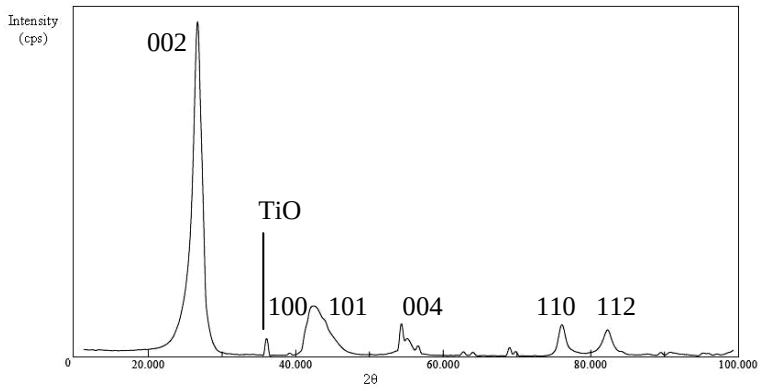

Fig. B.4.1. XRD pattern of hBN in presence of $Ti(NO_3)_4$ at 1050°C.

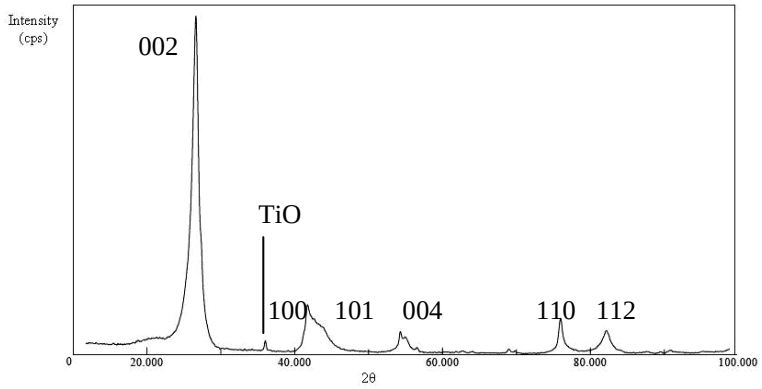

Fig. B.4.2. XRD pattern of hBN in presence of $Ti(NO_3)_4$ at 1250°C

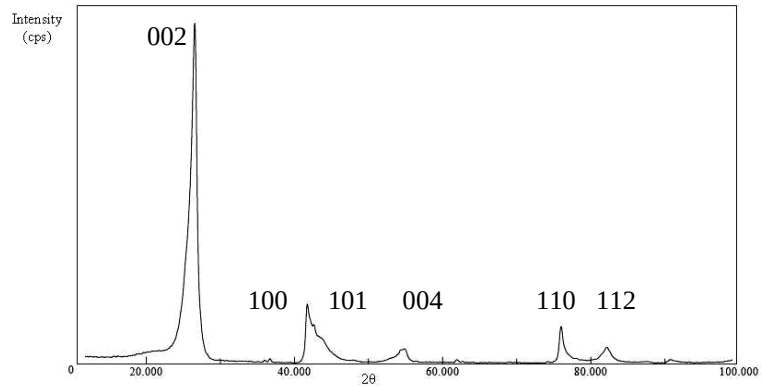

Fig. B.4.3. XRD pattern of hBN in presence of $Ti(NO_3)_4$ at 1450°C.

B.5. XRD pattern of hBN samples in presence of VO_2.

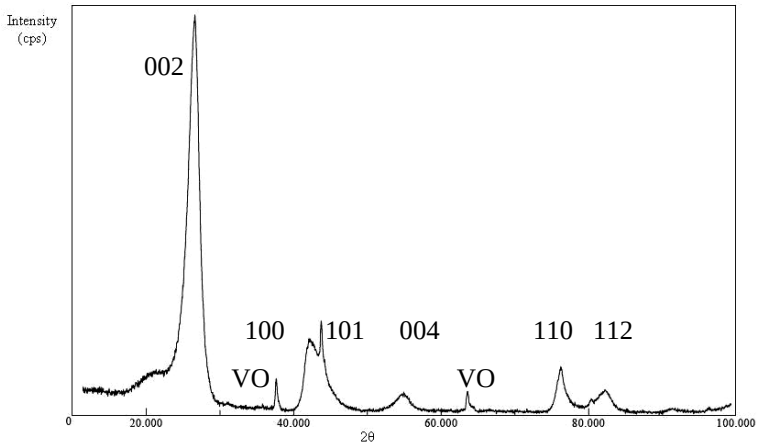

Fig. B.5.1. XRD pattern of hBN in presence of VO_2 at 1050°C.

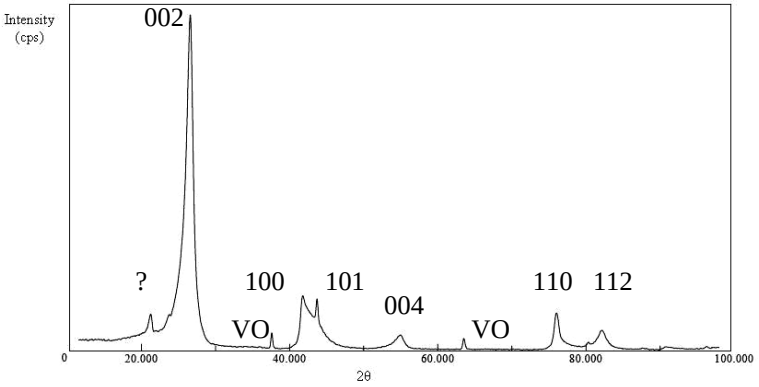

Fig. B.5.2. XRD pattern of hBN in presence of VO_2 at 1250°C.

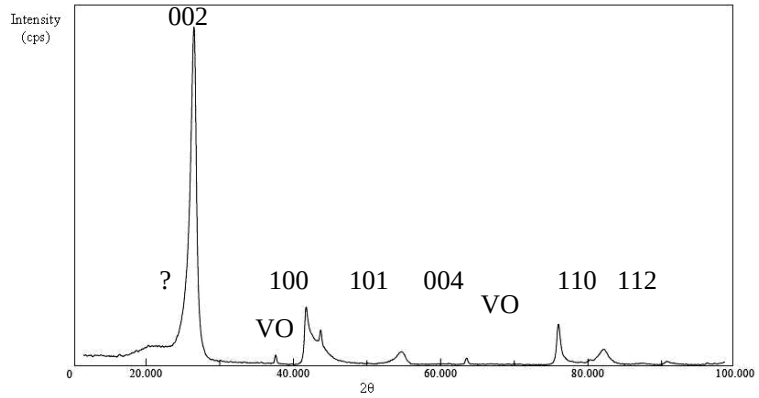

Fig. B.5.3. XRD pattern of hBN in presence of VO_2 at 1450°C

B.6. XRD pattern of hBN samples in presence of $Fe_2(SO_4)_3$.

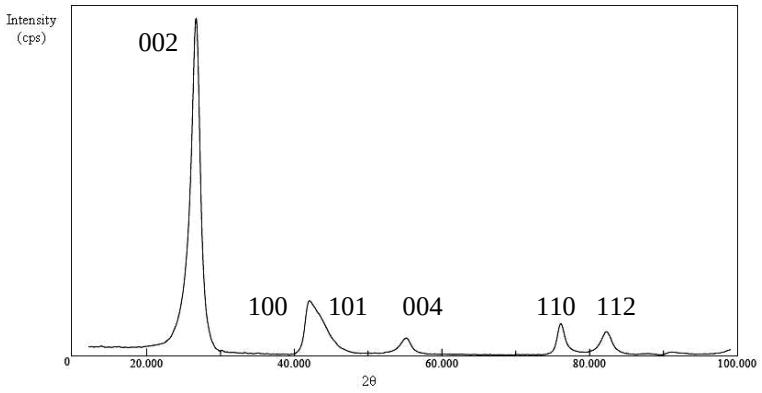

Fig. B.6.1. XRD pattern of hBN in presence of $Fe_2(SO_4)_3$ at 1050°C.

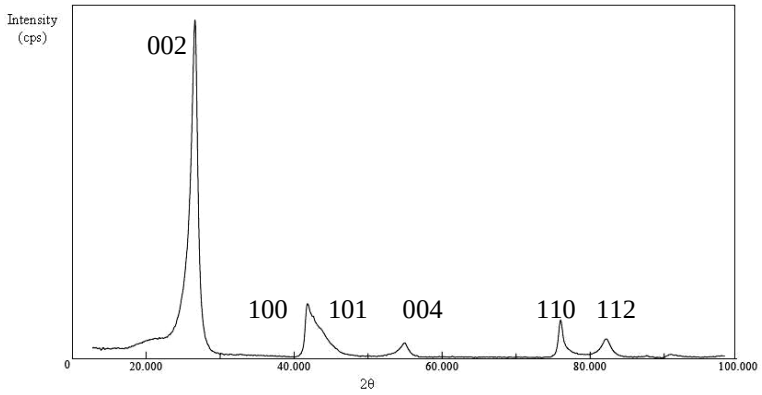

Fig. B.6.2. XRD pattern of hBN in presence of $Fe_2(SO_4)_3$ at 1250°C.

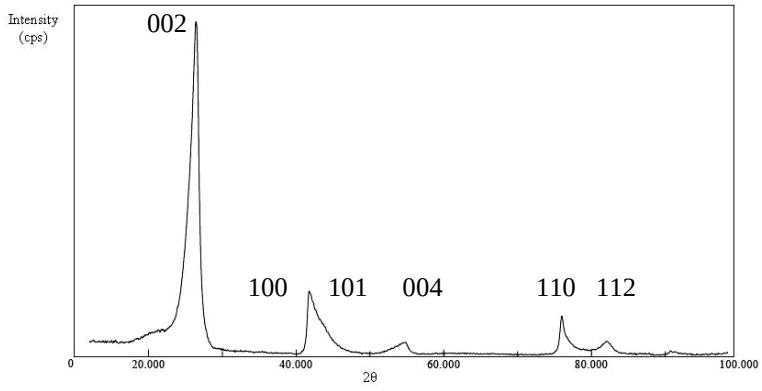

Fig. B.6.3. XRD pattern of hBN in presence of $Fe_2(SO_4)_3$ at 1450°C.

B.7. XRD pattern of hBN samples in presence of $FeBr_3$.

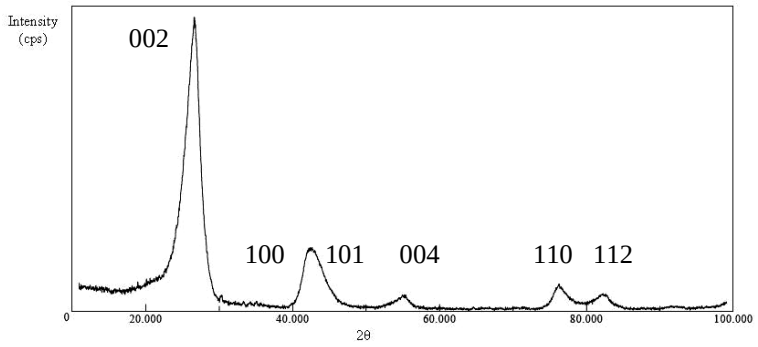

Fig. B.7.1. XRD pattern of hBN in presence of $FeBr_3$ at 1050°C.

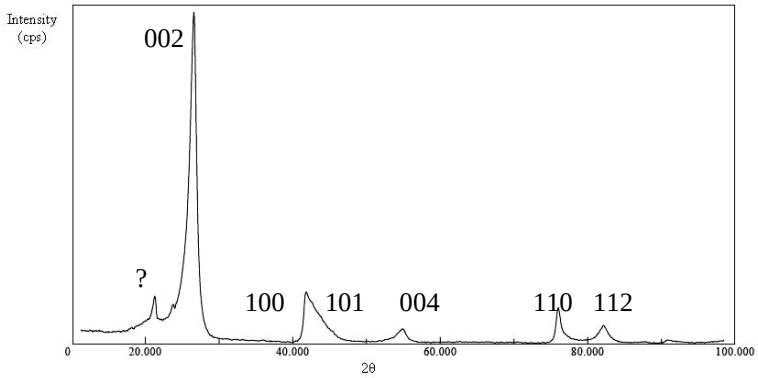

Fig. B.7.2. XRD pattern of hBN in presence of $FeBr_3$ at 1250°C.

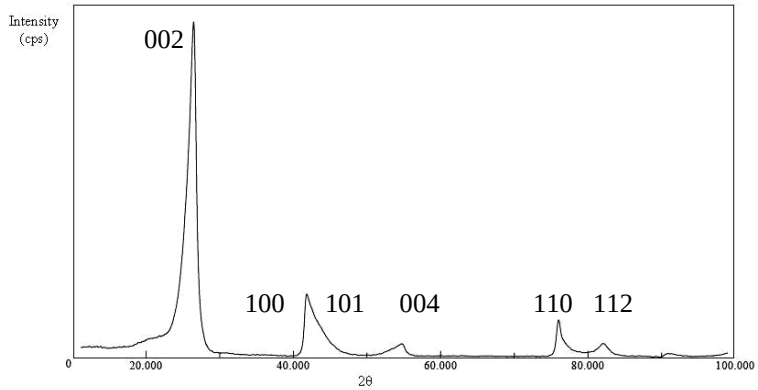

Fig. B.7.3. XRD pattern of hBN in presence of $FeBr_3$ at 1450°C.

B.8. XRD pattern of hBN samples in presence of FeF_3.

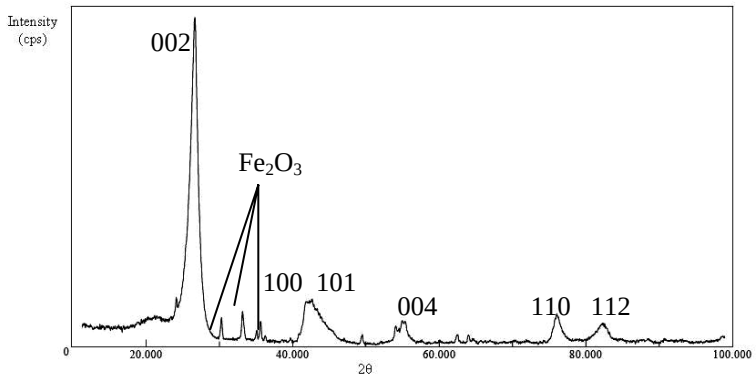

Fig. B.8.1. XRD pattern of hBN in presence of FeF_3 at 1050°C.

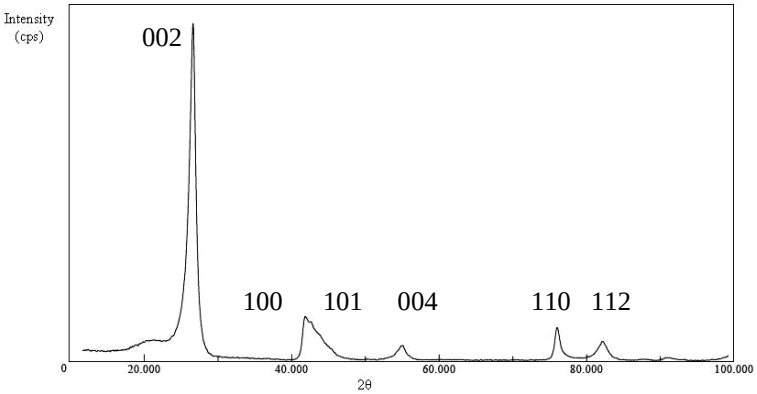

Fig. B.8.2. XRD pattern of hBN in presence of FeF_3 at 1250°C.

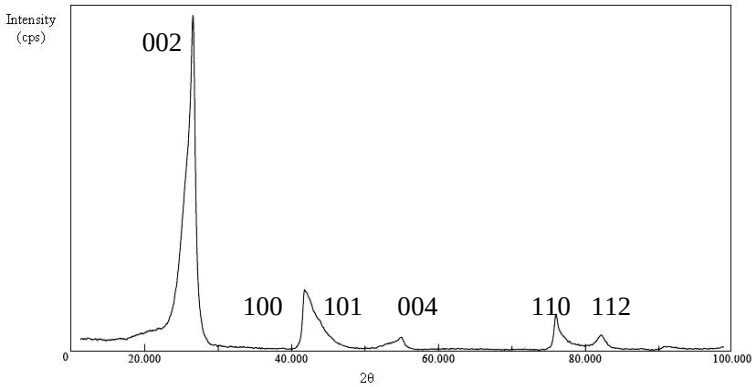

Fig. B.8.3. XRD pattern of hBN in presence of FeF_3 at 1450°C.

B.9. XRD pattern of hBN samples in presence of $Fe(NO_3)_3$.

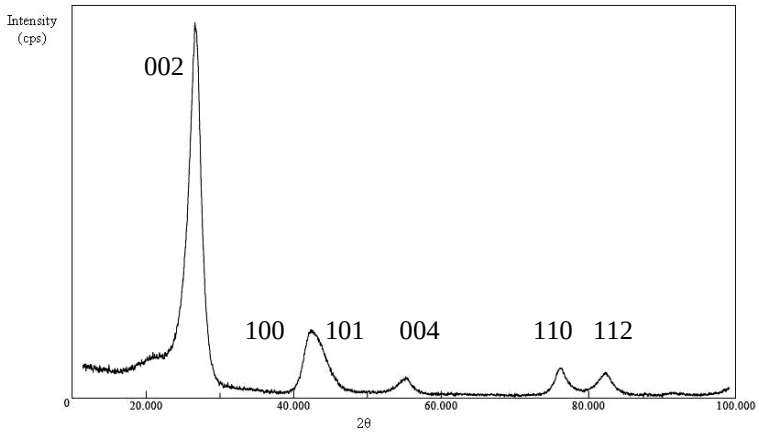

Fig. B.9.1. XRD pattern of hBN in presence of $Fe(NO_3)_3$ at 1050°C.

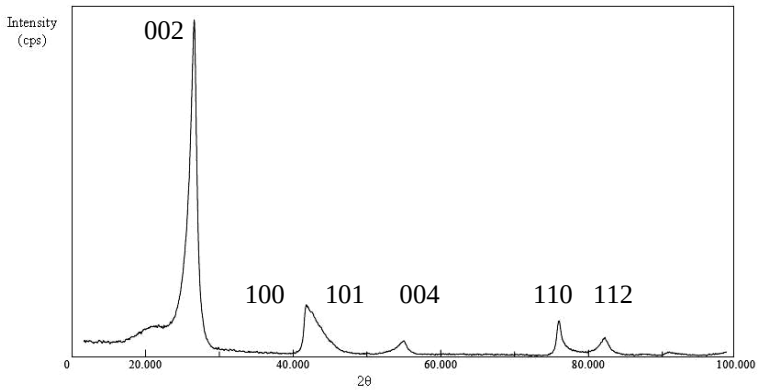

Fig. B.9.2. XRD pattern of hBN in presence of $Fe(NO_3)_3$ at 1250°C.

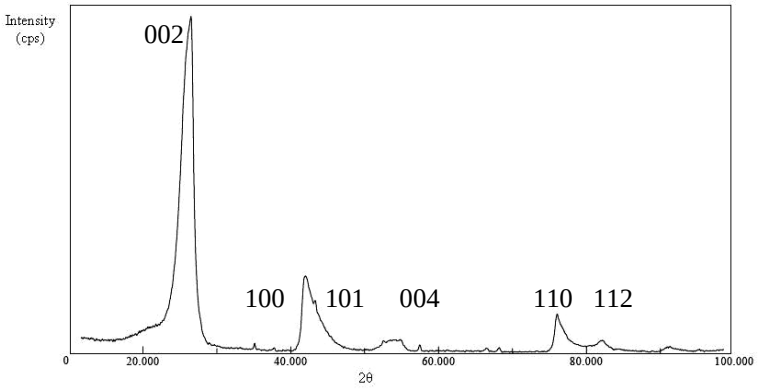

Fig. B.9.3. XRD pattern of hBN in presence of $Fe(NO_3)_3$ at 1450°C.

APPENDIX C

SEM IMAGES OF hBN SAMPLES

C. 1 SEM images of hBN in presence of KNO_3.

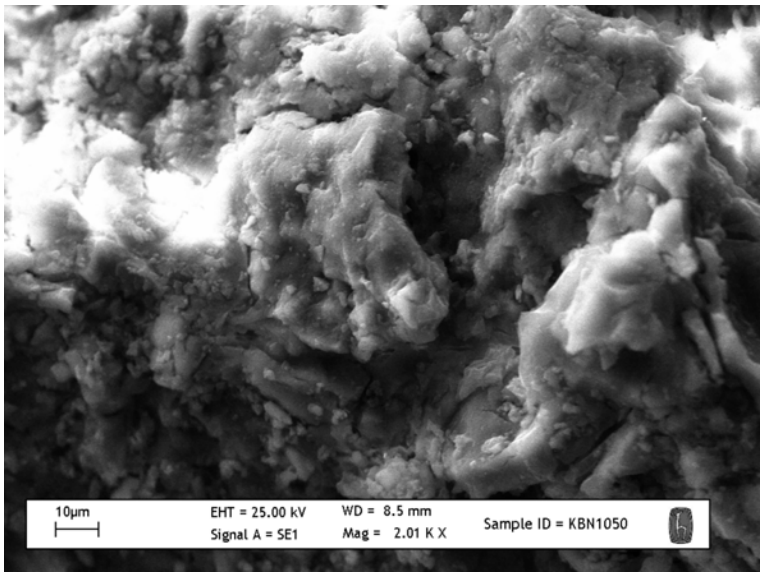

Fig. C.1.1. SEM images of hBN in presence of KNO_3 at 1050°C.

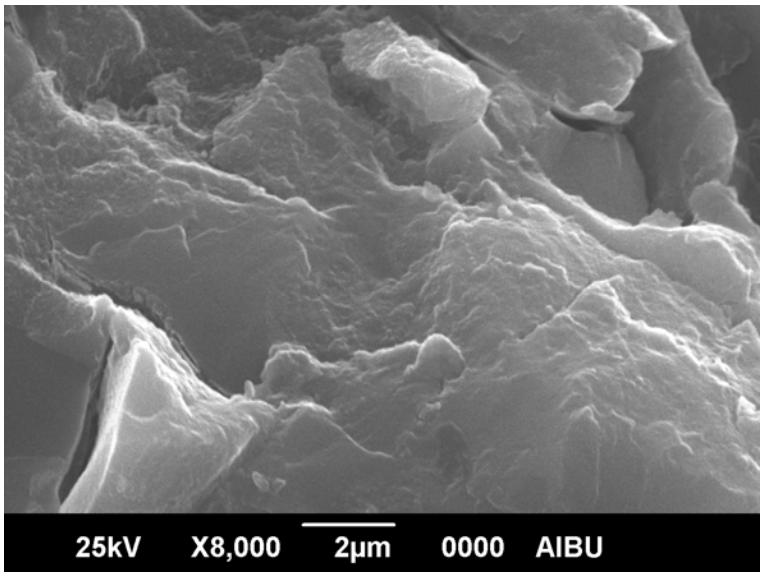

Fig. C.1.2. SEM images of hBN in presence of KNO_3 at 1050°C.

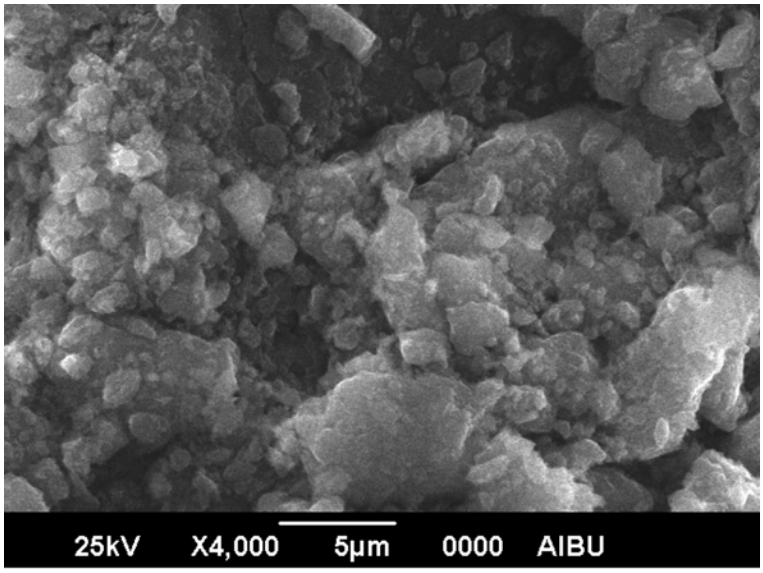

Fig. C.1.3. SEM images of hBN in presence of KNO_3 at 1250°C.

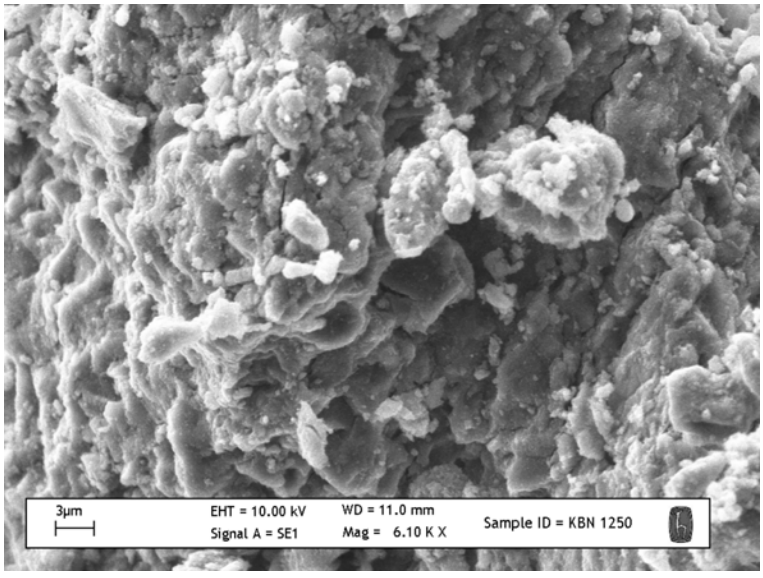

Fig. C.1.4. SEM images of hBN in presence of KNO_3 at 1250°C.

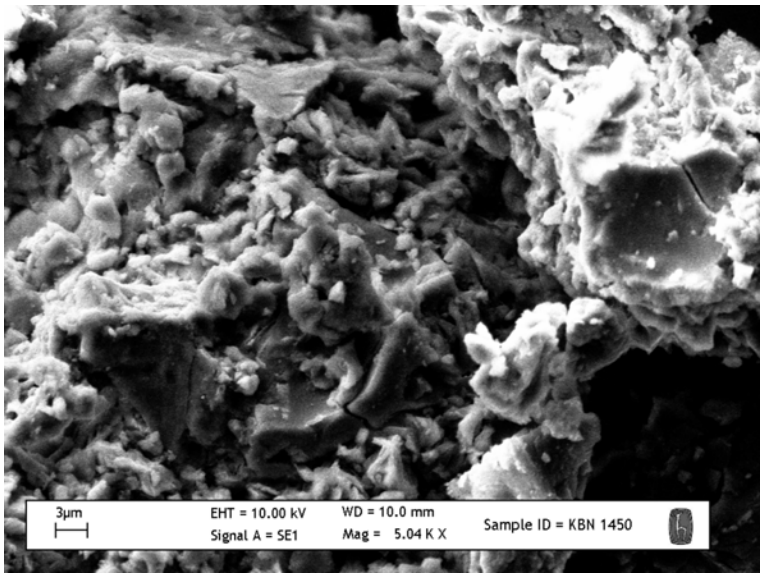

Fig. C.1.5. SEM images of hBN in presence of KNO_3 at 1450°C.

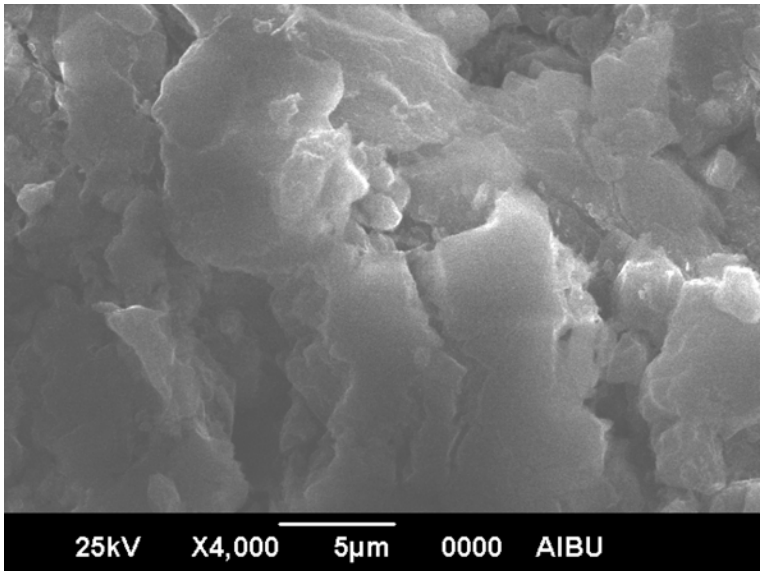

Fig. C.1.6. SEM images of hBN in presence of KNO_3 at 1450°C.

C. 2 SEM images of hBN in presence of $Ca(NO_3)_2$.

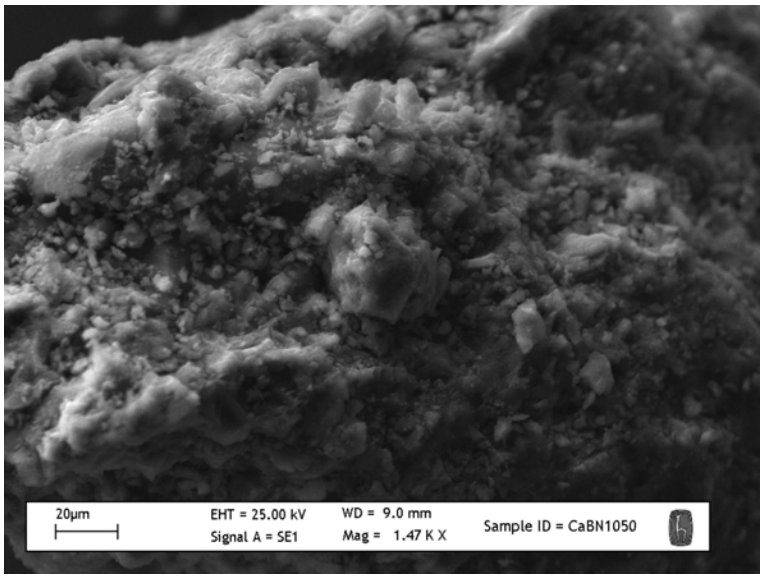

Fig. C.2.1. SEM images of hBN in presence of $Ca(NO_3)_2$ at 1050°C.

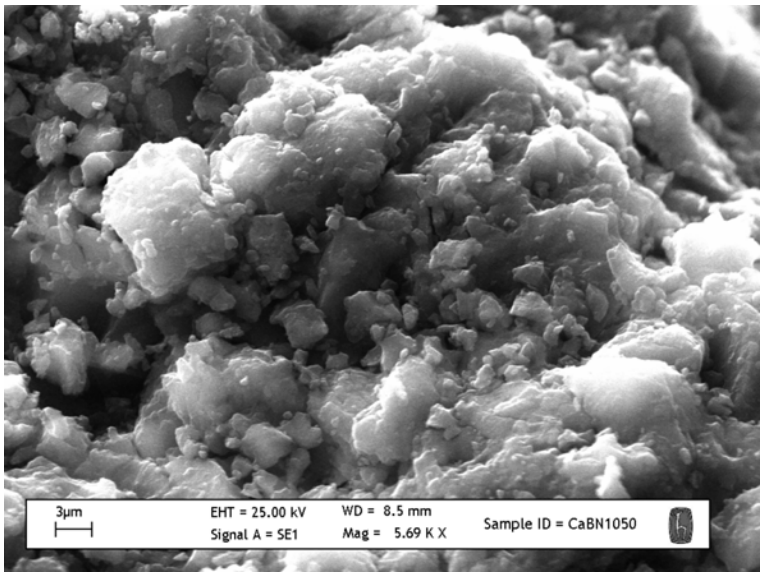

Fig. C.2.2. SEM images of hBN in presence of $Ca(NO_3)_2$ at 1050°C.

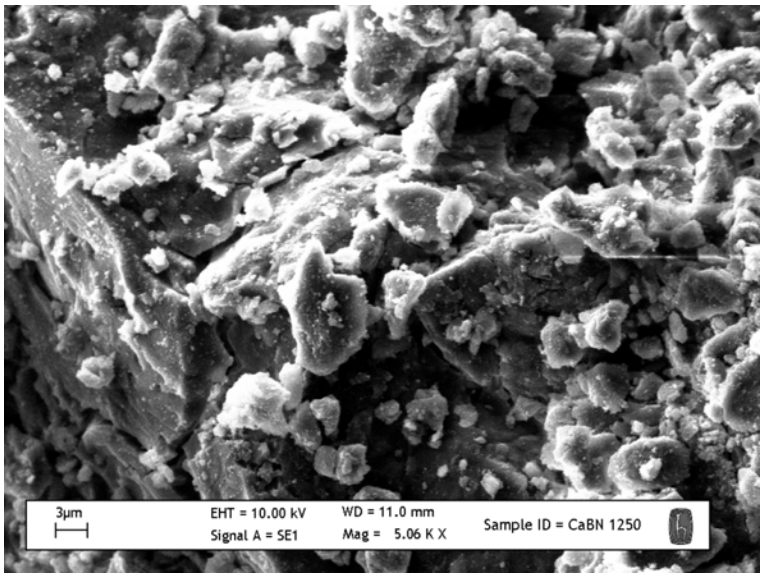

Fig. C.2.3. SEM images of hBN in presence of $Ca(NO_3)_2$ at 1250°C.

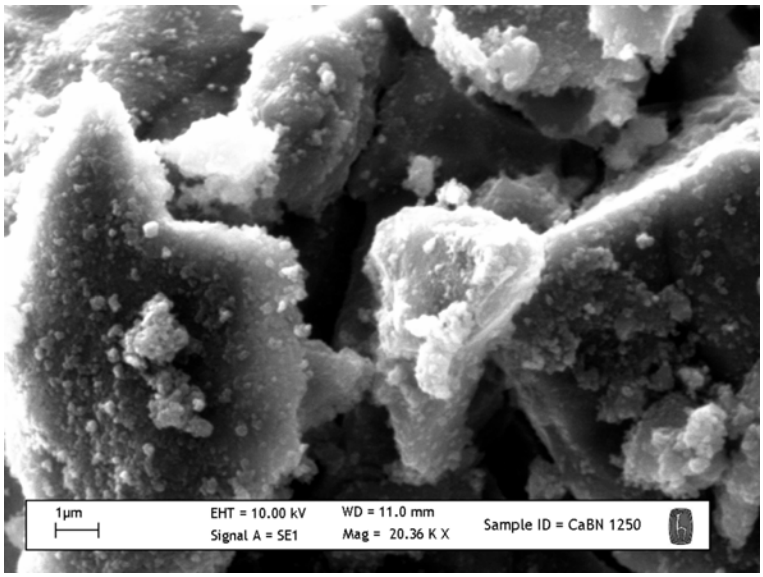

Fig. C. 2.4. SEM images of hBN in presence of $Ca(NO_3)_2$ at 1250°C.

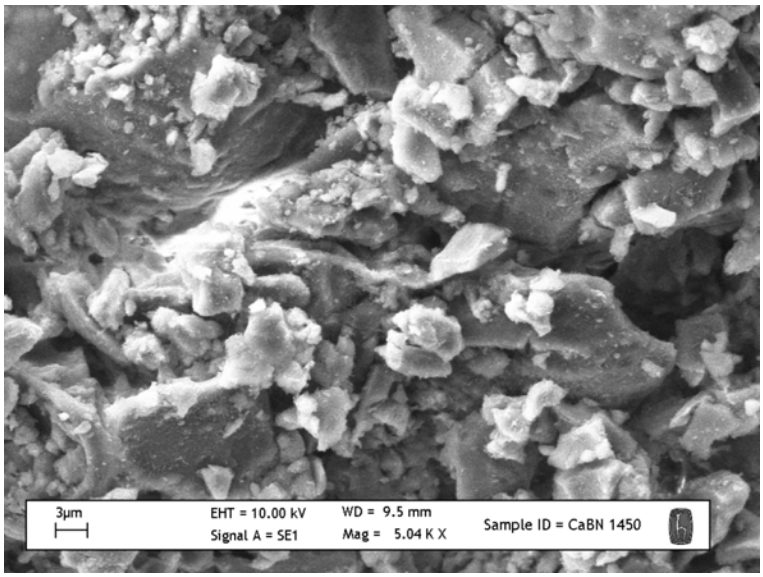

Fig. C.2.5. SEM images of hBN in presence of $Ca(NO_3)_2$ at 1450°C.

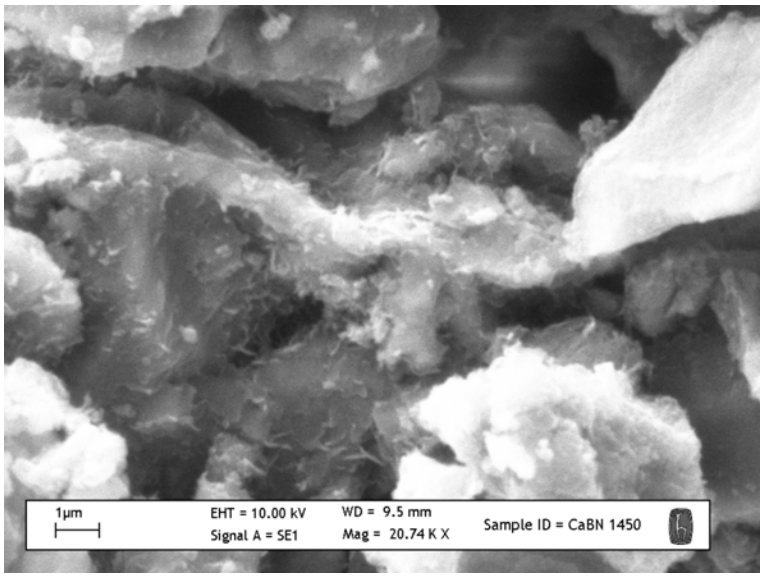

Fig. C.2.6. SEM images of hBN in presence of $Ca(NO_3)_2$ at 1450°C.

C. 3 SEM images of hBN in presence of $Sc(NO_3)_3$.

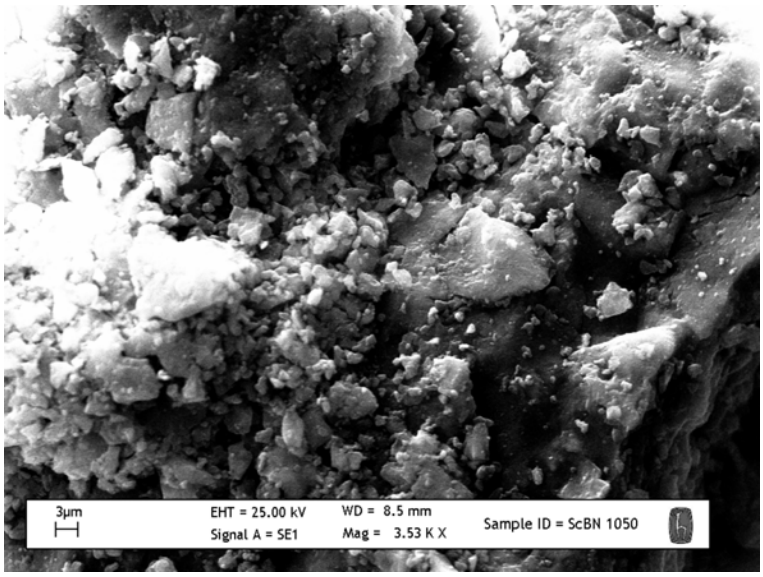

Fig. C.3.1. SEM images of hBN in presence of $Sc(NO_3)_3$ at 1050°C.

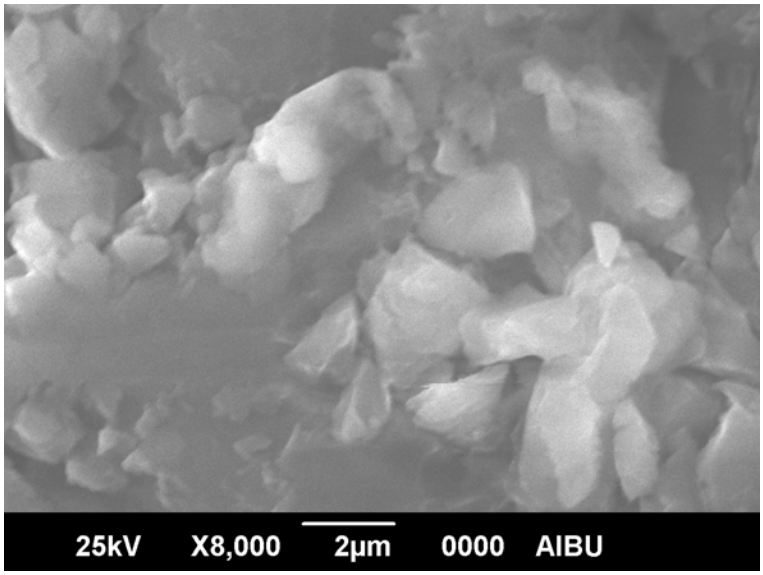

Fig. C.3.2. SEM images of hBN in presence of $Sc(NO_3)_3$ at 1050°C.

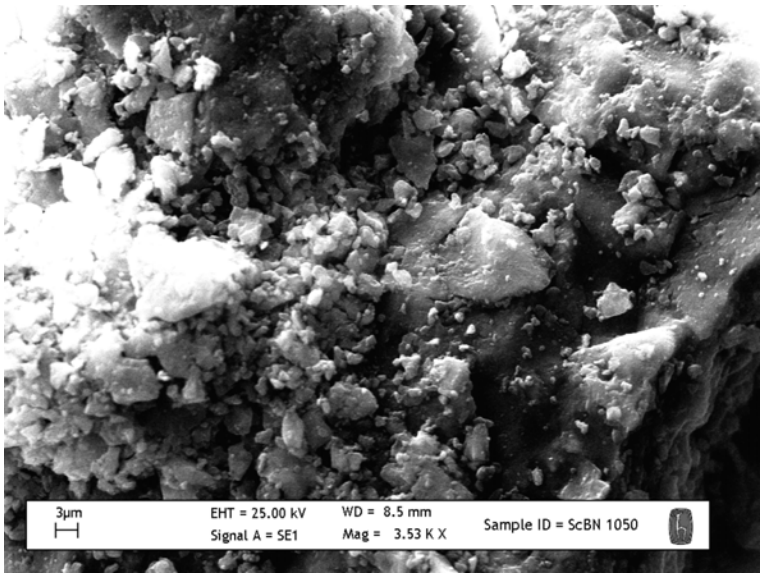

Fig. C.3.3 SEM images of hBN in presence of $Sc(NO_3)_3$ at 1250°C.

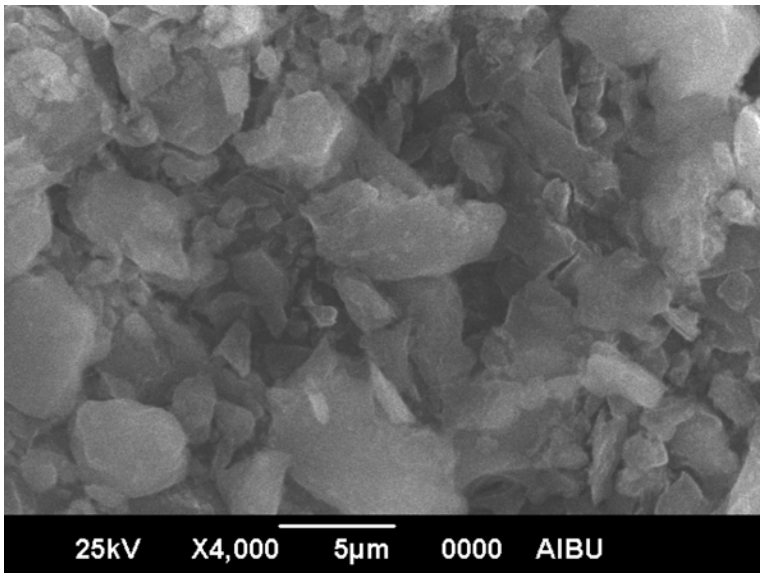

Fig. C.3.4. SEM images of hBN in presence of $Sc(NO_3)_3$ at 1250°C.

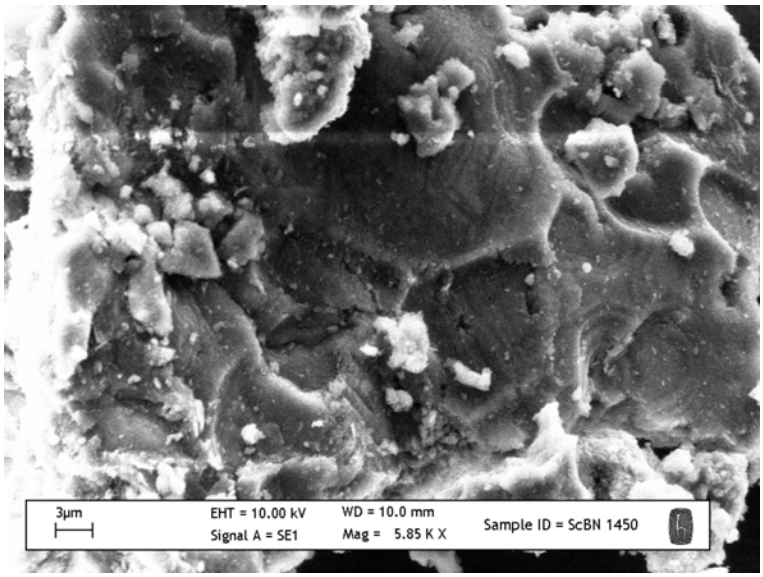

Fig. C.3.5. SEM images of hBN in presence of $Sc(NO_3)_3$ at 1450°C.

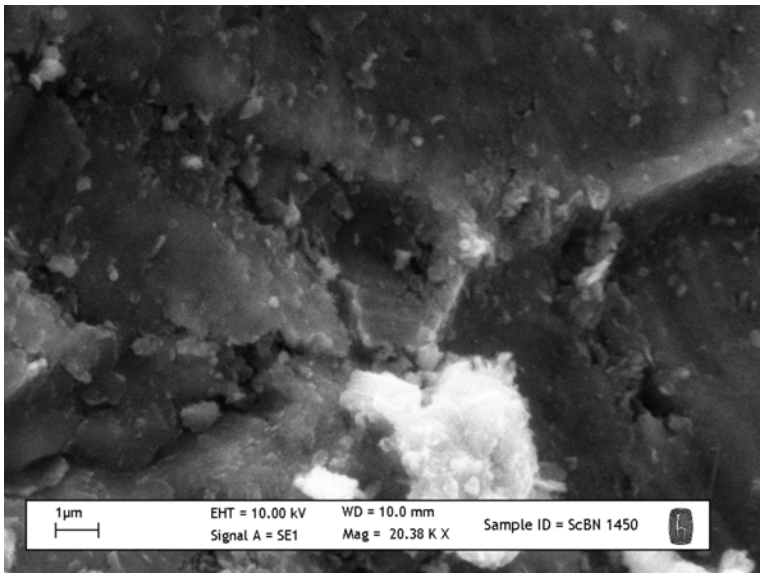

Fig. C.3.6. SEM images of hBN in presence of $Sc(NO_3)_3$ at 1450°C.

C. 4 SEM images of hBN in presence of $Ti(NO_3)_4$.

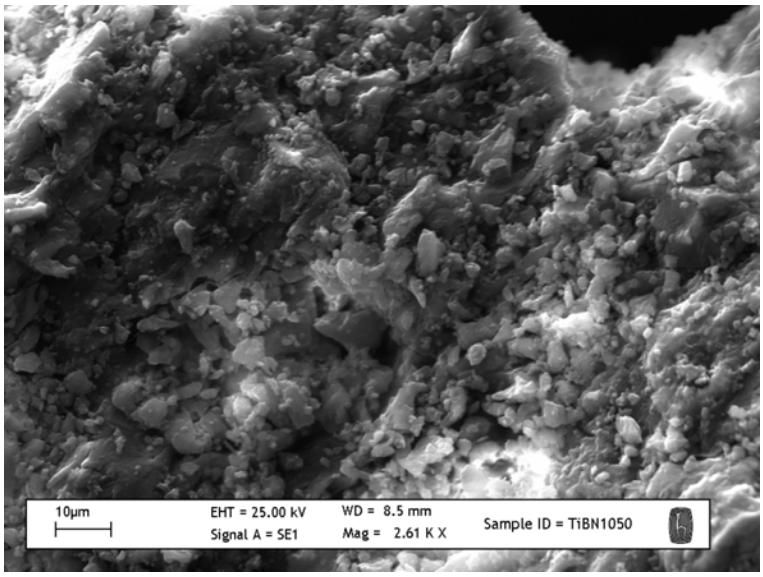

Fig. C.4.1. SEM images of hBN in presence of $Ti(NO_3)_4$ at 1050°C.

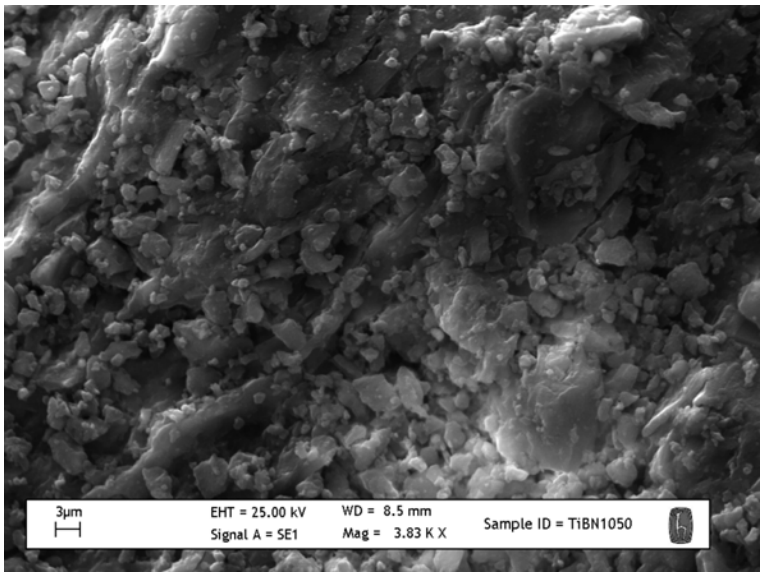

Fig. C.4.2. SEM images of hBN in presence of $Ti(NO_3)_4$ at 1050°C.

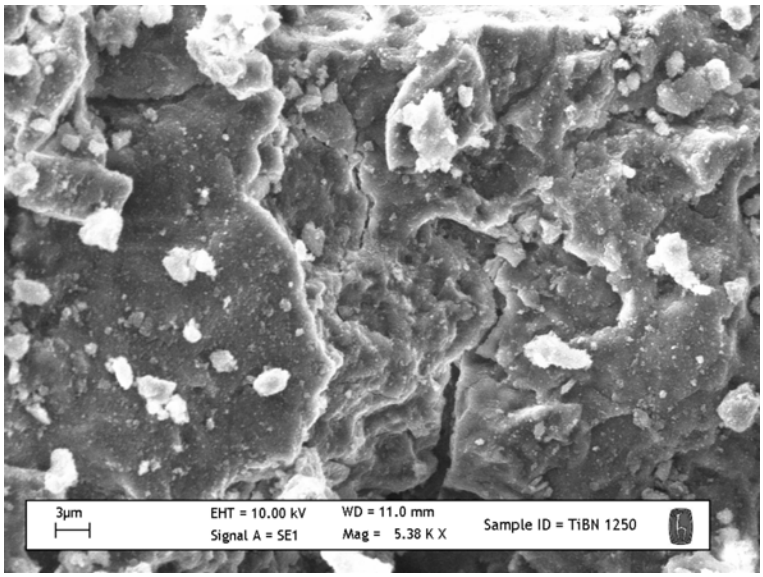

Fig. C.4.3. SEM images of hBN in presence of $Ti(NO_3)_4$ at 1250°C.

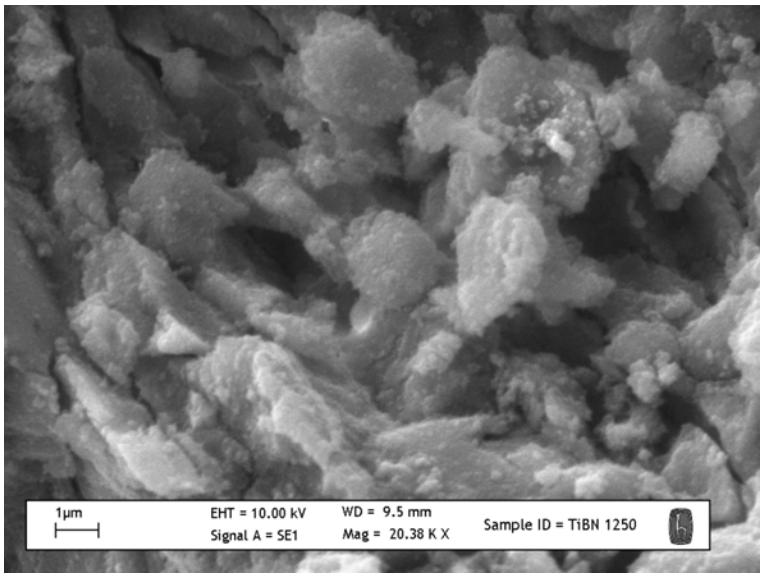

Fig. C.4.4. SEM images of hBN in presence of $Ti(NO_3)_4$ at 1250°C.

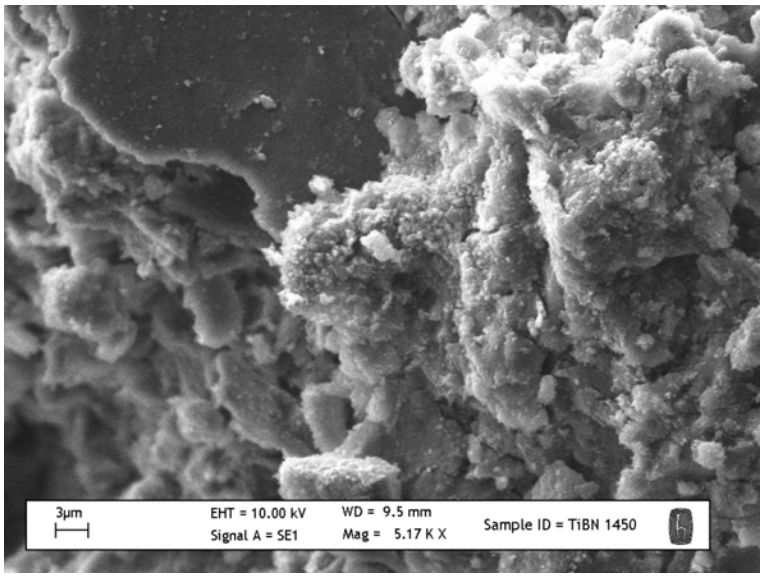

Fig. C.4.5. SEM images of hBN in presence of $Ti(NO_3)_4$ at 1450°C.

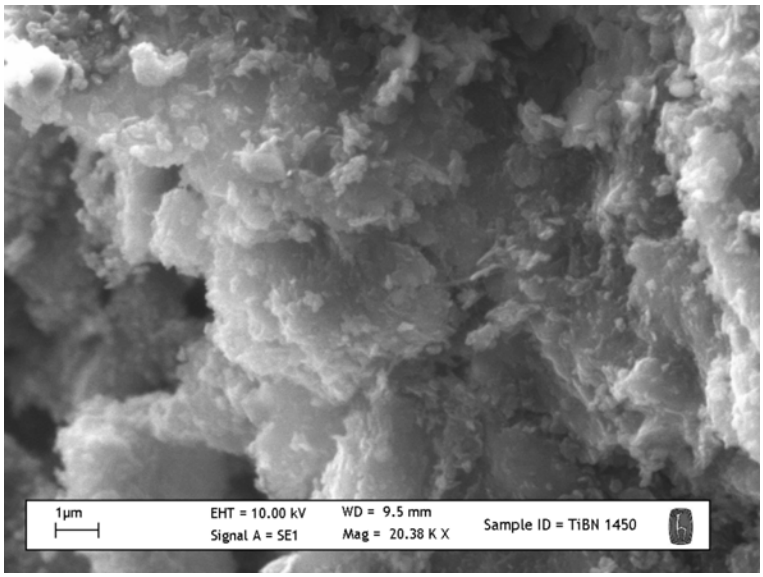

Fig. C.4.6. SEM images of hBN in presence of $Ti(NO_3)_4$ at 1450°C.

C. 5 SEM images of hBN in presence of VO_2.

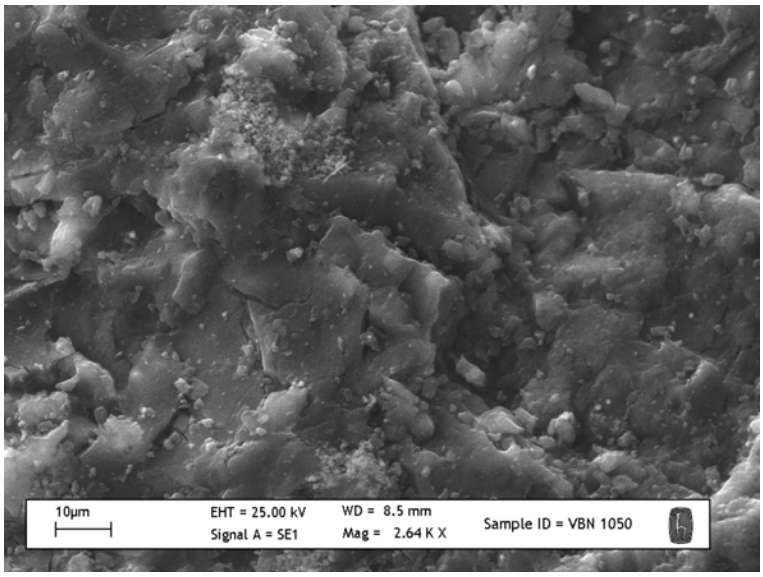

Fig. C.5.1. SEM images of hBN in presence of VO_2 at 1050°C.

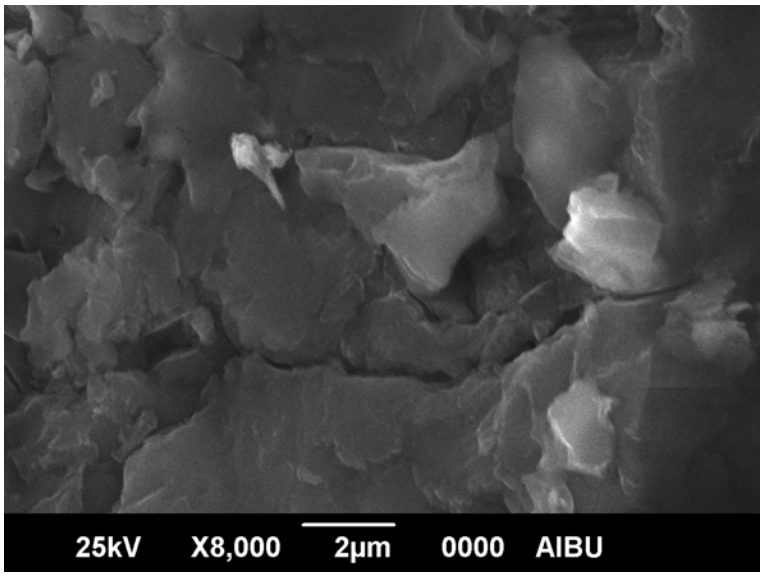

Fig. C.5.2. SEM images of hBN in presence of VO_2 at 1050°C.

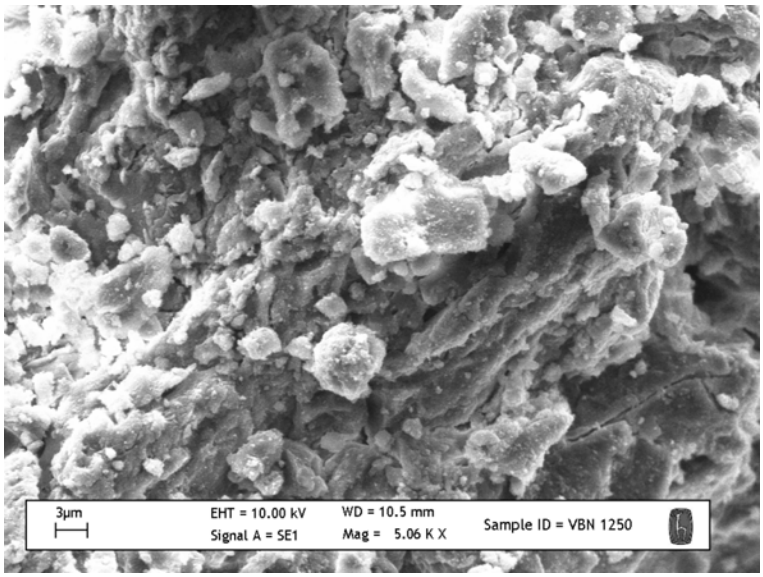

Fig. C.5.3. SEM images of hBN in presence of VO_2 at 1250°C.

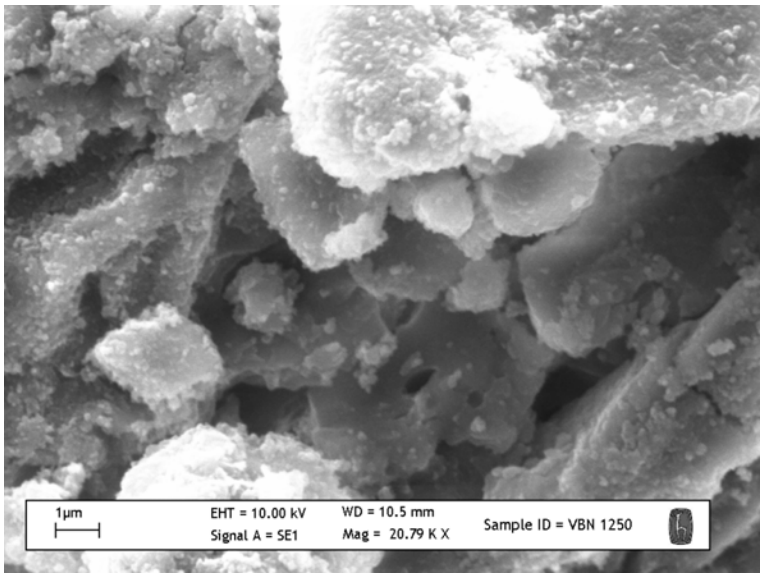

Fig. C.5.4. SEM images of hBN in presence of VO_2 at 1250°C.

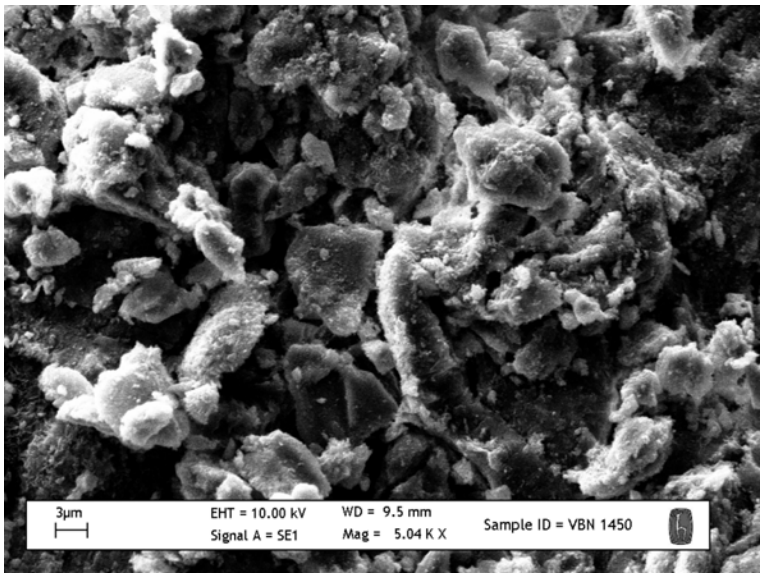

Fig. C.5.5. SEM images of hBN in presence of VO_2 at 1450°C.

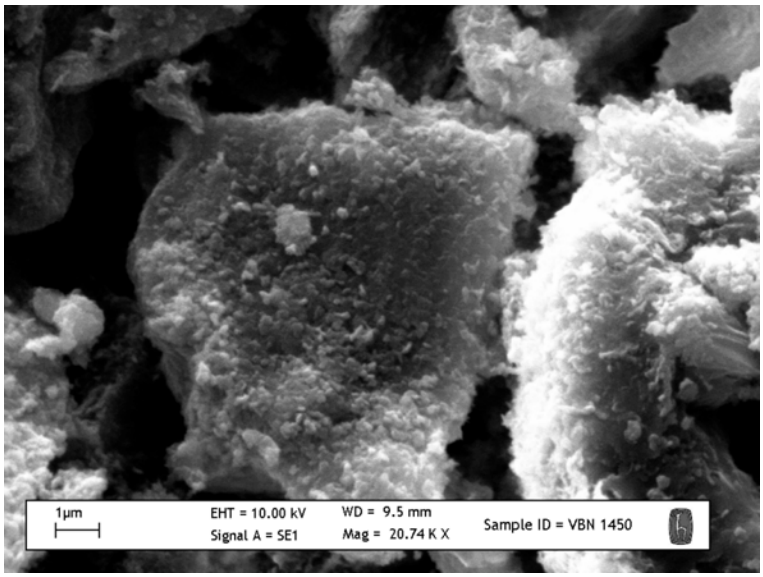

Fig. C.5.6. SEM images of hBN in presence of VO_2 at 1450°C.

C. 6 SEM images of hBN in presence of $Fe_2(SO_4)_3$.

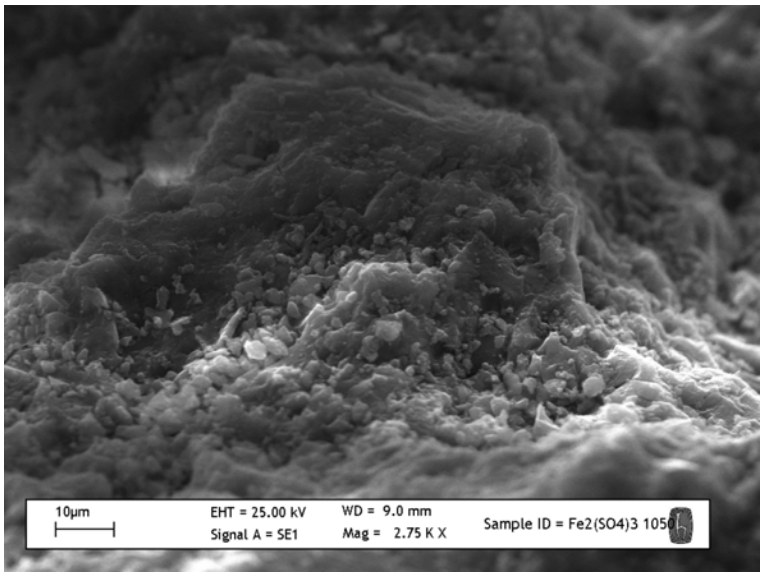

Fig. C.6.1. SEM images of hBN in presence of $Fe_2(SO_4)_3$ at 1050°C.

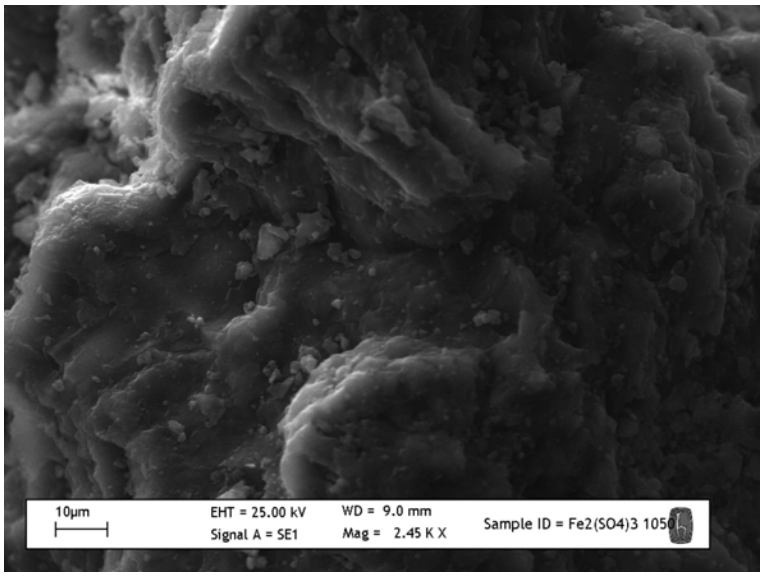

Fig. C.6.2. SEM images of hBN in presence of $Fe_2(SO_4)_3$ at 1050°C.

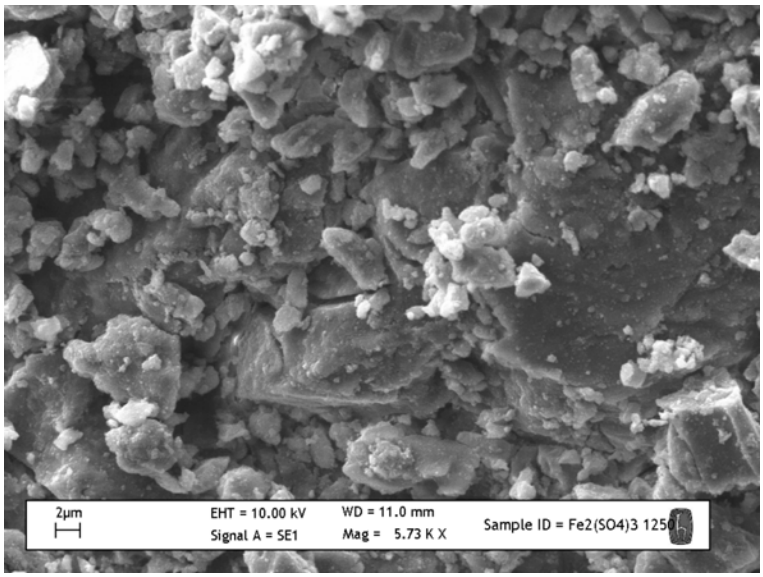

Fig. C.6.3. SEM images of hBN in presence of $Fe_2(SO_4)_3$ at 1250°C.

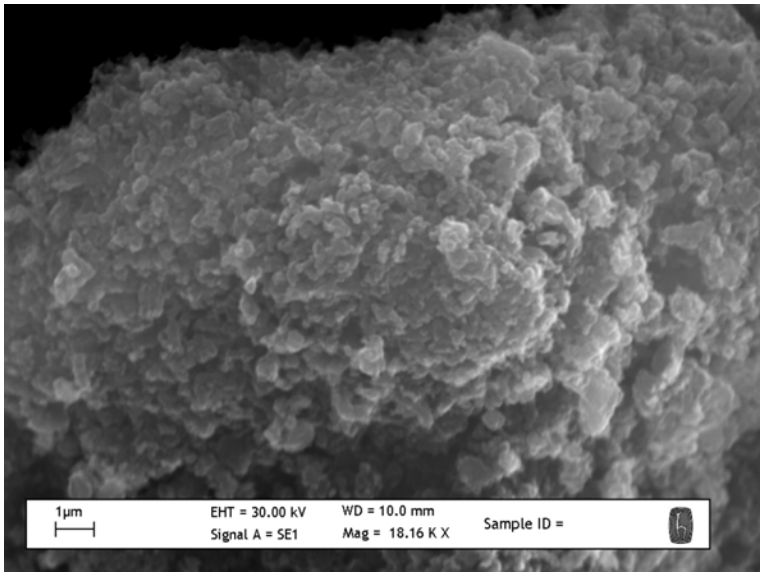

Fig. C.6.4. SEM images of hBN in presence of $Fe_2(SO_4)_3$ at 1250°C.

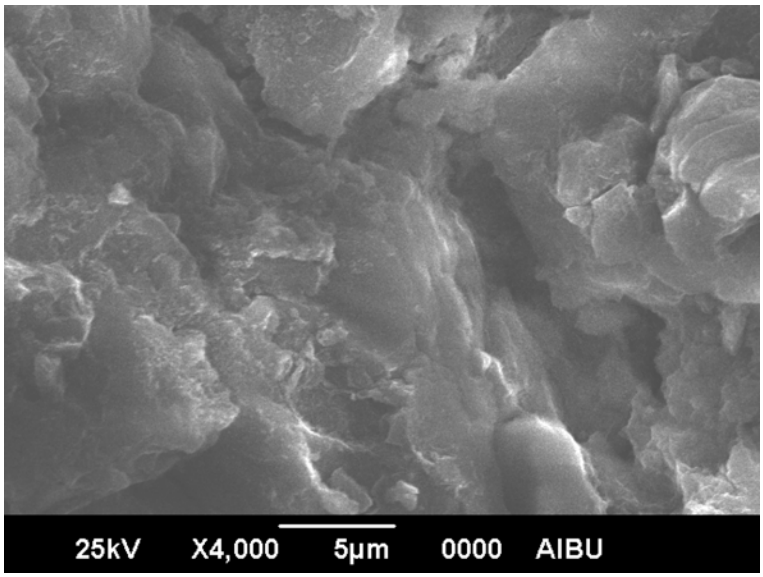

Fig. C.6.5. SEM images of hBN in presence of $Fe_2(SO_4)_3$ at 1450°C.

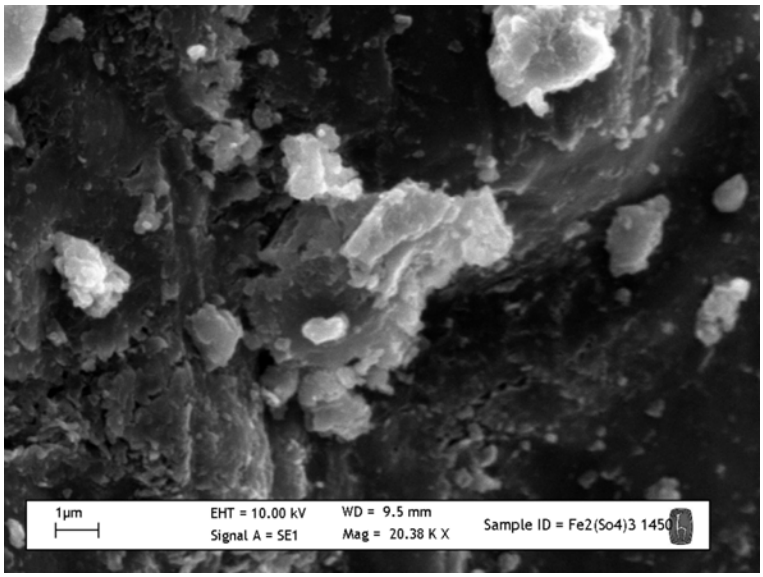

Fig. C.6.6. SEM images of hBN in presence of $Fe_2(SO_4)_3$ at 1450°C.

C. 7 SEM images of hBN in presence of $FeBr_3$.

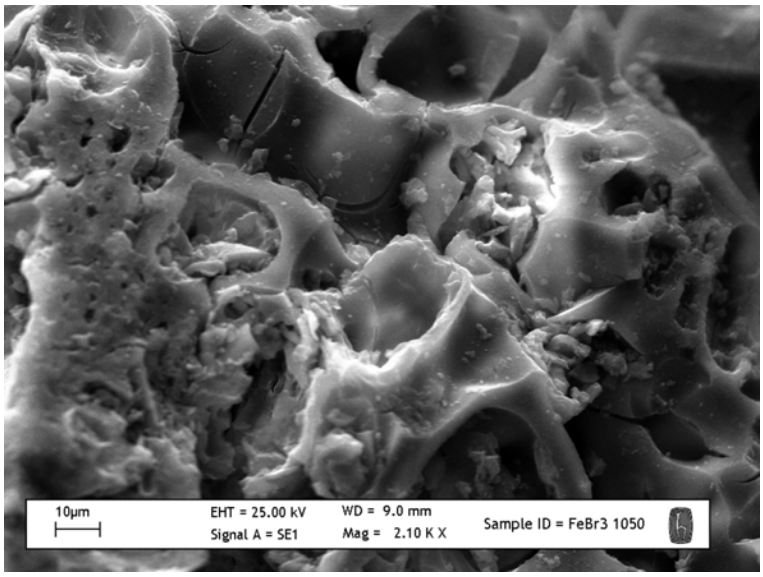

Fig. C.7.1. SEM images of hBN in presence of $FeBr_3$ at 1050°C.

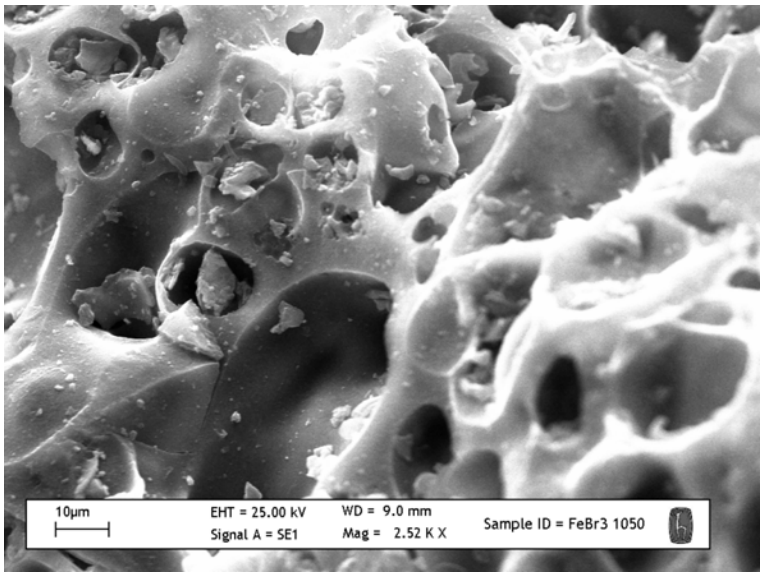

Fig. C.7.2. SEM images of hBN in presence of $FeBr_3$ at 1050°C.

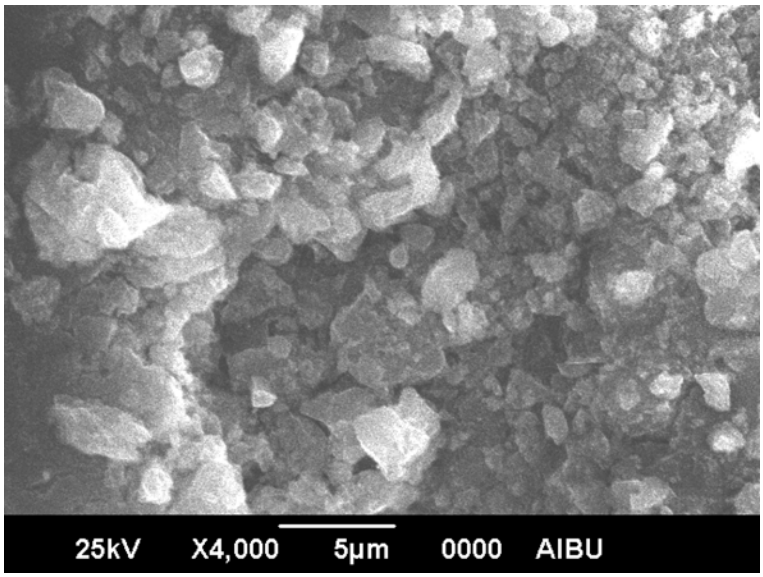

Fig. C.7.3. SEM images of hBN in presence of $FeBr_3$ at 1250°C.

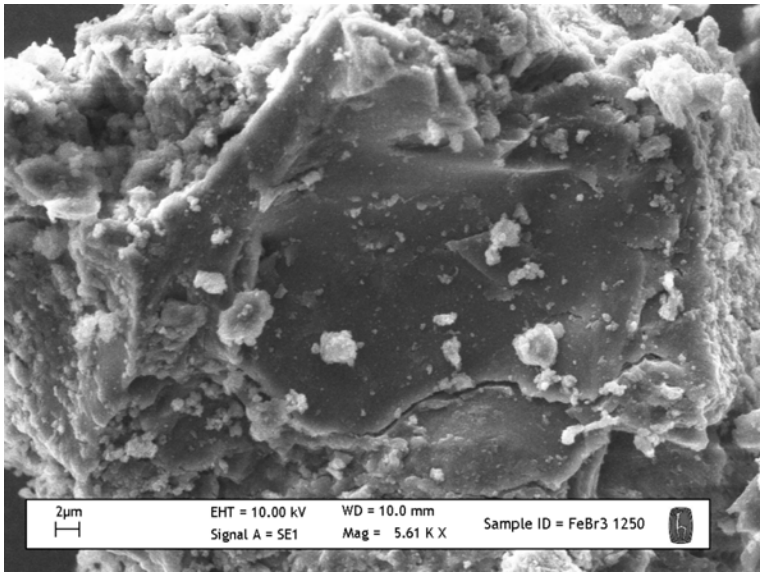

Fig. C.7.4. SEM images of hBN in presence of $FeBr_3$ at 1250°C.

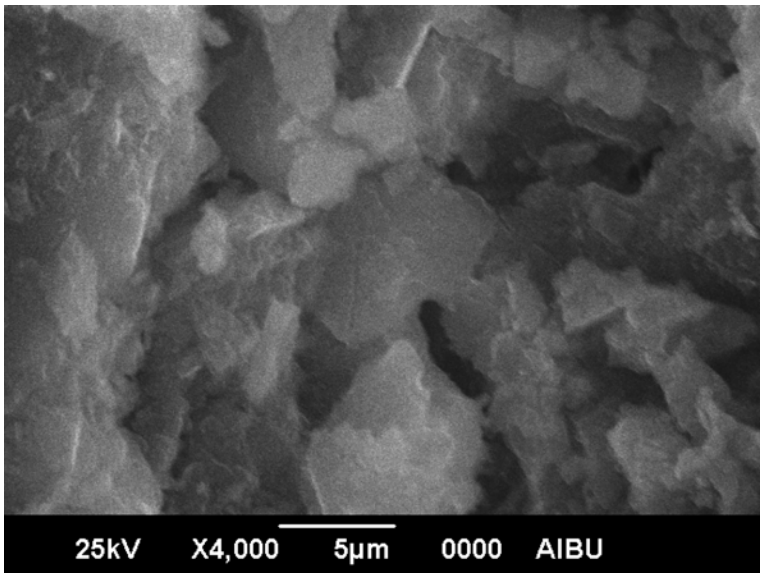

Fig. C.7.5. SEM images of hBN in presence of $FeBr_3$ at 1450°C.

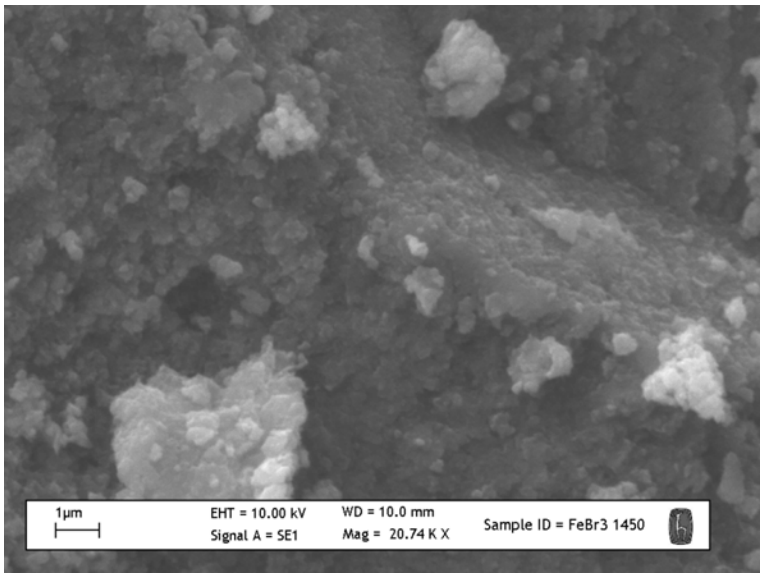

Fig. C.7.6. SEM images of hBN in presence of $FeBr_3$ at 1450°C.

C. 8 SEM images of hBN in presence of FeF_3.

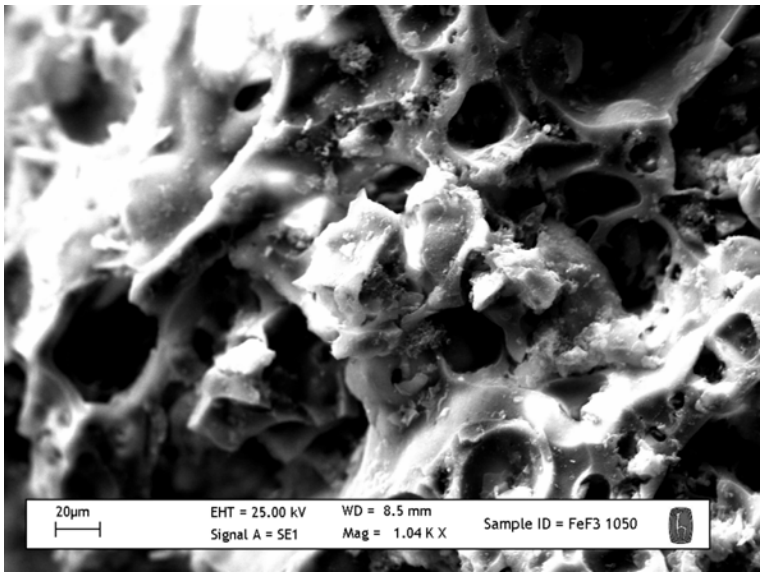

Fig. C.8.1. SEM images of hBN in presence of FeF_3 at 1050°C.

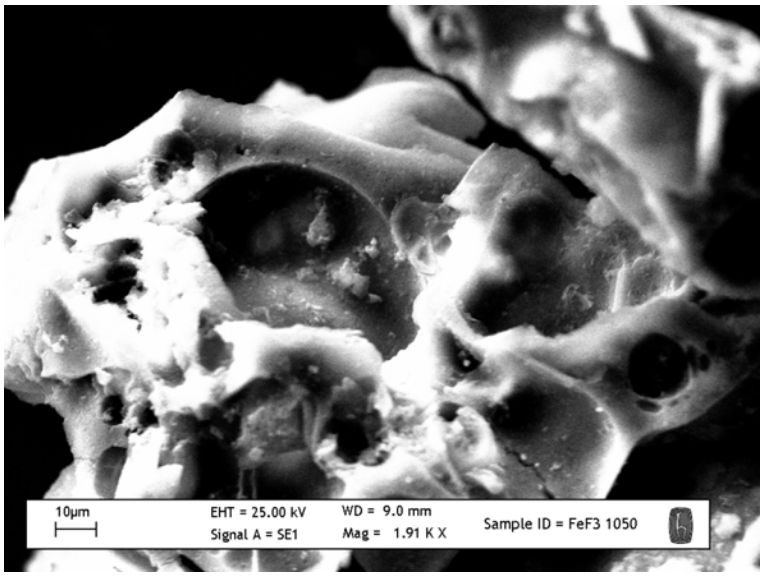

Fig. C.8.2. SEM images of hBN in presence of FeF_3 at 1050°C.

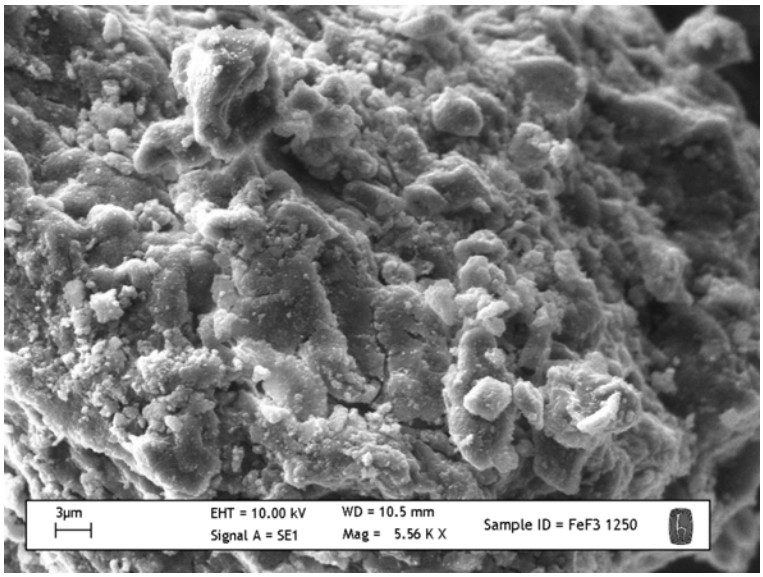

Fig. C.8.3. SEM images of hBN in presence of FeF_3 at 1250°C.

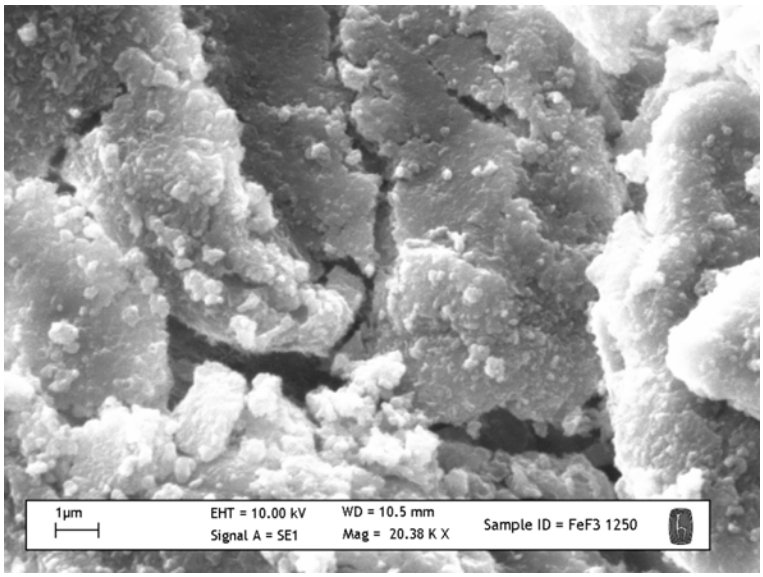

Fig. C.8.4. SEM images of hBN in presence of $FeBr_3$ at 1250°C.

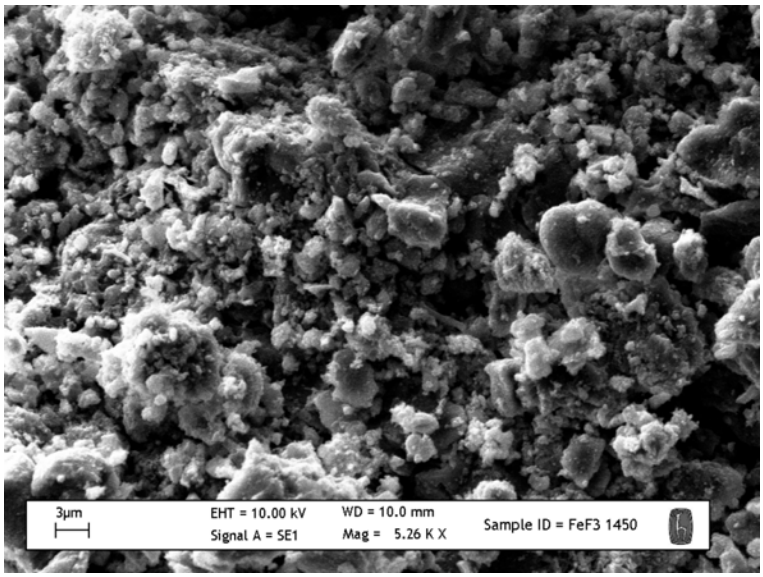

Fig. C.8.5. SEM images of hBN in presence of FeF_3 at 1450°C.

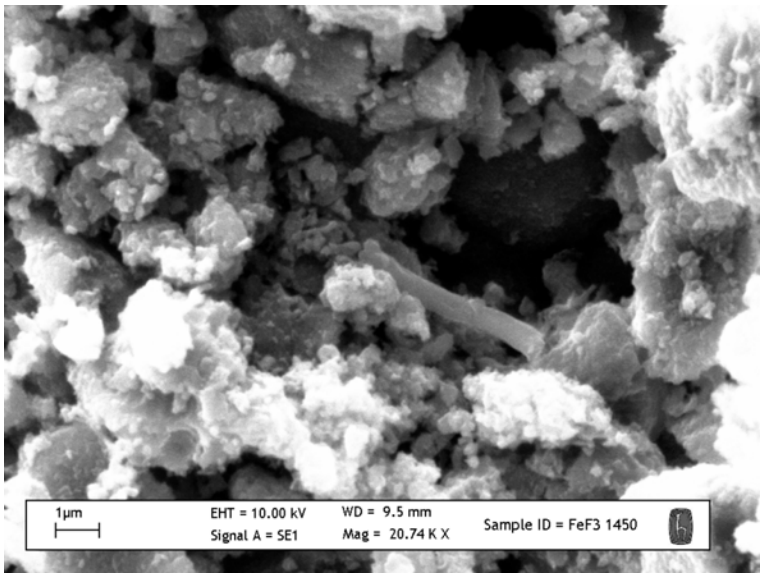

Fig. C.8.6. SEM images of hBN in presence of $FeBr_3$ at 1450°C.

C. 9 SEM images of hBN in presence of $Fe(NO_3)_3$.

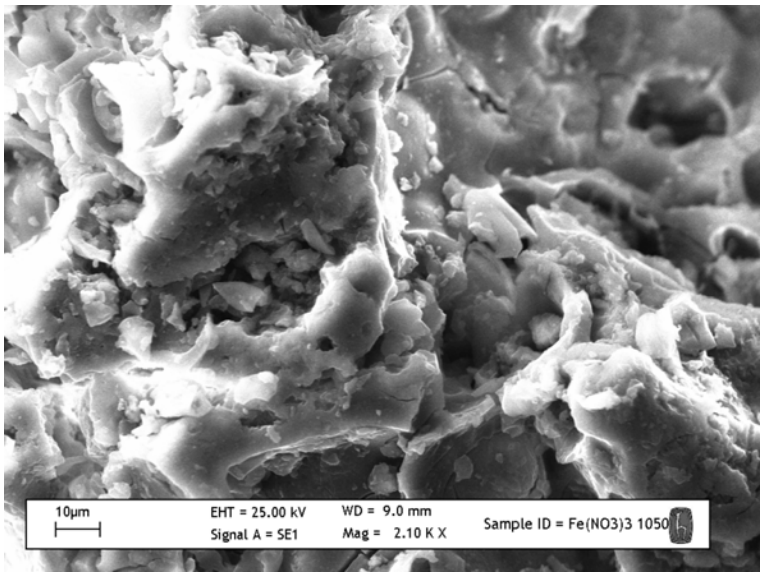

Fig. C.9.1. SEM images of hBN in presence of $Fe(NO)_3$ at 1050°C.

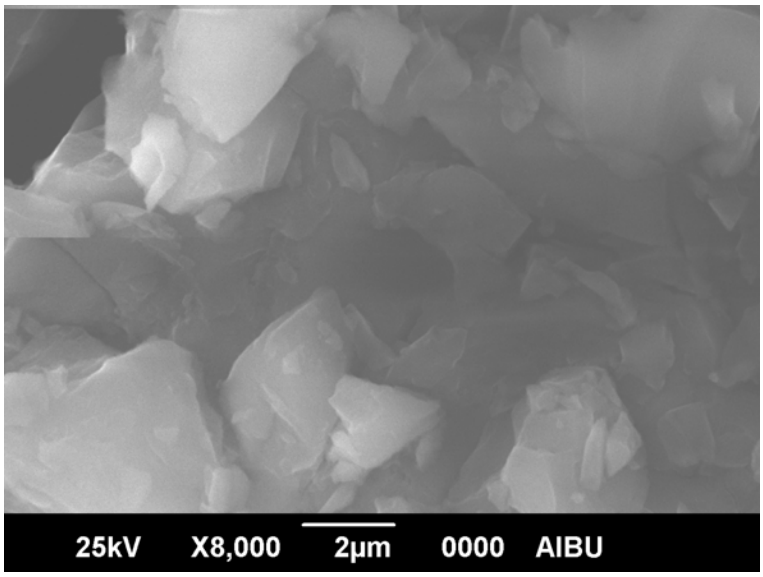

Fig. C.9.2. SEM images of hBN in presence of $Fe(NO)_3$ at 1050°C.

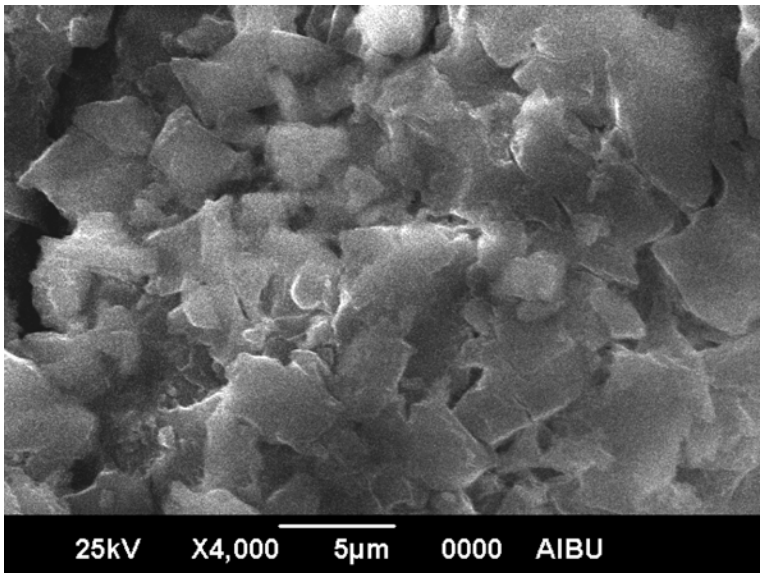

Fig. C.9.3. SEM images of hBN in presence of $Fe(NO_3)_3$ at 1250°C.

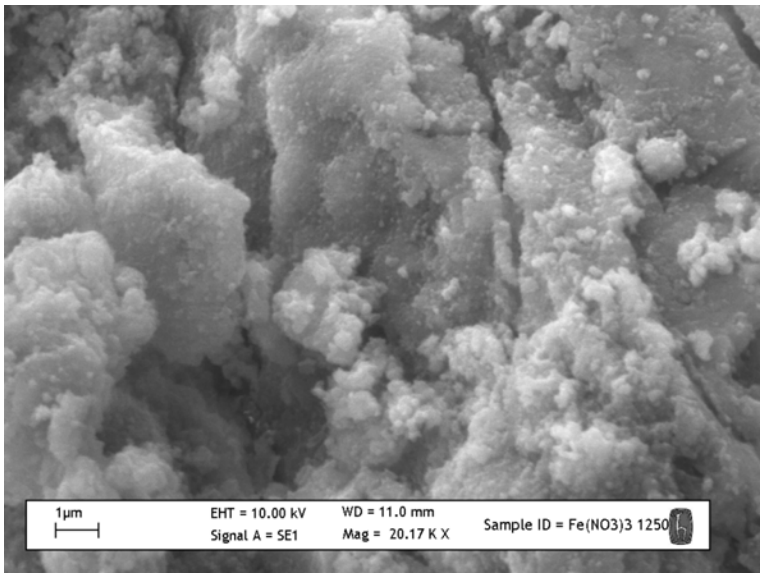

Fig. C.9.4. SEM images of hBN in presence of $Fe(NO_3)_3$ at 1250°C.

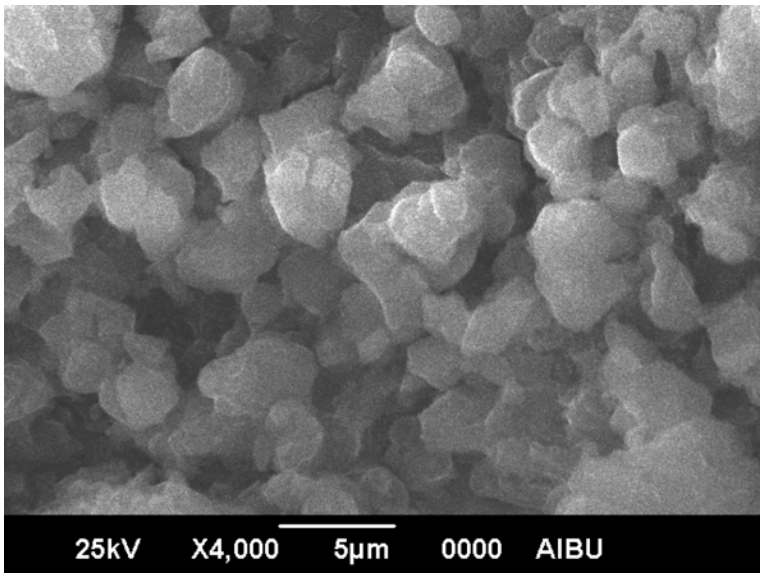

Fig. C.9.5. SEM images of hBN in presence of $Fe(NO_3)_3$ at 1450°C.

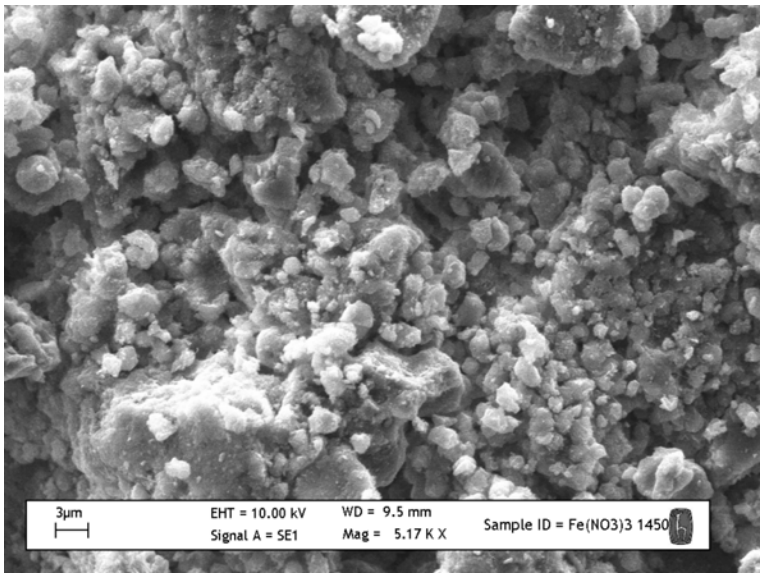

Fig. C.9.6. SEM images of hBN in presence of $Fe(NO_3)_3$ at 1450°C.

APPENDIX D

EDX ANALYSIS OF hBN SAMPLES

D.1. EDX analysis of some hBN samples prepared at 1050°C.

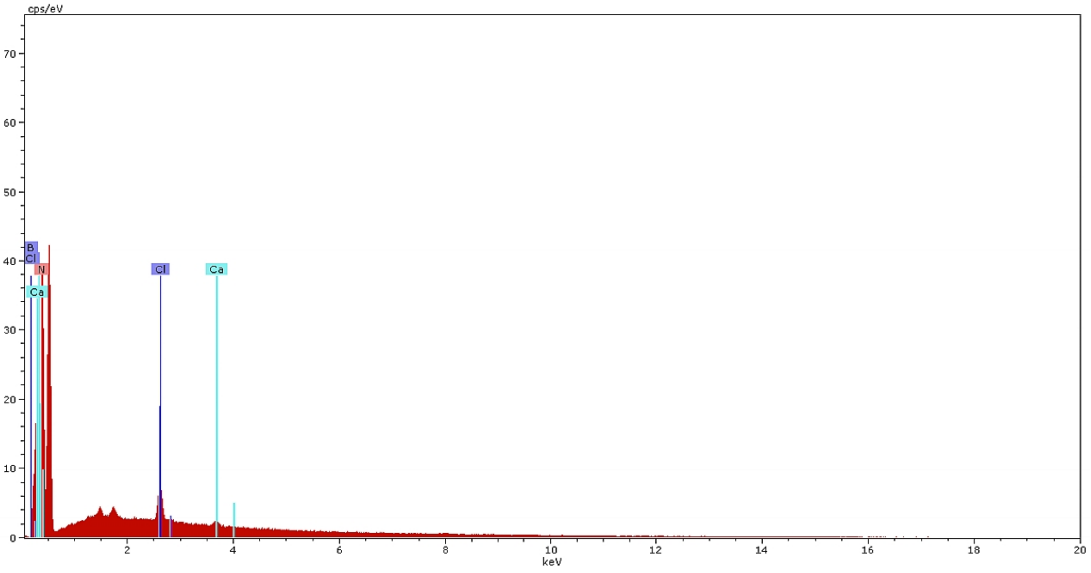

Fig. D. 1 EDX analysis of hBN in presence of $Ca(NO_3)_2$.

Element	[wt.-%]	[norm. wt.]	[norm.at.%]
Boron	23.72001385	23.72048826	28.79942001
Nitrogen	75.78238083	75.78389651	71.01778033
Chlorine	0.479360825	0.479370412	0.177479375
Calcium	0.016244497	0.016244822	0.005320285
Sum	99.998	100	100

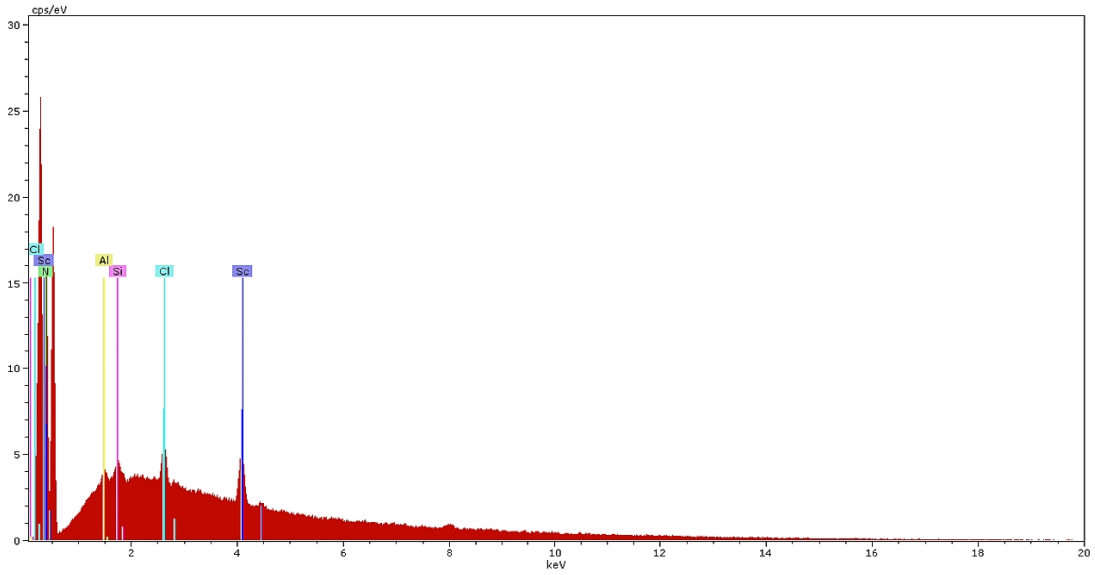

Fig. D. 2 EDX analysis of hBN in presence of $Sc(NO_3)_3$.

Element	[wt.-%]	[norm.wt.%]	[norm.at.-%]
Nitrogen	99.34915309	99.35014659	99.75080947
Aluminium	0.075939835	0.075940594	0.039581386
Silicon	0.079200798	0.07920159	0.039658427
Chlorine	0.181199602	0.181201414	0.071878003
Scandium	0.313506679	0.313509815	0.098072711
Sum:	99.999	100	100

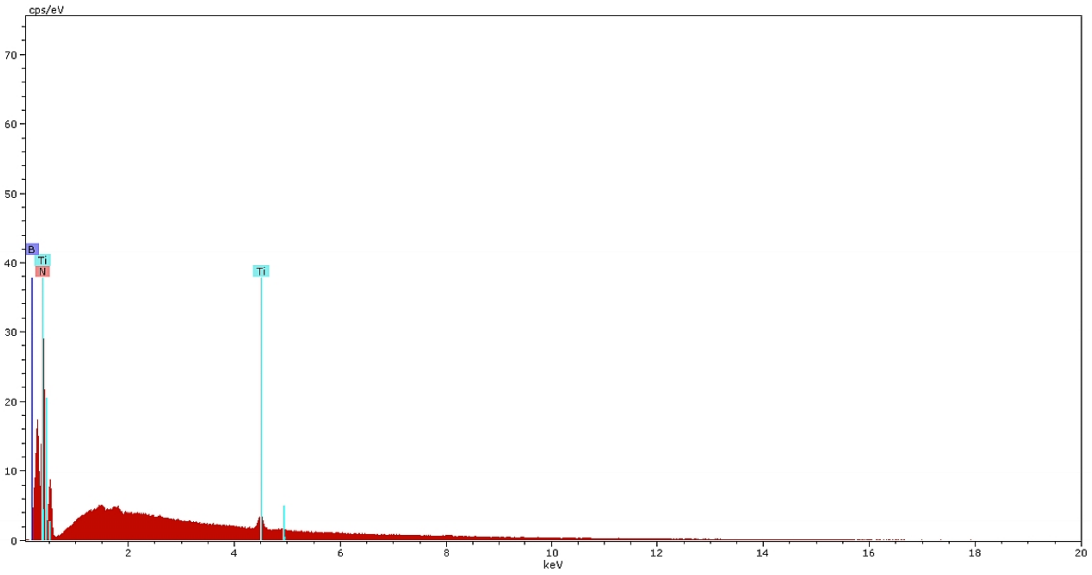

Fig. D. 3 EDX analysis of hBN in presence of $Ti(NO_3)_4$.

Element	[wt.-%]	[norm. wt.-%]	[norm.at.-%]
Boron	25.04581019	25.04631112	30.27003162
Nitrogen	74.66649924	74.6679926	69.65200593
Titanium	0.28569057	0.285696284	0.077962444
Sum:	99.998	100	100

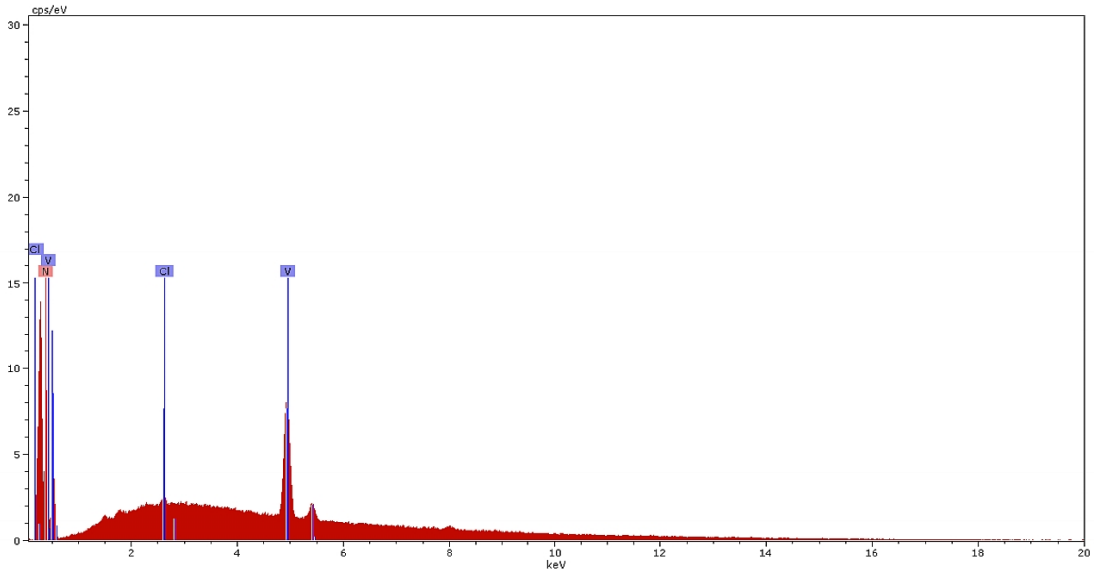

Fig. D. 4 EDX analysis of hBN in presence of VO_2.

Element	[wt.-%]	[norm.wt.%]	[norm.at.-%]
Nitrogen	98.72856984	98.72955713	99.64435439
Chlorine	0.025506127	0.025506382	0.010170467
Vanadium	1.244924038	1.244936487	0.345475148
Sum:	99.999	100	100

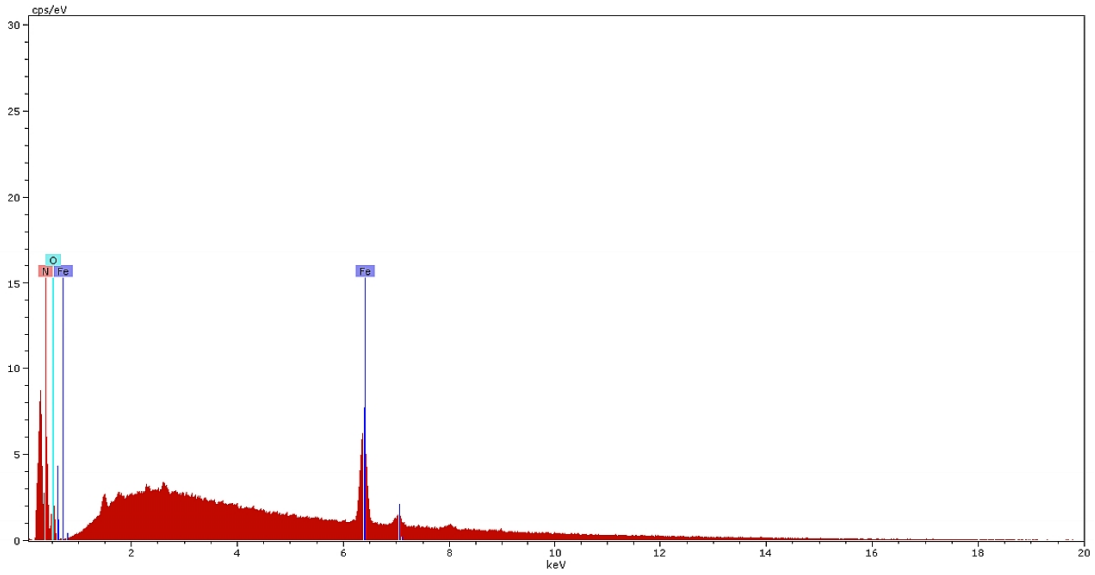

Fig. D. 5 EDX analysis of hBN in presence of $Fe_2(SO_4)_3$.

Element	[wt.-%]	[norm. wt.-%]	[norm. at.-%]
Nitrogen	64.99649565	64.99779561	68.63227341
Iron	1.49859407	1.498624042	0.396879266
Oxygen	33.50291028	33.50358035	30.97084732
Sum:	99.998	100	100

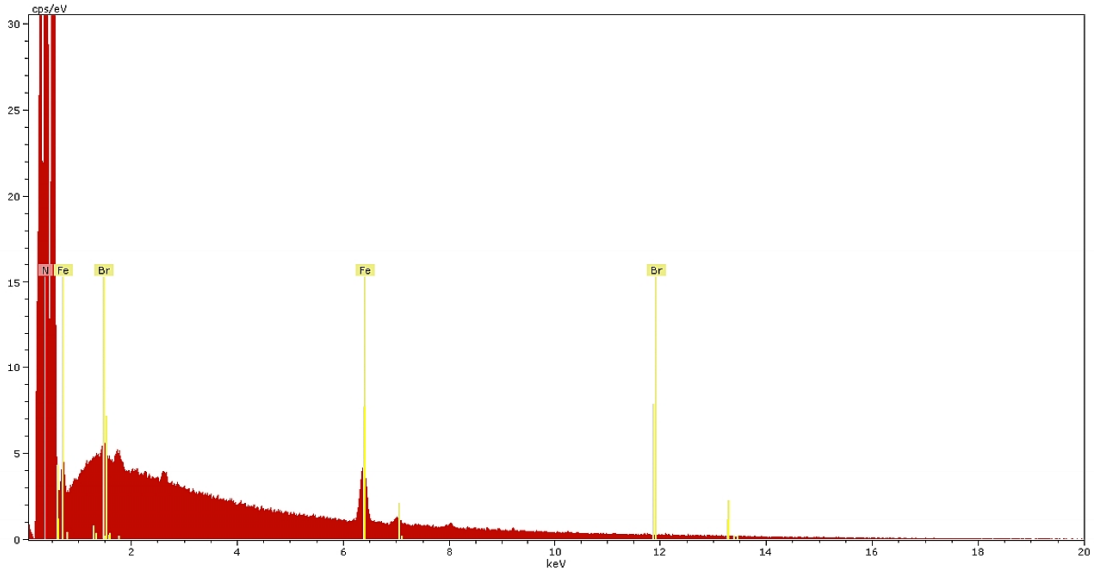

Fig. D. 6 EDX analysis of hBN in presence of $FeBr_3$.

Element	[wt.-%]	[norm. wt.-%]	[norm. at.-%]
Nitrogen	99.11667321	99.11766439	99.77725661
Iron	0.882020292	0.882029112	0.222689308
Bromine	0.000306495	0.000306498	5.40848E-05
Sum:	99.999	100	100

CIRRICULUM VITAE

Name **:** Erhan BUDAK

Permanent Address **:** Abant Izzet Baysal University Faculty of Art & Science of Chemistry 14280,Bolu

Degree and date to be conferred **:** Bs, 1999

Place, Date of Birth **:** Küçükçekmece, 13.12.1971

Secondory education **:** Aydınlıkevler Lisesi, Ankara

Collegiate instituons attended	**Dates**	**Degree**	**Date of degree**
Hacettepe University	1991-1997	Bs	1995
Abant Izzet Baysal University	1996-1999	Ms	1999

Publications:

Budak, E., Bozkurt, Ç. 2004. The Effect of Transition Metals on the Structure of hBN Intercalation Compounds. *J Solid State Chem*. 177: 1768- 1770.

Positions Held: Research Assistant at Abant Izzet Baysal University Faculty of Science & Letters Dept. Of Chemistry since 1996